Dissertation zur Erlangung des Doktorgrades der Technischen Fakultät der Albert-Ludwigs-Universität Freiburg im Breisgau

Mechanical Metamaterials with Engineered Responses

vorgelegt von

David Niels Schwarz

19.11.2025

Albert-Ludwigs-Universität Freiburg
Institut für Mikrosystemtechnik IMTEK



universität freiburg

Dekan

Prof. Dr.-Ing. Frank Balle

Referenten

Dr. Viacheslav Slesarenko

Prof. Dr.-Ing. Bastian E. Rapp

Datum der Promotion

03.02.2026

Bearbeitungszeitraum

November 2022 - November 2025

Contents

Abstract **1**

Zusammenfassung **3**

1 Introduction **5**
1.1 Engineered Materials 6
1.2 Motivation 7
1.3 Structure of the Thesis 8

2 Theoretical Background **9**
2.1 Mechanical Fundamentals 9
2.1.1 Stress and Strain 9
2.1.2 Hooke's Law 10
2.2 Mechanical Metamaterials 12
2.2.1 Auxetic Metamaterials 12
2.2.2 Metamaterials with Other Mechanical Responses 15
2.3 Fabrication of Advanced Materials and Metamaterials 16
2.3.1 Molding Based Manufacturing 17
2.3.2 Additive Manufacturing: Fused Filament Fabrication 19
2.3.3 Post-Processing and Functionalization 21

3 Mechanical Metamaterials with Engineered Responses **23**
3.1 Exploiting Self-Contact in Mechanical Metamaterials for New Discrete Functionalities 25
3.2 Correlating Fluorescence and Residual Stiffness in Self-Reporting Microcapsule Composites with an Intact Soft Matrix 36
3.3 Light Induced Training Enabled by Crosslinking in 3D Printed Mechanical Metamaterials 46

4 Conclusion **59**
4.1 Summary 59

4.2 Limitations and Outlook 60

5 Publications **63**

5.1 Publications as First Author 63

5.2 Publication as Co-Author 63

5.3 Presentations at Conferences 63

6 Scientific Curriculum Vitae **65**

Bibliography **71**

Abstract

This thesis develops approaches to engineer responses in mechanical metamaterials that enable new behaviors at the material level. Unlike traditional materials, mechanical metamaterials derive their unique responses to deformation from the geometry of their unit cell, rather than their composition. Furthermore, these geometry-driven responses can be enriched by additionally embedding functionality into the base material. This thesis makes three consecutive contributions utilizing geometry, composition, and their combination to engineer advanced responses in mechanical metamaterials.

The first contribution establishes the relationship between the unit cell's geometry and the resulting switch of Poisson's ratio during compression in a curved beam metamaterial. By means of experiments and simulations, the auxeticity switch is found to be accompanied by an expansion beyond the metamaterial's initial width. This switching response, which can be fine-tuned by geometric parameters, was harnessed in a discrete scales demonstrator, and also has the potential to be used in adaptive soft-robotic components. The second contribution deals with the modification of the base material by introduction of microcapsules in a soft matrix that can break when subjected to loading. Initially, the microcapsules contribute to the composite's stiffness. However, when overloaded, the microcapsules rupture, resulting in a significantly reduced stiffness of the composite. Subsequently, the capsules' released liquid content enables fluorescent self-reporting of the overloading event. The relationship between self-reporting and the drop in stiffness was found to be linearly correlated, but transient over time. The clear connection between the visual signal and the mechanical properties facilitates future mechanical metamaterial designs that can exploit local stress concentrations to release the capsule's contents in specific patterns upon deformation. The third contribution combines the geometrical design of a mechanical metamaterial with a responsive, UV-crosslinkable base material. Under UV irradiation, the 3D printable base material exhibits increased stiffness and accumulated shape changes, which were subsequently utilized in mechanical metamaterials. In a closed-loop setup with UV irradiation, a 3D printed

material system is achieved: the metamaterial's expansion upon compression triggers a UV light, resulting in stiffness and shape changes. Repeated stimuli can then be used to accumulate the property changes and demonstrate training of the material system.

Together, these contributions enable novel mechanical metamaterials that respond to their environment. By integrating "if-then" behavior, material softening, and adaptive stiffening, this work establishes a foundation for materials capable of responding and adapting to external stimuli.

Zusammenfassung

In dieser Dissertation werden Ansätze entwickelt, um auf Materialebene neue Funktionsweisen in mechanische Metamaterialien zu integrieren. Im Gegensatz zu konventionellen Werkstoffen erhalten mechanische Metamaterialien ihr außergewöhnliches Verhalten bei Verformung nicht durch ihre chemische Zusammensetzung, sondern durch die Geometrie ihrer Einheitszelle. Dieses geometriebasierte Verhalten lässt sich zudem erweitern, indem Grundwerkstoffe eingesetzt werden, die auf einen externen Reiz reagieren können. Die Arbeit besteht aus drei aufeinander aufbauenden Beiträgen, die die Geometrie, die Materialzusammensetzung sowie deren Kombination nutzen, um fortschrittliches Materialverhalten zu realisieren.

Der erste Beitrag untersucht den Zusammenhang zwischen der Geometrie einer Einheitszelle und dem Umschlag der Querkontraktionszahl bei Kompression eines Metamaterials aus geschwungenen Balkenelementen. Experimente und Simulationen zeigen, dass der Umschlag von auxetischer zu regulärer Querkontraktion mit einer lateralen Ausdehnung über die ursprüngliche Breite hinaus einhergeht. Diese Umschaltreaktion, die sich über geometrische Parameter gezielt einstellen lässt, wurde in einer diskreten Waage demonstriert und hat das Potenzial, adaptive Komponenten in der Softrobotik zu ermöglichen. Der zweite Beitrag befasst sich mit der Modifikation des Grundwerkstoffs, bei der Mikrokapseln in eine weiche Polymermatrix eingebettet werden. Zunächst erhöhen die Mikrokapseln die Steifigkeit des Komposits. Bei Überbelastung brechen die Kapseln jedoch und die Steifigkeit sinkt deutlich. Gleichzeitig ermöglicht die aus den Kapseln austretende Flüssigkeit eine Schadensanzeige mittels Fluoreszenz infolge der Überbelastung. Es zeigt sich, dass die visuelle Schadensanzeige und der Abfall der Steifigkeit linear korrelieren, sich dieser Zusammenhang jedoch mit der Zeit ändert. Diese direkte Kopplung zwischen optischem Signal und mechanischer Antwort eröffnet neue Gestaltungsmöglichkeiten für mechanische Metamaterialien. Diese könnten lokale Spannungsspitzen gezielt nutzen, um bei Verformung die Kapselinhalte in definierten Mustern freizusetzen. Der dritte Beitrag kombiniert die Geometrie eines Metamaterials mit einem reaktionsfähigen, UV-vernetzbaren Grundwerkstoff. Das 3D-druckbare Material passt

sich unter UV-Bestrahlung in seiner Form an und erhöht gleichzeitig seine Steifigkeit. Diese Eigenschaften können anschließend gezielt in einem Metamaterial genutzt werden. In einem geschlossenen Regelkreis entsteht so ein 3D-gedrucktes Materialsystem: Die laterale Ausdehnung des Metamaterials bei Kompression aktiviert eine UV-Lichtquelle, die eine Steifigkeits- und Formänderung auslöst. Durch wiederholte Stimuli werden diese Veränderungen akkumuliert, das Materialsystem kann „trainiert“ werden.

Gemeinsam ermöglichen diese Beiträge neuartige mechanische Metamaterialien, die aktiv auf ihre Umgebung reagieren können. Durch die Integration von „Wenn-dann“-Verhalten, Steifigkeitsabfall auf Materialebene und adaptiver Steifigkeitserhöhung legt diese Arbeit die Grundlage für Materialien, die sich anpassen und auf externe Reize reagieren können.

1 Introduction

Thanks to advancements in additive manufacturing techniques, we can process a wide range of materials and fabricate highly complex geometries. One such geometry is the gyroid lattice, which occurs naturally in the scales that cover butterfly wings and give them their striking colors [1]. The gyroid lattice additionally exhibits high stiffness while maintaining low relative density, which stems from the shape of its smallest repeated building block, the unit cell [2]. By designing the unit cell of an artificial material, it is possible to achieve mechanical responses that are dictated by geometrical features rather than composition. These so-called mechanical metamaterials can exhibit rather exotic responses to deformation, such as negative Poisson's ratio, rotation, and logic [3–5]. Additionally, changing the composition of a mechanical metamaterial's base material can enrich the response to external stimuli.

The rational design of mechanical metamaterials can be used to achieve new responses to external stimuli. Nonlinearities that occur upon deformation, such as self-contacts or instabilities, are intriguing because they enable mechanical metamaterials to switch stiffness or shape [5]. Inspired by nature, another response to mechanical loading is self-reporting. Similar to bleeding from a wound, materials can be designed to indicate damage by release of a liquid dye. This response can be achieved by a composite material with embedded microcapsules [6]. When the material is deformed, the capsules break and release their encapsulated dye, providing a visual indication of overload. However, the broken capsules result in reduced stiffness of the composite material. Consequently, establishing a connection between visually reported damage and the remaining mechanical properties is a challenge for applications. Mechanical metamaterials fabricated from a microcapsule composite can harness local stress concentrations upon deformation to deliberately rupture capsules. This can reveal predefined, self-reporting patterns or enable local stiffness changes. Finally, combining the unit cell's response with the base material's composition-driven response allows for novel, adaptive behavior. The geometry-driven response to deformation can be used to trigger a stiffness change in a respon-

sive base material. When connected in a closed-loop system, this approach has the potential to accumulate changes and enable trainable behavior.

This thesis focuses on three core approaches to engineered responses in mechanical metamaterials: *structural design* to harness a nonlinear mechanical response, *composition* to facilitate self-reporting, and the *combination of structural design and composition* to enable trainable behavior.

1.1 Engineered Materials

Traditionally, materials are used as rather passive structural building blocks in designs. Concrete is typically used to withstand compression in building foundations, while steel is often used to bear bending or tensile loads in trusses and beams [7]. These materials often have nearly constant properties in their operating conditions, and consequently, their functionality is often limited to providing structural integrity. However, by shaping the material deliberately, we can significantly extend its functionality and tailor its response to deformation: metal is already linear elastic, but by shaping it into a spring, we can make it more compliant and store energy, enabling applications in measurement devices or as vibration isolators.

When this concept of structural modification is applied at the micro- or macroscale, we can change a material's mechanical behavior significantly compared to its homogeneous counterpart. A polymer foam exhibiting unusual behavior when compared with the base material was reported by Lakes [8]. Upon compression, the foam contracted laterally, exhibiting a negative Poisson's ratio. The foam's microstructure can be described by its reentrant unit cell. By controlling the design of the unit cell, different responses upon mechanical loading can be engineered, like switching between stiffnesses [5] or expansion-contraction behaviors [9].

Besides structuring, responses to external triggers can also be engineered through the base material's intrinsic chemistry. These responsive materials can change their properties in response to external triggers. For example, such a material can change its stiffness in response to heat, magnetic fields, or light, thus enabling applications like shape morphing structures [10, 11]. This opens up new possibilities for engineering responses into materials, especially when combined with the deformation-driven responses of mechanical metamaterials.

1.2 Motivation

Mechanical metamaterials' responses to deformation have gained wide interest, from fundamental scientific research [12] to engineering applications [13]. Their rational design allows loading-dependent responses, which can yield improved properties in specific applications or even introduce novel functionalities. By functional integration of geometric design, material composition, and a combination of both, novel mechanical metamaterials can achieve more complex, adaptive responses. Such responses can range from nonlinear mechanical behavior to stiffness changes and loading history dependent adaptations. Mechanical metamaterials exhibiting such responses can contribute to more life-like material systems, capable of performing autonomously in their environment. However, realizing such responsive materials remains challenging. Prior to this thesis, Pishvar and Harne [14] identified several technical challenges in the field of autonomous engineered matter. These challenges included optimization and design, creating graded mechanical properties, integrating actuation, and manufacturing. The following three parts outline different strategies for overcoming these challenges.

The first part focuses on the shape of a metamaterial's unit cell and how its design can be tailored to achieve a nonlinear response at a predefined level of deformation. Mechanical metamaterials typically have a constant, predefined response to loading, such as rotation [4] or contraction [3] upon compression. Beyond these fixed responses, it has been shown that also discontinuous behaviors during loading can be designed [5, 15]. Here, the curvy beam metamaterial is intriguing, because because it exhibits self-contact during compression, that results in a switch from auxetic contraction to regular expansion. However, the explicit connection between the auxeticity switch and the geometry of the unit cell remains unclear. Establishing this geometry-driven response is essential to enable the application-specific design of such mechanical metamaterials.

The second part shifts to an engineered response based on the material's composition. Embedding stiff, liquid-filled microcapsules in a soft polymer matrix can significantly contribute to the composite's mechanical properties [16]. However, when the material is overloaded, the capsules rupture and no longer contribute to the material's mechanical properties, resulting in decreased stiffness. At the same time, the released liquid enables a fluorescent color change, self-reporting the local overloading [6, 17]. Consequently, when the matrix stays intact during the loading event, the fluorescence signal is intrinsically connected to a change in mechanical

properties. Therefore, to use these materials for mechanical metamaterial applications, it is crucial to understand the relationship between the self-reporting signal and the change in mechanical properties.

The third part covers the combination of the unit cell's geometry-driven response and the base material's composition-based response. A thermoplastic polymer modified for UV-crosslinking, as described by Liotier et al. [18], enables 3D printed specimens that can undergo stiffness changes upon irradiation. Hence, a mechanical metamaterial printed from this polymer can respond to UV irradiation. When compressed, the metamaterial's geometry-driven expansion can be utilized to close an electrical circuit and activate a UV light. Consequently, the mechanical metamaterial stiffens by UV irradiation in response to external loading. Thus, establishing this connection between the two responses has the potential to enhance soft robotics and other applications that benefit from adaptive, stimuli-responsive behavior.

1.3 Structure of the Thesis

The thesis is based on three consecutive peer reviewed journal articles that contribute to the field of mechanical metamaterials in terms of unit cell design, material composition, and a combination of both.

Chapter 2 lays the theoretical foundation in solid mechanics, mechanical metamaterials, and manufacturing techniques.

Chapter 3 includes the publications, each introduced by a personal assessment of the field and the contributions made to it.

Chapter 4 summarizes the work and gives an outlook.

Chapter 5 lists all scientific publications contributed to the field during the work on the thesis.

2 Theoretical Background

2.1 Mechanical Fundamentals

The engineered responses of mechanical metamaterials depend on how their unit cells deform under mechanical loading. The following section introduces the mechanical fundamentals of stress, strain, and their constitutive laws. Together, these concepts form the basis for the working principles of mechanical metamaterials.

2.1.1 Stress and Strain

When a body is subjected to external loading, internal stresses arise. At a given point on a cross-section of the body, these stresses are described by a normal stress σ, and shear stress τ (Figure 2.1A). The normal stress is perpendicular and shear stress is tangential to the cross-section. Independent of the cross-section's orientation, each point in the body is characterized by three normal stresses and six shear stresses, which together form the three-dimensional stress state (Figure 2.1B) [19].

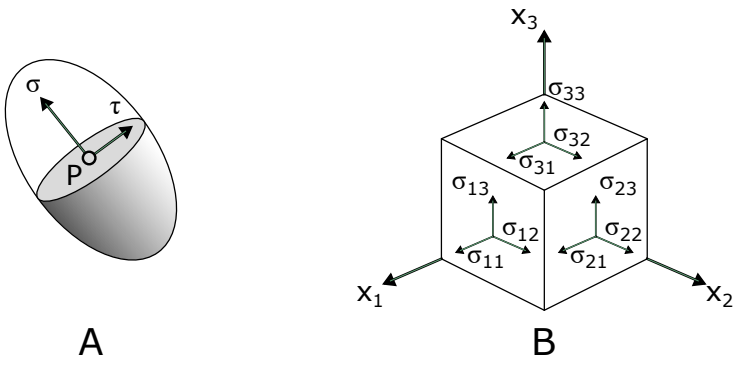


Figure 2.1: Stress state in a solid. A: Stress in point P in a cross-section of a solid, with normal stress σ and shear stress τ B: Stress tensor. Adapted from [19].

These stress components form the stress-tensor $\boldsymbol{\sigma}$, with the normal stresses on the diagonal and the shear stresses off-diagonal:

$$\boldsymbol{\sigma} = \begin{bmatrix} \sigma_{xx} & \tau_{xy} & \tau_{xz} \\ \tau_{yx} & \sigma_{yy} & \tau_{yz} \\ \tau_{zx} & \tau_{zy} & \sigma_{zz} \end{bmatrix} = \begin{bmatrix} \sigma_{11} & \sigma_{12} & \sigma_{13} \\ \sigma_{21} & \sigma_{22} & \sigma_{23} \\ \sigma_{31} & \sigma_{32} & \sigma_{33} \end{bmatrix} \tag{2.1}$$

The stress tensor $\boldsymbol{\sigma}$ is symmetric $\sigma_{ij} = \sigma_{ji}$, meaning it contains six independent components. During deformation, a displacement field describes the movement of the body's points. For small displacements, the strain tensor is approximated from the gradient of displacement u_i, as given in the following equation:

$$\varepsilon_{ij} = \frac{1}{2}(u_{i,j} + u_{j,i}) \tag{2.2}$$

Analogous to stresses, strains are consolidated in a tensor $\boldsymbol{\varepsilon}$:

$$\boldsymbol{\varepsilon} = \begin{bmatrix} \varepsilon_{11} & \varepsilon_{12} & \varepsilon_{13} \\ \varepsilon_{21} & \varepsilon_{22} & \varepsilon_{23} \\ \varepsilon_{31} & \varepsilon_{32} & \varepsilon_{33} \end{bmatrix} = \begin{bmatrix} \varepsilon_x & \frac{1}{2}\gamma_{xy} & \frac{1}{2}\gamma_{xz} \\ \frac{1}{2}\gamma_{yx} & \varepsilon_y & \frac{1}{2}\gamma_{yz} \\ \frac{1}{2}\gamma_{zx} & \frac{1}{2}\gamma_{zy} & \varepsilon_z \end{bmatrix} \tag{2.3}$$

Here, the diagonal elements represent the normal strains along the coordinate axes, and off-diagonal elements represent shear strains [19]. Constitutive laws then combine stress and strain to describe a material's response to mechanical loading.

2.1.2 Hooke's Law

In materials, stress and strain are connected properties, hence they need to be related by constitutive laws. For linear elastic materials, this relationship is provided by Hooke's law [20]:

$$\sigma_{ij} = C_{ijkl}\varepsilon_{kl} \tag{2.4}$$

Here, stress σ_{ij} and strain ε_{kl} are combined with the elasticity tensor C_{ijkl}, which contains the elastic constants. For isotropic materials, Hooke's law is written as [20]:

$$\begin{bmatrix} \varepsilon_{11} \\ \varepsilon_{22} \\ \varepsilon_{33} \\ 2\varepsilon_{12} \\ 2\varepsilon_{23} \\ 2\varepsilon_{31} \end{bmatrix} = \begin{bmatrix} \frac{1}{E} & -\frac{\nu}{E} & -\frac{\nu}{E} & 0 & 0 & 0 \\ & \frac{1}{E} & -\frac{\nu}{E} & 0 & 0 & 0 \\ & & \frac{1}{E} & 0 & 0 & 0 \\ & & & \frac{1}{G} & 0 & 0 \\ & & & & \frac{1}{G} & 0 \\ sym. & & & & & \frac{1}{G} \end{bmatrix} \begin{bmatrix} \sigma_{11} \\ \sigma_{22} \\ \sigma_{33} \\ \sigma_{12} \\ \sigma_{23} \\ \sigma_{31} \end{bmatrix} \tag{2.5}$$

Here, E is Young's modulus, and G is the shear modulus, which is defined by [20]:

$$G = \frac{E}{2(1+\nu)} \tag{2.6}$$

with Poisson's ratio ν, given by [21]:

$$\nu = -\frac{\varepsilon_x}{\varepsilon_y} \tag{2.7}$$

with transverse strain ε_x, orthogonal to the applied longitudinal strain ε_y, both are nominal strains in $\boldsymbol{\varepsilon}$ (Equation 2.3). Hooke's law is valid only in the linear elastic regime, which, for tensile loading of brittle materials, is until failure. While linear elastic deformation is reversible when the load is removed, ductile materials, such as metals and some polymers, exhibit plasticity above yield stress σ_y, which is permanent after unloading. In this nonlinear regime of the stress-strain curve, necking occurs in the specimen, which means that two types of stress can be determined: true stress σ_{true} references the specimen's current (necked) cross-section, or engineering stress σ_{eng}, which references the initial cross-section (Figure 2.2) [22].

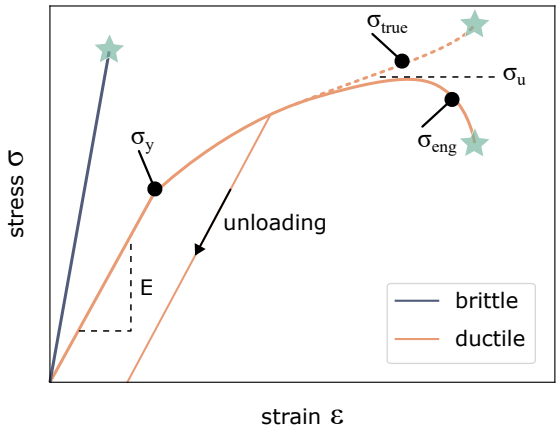


Figure 2.2: Schematic stress-strain curves of brittle and ductile materials up to failure (star). Brittle materials (blue curve) exhibit linear elastic behavior until failure. Ductile materials (orange curve) exhibit initially linear elastic stress-strain behavior, from which Young's modulus E can be determined. Above the yield stress σ_y, plastic deformation occurs, and the stress-strain relation becomes nonlinear, its maximum is ultimate strength σ_u. Plastic deformation is permanent, leaving the material deformed upon unloading (black arrow). Engineering stress σ_{eng} is calculated with respect to the initial cross-section, true stress σ_{true} is calculated with respect to the current (necked) cross-section. Adapted from [7, 22].

2.2 Mechanical Metamaterials

Materials play a central role in everyday life, from the concrete that supports the roofs above our heads, to the sheet metal that forms the aerodynamic exterior of cars. Material selection for a given application is primarily determined by intrinsic mechanical properties: concrete cast into the shape of a pillar yields a structure with high compressive strength, making it well suited for its intended use [7].

Mechanical metamaterials, comprised of the Greek word *meta*, meaning "beyond", and *mater*, the Latin word for "matter", exceed common associations we have with materials: their mechanical properties and embedded functionalities are defined by the material's periodic microstructure, rather than by chemical composition. The material's response to mechanical loading is governed by its smallest building block, the unit cell [23–25]. This geometry-driven behavior is in stark contrast to classical materials used in engineering, such as the aforementioned concrete or sheet metal. The following chapter gives an overview of achievable responses found in mechanical metamaterials.

2.2.1 Auxetic Metamaterials

Almgren [3] proposed a unit cell of rods connected by elastic hinges, periodically repeated to form a material with Poisson's ratio of -1 (Figure 2.3). This implies that Almgren's structure contracts laterally upon axial compression, a rather exotic behavior rarely found in engineering or biological materials. A three-dimensional version of Almgren's unit cell occurs in polymer foams and became known as the reentrant unit cell [8]. Metamaterials with negative Poisson's ratio, also called auxetics, show intriguing benefits in multiple applications. Auxetic materials have favorable acoustic [26, 27], bio-compatibility [28], and energy absorption [29] properties.

Auxetic behavior is not limited to reentrant unit cells. Auxetic characteristics can be found in various other unit cells, distinguished by their internal connectivity and deformation mechanisms. Similar to reentrant unit cells, double arrowhead structures employ straight beams connected by deformable hinges. By optimizing the hinge angles, Larsen et al. [30] tuned Poisson's ratio and implemented the structure in micromechanisms. Alderson et al. [31] modified the reentrant unit cell by replacing the elastic hinges with cylinders in their so-called cylinder-ligament honeycombs. This allowed for an angle-dependent Poisson's ratio, with additional flexion of the connecting filaments. Körner and Liebold-Ribeiro [32] showed that

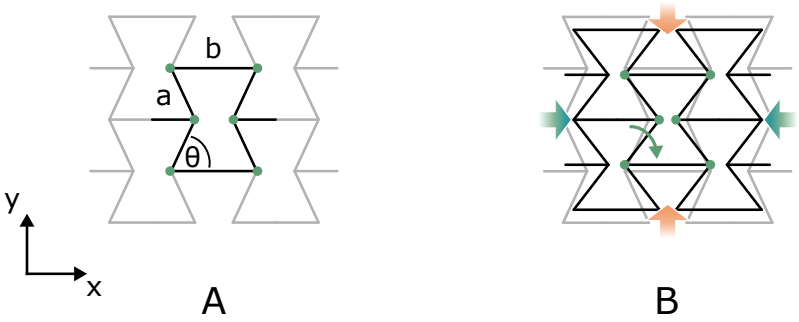
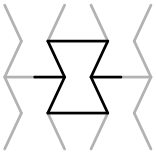
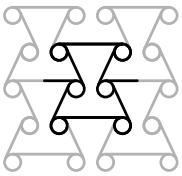
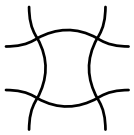
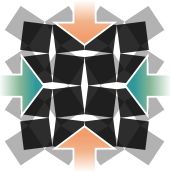
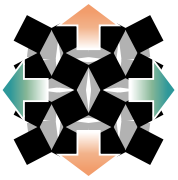
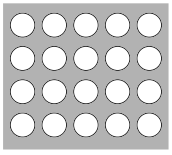
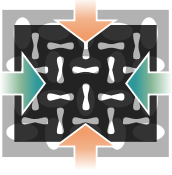


Figure 2.3: Working principle of the reentrant auxetic, as described by Almgren [3]. A: The unit cell (black) consists of beams (length a and b, with angle θ) and elastic hinges (green), which are periodically patterned (grey). B: Negative Poisson's ratio: Upon vertical compression (orange arrows), the reentrant contracts laterally (green arrows), facilitated by rotation about the nodes (bent green arrow).

eigenfrequency analysis of a quadratic lattice also leads to new auxetic unit cell designs. This method can also be extended to other 2D base structures, such as hexagonal or triangular lattices.

However, not all auxetic unit cells rely on deformable beam connections. Rotating squares achieve auxeticity by rigid body rotation at connecting nodes, eliminating deformation of the elements [33, 34]. Similarly, sheets with alternating vertical and horizontal cuts can show analogous auxetic characteristics, closely resembling the geometry of rotating squares [35]. In a similar approach, Grima et al. [36] have shown varying auxetic responses for randomized cuts in sheets. Auxeticity can also emerge from elastic instabilities, as shown by Bertoldi et al. [9]. Here, an intriguing characteristic of a block with a grid pattern of holes appears upon compression: the holes collapse into horizontal and vertical elliptical shapes. The resulting structure closely resembles that of the rotating squares, exhibiting significant lateral contraction. A representative selection of auxetic unit cells is summarized in Table 2.1.

Table 2.1: Overview of selected auxetic metamaterials with their mechanical response (green arrows) when subjected to vertical loading (orange arrows).

	Unit cell	Mechanical response	Geometric features	Citation
Reentrant			Beams + elastic hinges	[3]
Double arrowhead			Beams + elastic hinges	[30]
Reentrant chiral			Beams + circle connections	[31]
Sinusoidal			Curved beams + elastic hinges	[32]
Rotating squares			Rigid squares + elastic hinges	[33, 34]
Cuts			Slit perforations	[35, 37]
Instability			Circular voids collapse	[9]

2.2.2 Metamaterials with Other Mechanical Responses

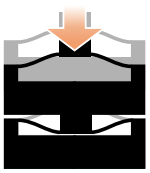
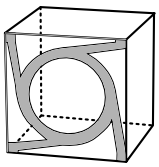
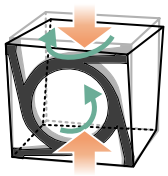
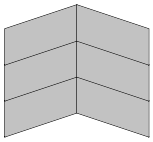
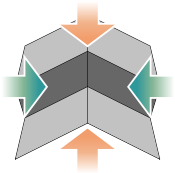
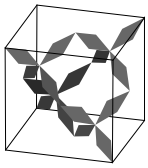
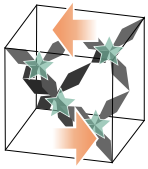
Beyond negative Poisson's ratio, rational unit cell design enables a broad spectrum of achievable characteristics. By assembling a metamaterial from unit cells of different Poisson's ratios, more complex shape changes are possible: expanding and contracting parts can be combined, leading to a different shape under load. Depending on the unit cell's design, the overall shape change during loading can be smooth [38] or discrete at predefined deformation thresholds [5]. Such discrete responses effectively embed mechanical logic because the shape change of the unit cells is tied to an "if-condition" of applied deformation.

Bistable unit cell designs further extend this concept. Che et al. [39] utilized bistable beams in a metamaterial's unit cell by specifically tuning the snapping sequence of a unit cell series. This yields a multistable metamaterial: specific regions of the metamaterial collapse upon predefined levels of loading. Due to the bistable characteristic, the deformed shape of the metamaterial is conserved upon unloading. Moreover, during loading, the bistable snap of the unit cell is accompanied by negative stiffness. Designing unit cells with a three-dimensional response opens new possibilities: Frenzel et al. [4] designed a chiral unit cell capable of a twist degree of freedom. Upon compression, rings on the sides of the unit cell start rotating, eventually twisting the unit cell about its central axis.

Origami-based metamaterials build on the concept of rational unit cell design. Their mechanical behavior is tuned by deliberate folding of planar sheets. Depending on the folding angle, Poisson's ratio can be deliberately tuned to fulfill desired mechanical characteristics [40, 41]. Origami metamaterials and the previously discussed unit cells rely on bending or elastic hinges, which leads to a comparatively low bulk modulus.

Contrasting the low bulk modulus of origami metamaterials, pentamode metamaterials exhibit an extremely low shear modulus while maintaining high compressive stiffness [42]. In pentamodes, the rods forming the unit cell only have minimal points of contact, rather than elastic hinges (as in the reentrant auxetic). These point-like connections can withstand compression; however, they shear off easily, giving the resulting metamaterial its low shear modulus [43–45]. Representative non-auxetic metamaterials are summarized in Table 2.2.

Table 2.2: Overview of selected metamaterials with their mechanical response (green arrows) when subjected to vertical loading (orange arrows).

	Unit cell	Mechanical response	Citation
Logic		 Preprogrammed shape change	[5]
Bistable beams		 Negative stiffness	[39]
Chiral		 Rotation	[4]
Origami		 Contraction, rotation	[40, 41]
Pentamode		 Minimal shear modulus	[42, 43]

2.3 Fabrication of Advanced Materials and Metamaterials

The reentrant metamaterial (Figure 2.3) can be easily assembled from rods and flexible connectors. In contrast, more complex geometries, like the 3D chiral unit cell designed by Frenzel et al. [4] (Table 2.2) demand more advanced manufacturing approaches to translate theoretical design into working physical representations. While 2D unit cells can be manufactured by molding or subtractive methods, such as milling or laser cutting, the fabrication of complex 3D unit cells typically requires

additive manufacturing techniques. The following chapter elaborates on manufacturing techniques applicable to advanced materials and mechanical metamaterials.

2.3.1 Molding Based Manufacturing

Polymers offer a broad spectrum of manufacturing techniques. For thermoplastics, their malleability above glass transition temperature makes thermoforming possible, while, at higher temperatures, they become liquid and can therefore be extruded or injection molded into complex shapes [46]. In contrast, thermosetting elastomers like Poly(dimethylsiloxane) (PDMS) do not show a temperature dependent phase change and can only be molded before they are cured. PDMS is typically prepared by mixing a silicone elastomer with an initiator. The mixture's relatively slow crosslinking reaction provides sufficient working time for degassing and pouring it into molds of desired shape [47] (Figure 2.4). This molding process is capable of achieving the high accuracy required to even resolve microstructures [48] and is particularly suitable for fabricating 2D mechanical metamaterials. Their functionality can even be enriched by combining two phases with different stiffnesses of PDMS, as shown by Li et al. [49].

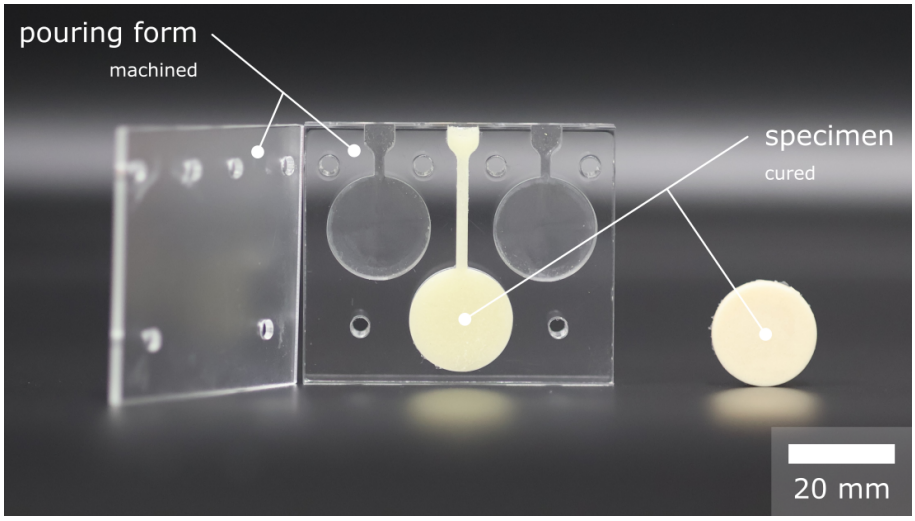


Figure 2.4: Acrylic two-piece mold, lid opened and the central specimen cavity filled with silicone. Post-processed specimen to the right of the pouring form.

Mechanical metamaterials get their properties from their unit cell's geometry, as described in Section 2.2. However, properties also arise from composition, like high tensile strength of a carbon fiber and large deformation before failure of an elas-

tomer. To further enhance properties, composites have been established, such as carbon fiber reinforced plastics (CFRP). By embedding high-strength carbon fibers in a polymer matrix, CFRPs exhibit improved stiffness at low weight [7]. Beyond fibrous reinforcements, spherical inclusions can also improve a composite's mechanical properties [50, 51], typically by a homogeneous dispersion of the filler within the matrix material. Going beyond the sole mechanical benefits of spherical inclusions, filled microcapsules introduce new functionalities. Capsule composites utilize liquid filled inclusions to enable, for example, self-healing [52, 53] or self-reporting [6]. Their fabrication introduces unique challenges: producing stable capsules that enclose the liquids, homogeneously dispersing them in the matrix, and subsequently shaping the composite into its final form.

The first step in capsule composite manufacturing is capsule synthesis. Robb et al. [6] established a process for producing self-reporting microcapsule composites containing 1,1,2,2-tetraphenylethylene (TPE) as a luminogen. TPE exhibits aggregation-induced emission (AIE): it is non-emissive when dissolved in hexyl acetate but fluoresces bright blue under UV irradiation once the solvent evaporates and TPE aggregates. The encapsulation process is described by Caruso et al. [54] for poly(urea formaldehyde) (PUF). In this process, a prepolymer is introduced in the core-liquid and stirred into an emulsion. Under constant agitation, polymerization forms a shell, which encloses the solvent-luminogen mixture. The capsule size is primarily determined by the stir rate [54], and the capsules are subsequently recovered by filtration, drying, and sieving. While emulsion-based techniques are scalable and well established, they often result in broad size distributions. To achieve tighter control of capsule parameters, alternative fabrication methods employ microfluidic devices, which allow precise tuning of capsule radius and shell thickness [55].

Once fabricated, the microcapsules can be incorporated into a matrix material. Robb et al. [6] demonstrated their successful incorporation into the polymer matrix of CFRPs, while other studies have included them into adhesives to enable debonding-on-demand through a triggered release of solvents [56]. In all cases, the capsules must be distributed throughout the matrix material before it solidifies. As described above, crosslinked polymers like PDMS offer a processing window for pouring before the silicone-initiator mix sets. Poured into two-piece molds, often machined from acrylic, a wide range of geometries can be manufactured. However, molding is inherently restricted to parts without complex internal structures, especially when compared to additive manufacturing methods.

2.3.2 Additive Manufacturing: Fused Filament Fabrication

In 1981, Kodama introduced a process of manufacturing three-dimensional polymer objects by using a layer-by-layer approach, in which a photosensitive polymer is selectively hardened by a light source [57]. This enabled the manufacturing of previously unattainable geometries, such as enclosed internal structures. The process later became known as stereolithography (SLA), developed and commercialized by Charles Hull [58]. SLA marked the beginning of additive manufacturing (AM) and sparked the development of numerous other processes. Today, one of the most common processes is fused filament fabrication (FFF).

Originally developed and patented by Stratasys under the trademark fused deposition modeling (FDM), FFF is based on the extrusion of a thermoplastic polymer in successive layers [59, 60]. The workflow begins by modeling a 3D part in computer aided design (CAD) software, which is then exported in a tessellated stereolithography (STL) format. A slicing program cuts the STL file into a sequence of 2D cross-sections (slices) and generates the machine instructions in g-code format. During printing, a polymer filament is pushed into a heated extrusion head (hotend) by a gear-driven feed mechanism. Inside the hotend, the polymer is melted and forced through the nozzle, which deposits the material onto the build plate along the instructed toolpath. The extruded polymer solidifies upon deposition, forming each layer. By repeating the process, the 3D part is built in a layer-by-layer fashion [58, 60] (Figure 2.5). The fidelity and mechanical properties of a printed part result from the interplay of multiple process parameters [61]. Among those parameters, we see line width, layer thickness, and print speed [62]. Additional parameters include air gap, build orientation, and extrusion temperature [61].

In addition to appropriately chosen process parameters, effective design for additive manufacturing is important for achieving high-quality results. Medellin-Castillo and Zaragoza-Siqueiros [63] outline key strategies for FFF, one of which is the consideration of geometric constraints. The layered process does not allow for printing large overhangs. Because each new layer must be attached to the previous one, support structures are necessary to bridge the gaps introduced by overhangs. Furthermore, the smallest resolvable features are limited by layer thickness and nozzle diameter. Build orientation should be optimized during the design process to ensure high accuracy, good surface finish, and sufficient mechanical properties. Path planning, both for external and internal extrusion trajectories, significantly influences the part's final properties, such as bending stiffness and mass distribution. Finally,

part dimensions are restricted by the machine's build volume [63]. In addition to these design guidelines, standards have been established to support both the design [64] and qualification [65] of additively manufactured parts.

FFF manufacturing is predominantly used with thermoplastic polymers that exhibit suitable melt viscosities for extrusion while still maintaining structural integrity after deposition. Typical polymers include polycarbonate (PC), acrylonitrile butadiene styrene (ABS), polylactic acid (PLA), and Nylon [66]. Water-soluble polymers like polyvinyl alcohol (PVA) are used to create (internal) support structures, which can be dissolved post printing [67]. To overcome the limitations of homogeneous polymers, composite filaments have been developed to enhance functionalities and physical properties. These can include copper or aluminium oxide particles to improve the thermal conductivity or frictional coefficient [66]. To improve part stiffness, carbon fibers can be introduced [58, 68]. Particularly relevant for mechanical metamaterial manufacturing, thermoplastic polyurethane (TPU) enables the fabrication of flexible architectures [69]. Additionally, functionalization is also possible through conductive parts and fillers, enabling mechanical metamaterials with integrated sensing capabilities and embedded logic [70, 71].

While the aforementioned material palette for FFF enables a wide range of structures, the process remains restricted to mostly thermoplastic polymers. Other inherent drawbacks include visible layer lines, which affect the surface finish [58], and orthotropic mechanical properties [63]. The mechanical properties are further impaired by potentially suboptimal process parameters [61], leading to significant warping or distortion [63]. Even under ideal conditions, FFF is generally slower than traditional manufacturing techniques, such as injection molding, employed for thermoplastic polymers.

Nevertheless, the aforementioned restrictions can be acceptable or even advantageous, depending on the intended application. Certain geometries, such as the chiral mechanical metamaterial designed by Frenzel et al. [4], could not be manufactured using traditional manufacturing techniques due to complex, enclosed voids. Also, exploring these complex designs is possible because FFF allows for rapid iterations, since no additional tooling is required. FFF's high degree of flexibility supports the production of highly customized products [63] and on-demand manufacturing of spare parts, reducing storage costs and down time [58]. These advantages have driven the widespread adoption of FFF, not only for prototyping, but extending into engineering applications and scientific research.

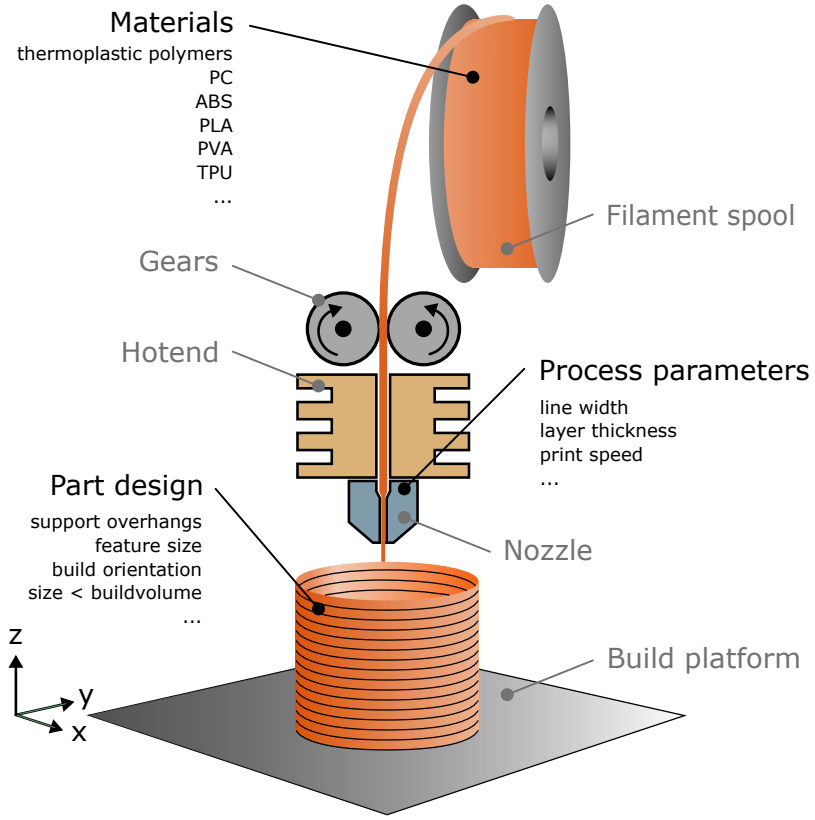


Figure 2.5: Working principle of fused filament fabrication (FFF), highlighting considerations for material choice, process parameters and part design. Components are indicated in grey.

2.3.3 Post-Processing and Functionalization

Post-processing requirements depend on the chosen manufacturing technique and directly influence the final geometry, surface quality, and mechanical performance of the part. For FFF manufactured parts, mechanical post-processing is often necessary to achieve the desired surface finish or dimensional accuracy. Typical steps include the removal of support structures and sanding [72]. Similarly, injection molded parts require removal of the sprue and runner geometries used to fill the mold. Additional operations, such as deburring [73], polishing [74], or machining [75] are deployed to refine accuracy or finish. These mechanical methods can be supplemented by chemical treatments, such as polymer coatings or acetone vapor smoothing, which can further enhance surface quality [72].

In addition to mechanical and chemical treatments, physical processes are commonly used for post-processing. Annealing semi-crystalline polymers such as PLA increases crystallinity, resulting in improved tensile strength [76], and can positively impact shrinkage or warping [77]. For composite filaments used in FFF containing high fractions of metal powder, post-processing involves multiple steps: after printing, the polymer binder is removed, and the part is then sintered at temperatures above 1300 °C to achieve a metal part with a density exceeding 90% [78]. Additive processes involving photopolymers also require post-processing. After support removal, parts must be washed, and finally UV cured [72]. UV curing increases the crosslink density on the part's surface, thereby increasing the mechanical properties, while elevated curing temperatures improve surface smoothness. However, the sequence of operations is important: subtractive machining should be performed prior to curing, as machinability is reduced once the part is fully crosslinked [79].

Beyond mechanical and surface improvements, post-processing can also involve functionalization of parts. By exploiting distinct material properties in multimaterial parts, final functionality might only be achieved after a final processing step. Chi et al. [80] combined thermosets and thermoplastics in a multimaterial print. Only after melting the transparent thermoplastic in the thermoset frame, an array of lenses was formed as a result of the thermoplastic's viscous flow at elevated temperatures. In a different approach of adding functionality post manufacturing, thermoplastic polymers and post-processing by UV curing can be combined. C,H insertion chemistry allows functionalization of thermoplastic polymers, facilitating controlled crosslinking upon UV exposure [18]. This strategy allows tailoring of mechanical properties even after the part has been additively manufactured.

3 Mechanical Metamaterials with Engineered Responses

Engineering responses into devices on a material level has great potential: functional integration can enable embedded logic [5], but also structural health monitoring [81], or life-like adaptive behavior [10]. Such functionalities can be integrated into mechanical metamaterials, which is why they have attracted attention in fundamental [82] and applied research, such as for biomedical devices [83]. Because they derive their behavior from geometric design, they are capable of responding directly to deformation, hence their application can involve mechanical triggering, such as the deployment of auxetic stents [28]. This geometry-driven behavior holds the potential of being enriched by a responsive base material. Such base materials can be composites, which achieve property improvements or embedded functionality by the combination of at least two components [84, 85]. However, engineering mechanical metamaterials beyond a single, predefined response poses multiple challenges, from designing the unit cell to integrating a material response and the combination of both.

The first work (Section 3.1) focused on the systematic assessment of a sinusoidal mechanical metamaterial (see Table 2.1) that exhibits a nonlinear response to compression. While the switch between negative and positive Poisson's ratio during compression is known [86], the explicit connection between the switching behavior and the unit cell's design parameters had not been established. Consequently, a parametrized unit cell model was developed, and its mechanical response was analyzed by simulations and experimental validation. The resulting framework can be used to obtain a unit cell geometry tailored to a specific response. Finally, a discrete scales device showed the applicability of the approach.

The second work (Section 3.2) shifted from a homogeneous material to a microcapsule composite capable of self-reporting mechanical damage. Although UV fluorescence due to aggregation-induced emission (AIE) upon capsule rupture is well

described, previous works lacked the quantitative link between self-reporting and mechanical properties [6, 17]. This work closed this gap for a soft silicone matrix with embedded, liquid-filled microcapsules. During tensile testing, the composite was able to self-report while the matrix material stayed intact. Tracking over time revealed the linear correlation between applied load, stiffness reduction, and fluorescence intensity for any point in time. Knowing the transient changes of this relation over time allows one to accurately connect the material's remaining stiffness and visual signal after loading. The results provide a foundation for employing microcapsule composites as responsive base materials for mechanical metamaterials.

The third work (Section 3.3) combined the approaches of engineered responses on a geometrical (metamaterial) and composition (base material) level to realize a trainable material system. Although combinations of metamaterial geometries with responsive base materials have been demonstrated [87], they lack a closed-loop coupling of both responses. To overcome this, we combined the response to deformation of a mechanical metamaterial with C,H insertion chemistry, enabling UV induced stiffness changes in a single system. After characterizing the modified, 3D printable TPU under UV irradiation, several demonstrations were realized. Local stiffening in an instability driven mechanical metamaterial was followed by a closed-loop trainable system. Here, the metamaterial's expansion under compression triggered a UV light, which led to permanent shape and stiffness changes. Finally, threshold training was demonstrated, in which the system was trained to resist a force after repeated, planned loading cycles.

Together, the following sections form the core of this dissertation, highlighting the contributions made to *mechanical metamaterials with engineered responses* from geometric design, to base material functionality, to coupling of both design principles. This aims to advance the field towards stimuli-responsive material systems capable of exhibiting life-like behavior.

3.1 Exploiting Self-Contact in Mechanical Metamaterials for New Discrete Functionalities

Authors: David Schwarz, Gerrit Felsch, Falk Tauber, Stefan Schiller, Viacheslav Slesarenko
Journal: Materials & Design
Date: 13.11.2023
DOI: https://doi.org/10.1016/j.matdes.2023.112468

Author	Contributions
David Schwarz	Conceptualization, data curation, formal analysis, investigation, methodology, visualization, writing – original draft
Gerrit Felsch	Methodology, validation
Falk Tauber	Conceptualization
Stefan Schiller	Conceptualization
Viacheslav Slesarenko	Conceptualization, funding acquisition, project administration, supervision, writing – original draft, writing – review & editing

The article is open access under the CC BY license (http://creativecommons.org/licenses/by/4.0/) and reprinted without changes.

Context and Personal Assessment

We typically expect responses upon interaction from devices, like door handles or push buttons, rather than from homogeneous blocks of material. However, mechanical metamaterials exhibit responsiveness intrinsically by the design of their unit cell [23]. As described in Section 2.2, various unit cells have demonstrated auxetic behavior [8, 9], rotation [4], or bistability [39]. Their mechanical response can be tuned by the unit cell's geometry. For example, different Poisson's ratios can be realized by systematic alterations of geometric features [88].

Altering geometric features can enable a switch of auxeticity, as shown in thermo-responsive hydrogels [87]. In contrast to this swelling-driven response, an instant, purely geometric switch of properties during mechanical loading can be achieved by metastable [89] or self-contacting [5, 90] features of the unit cell. Such geometric responses have enabled metamaterial-based devices capable of mechanical computing [91] or triggering preprogrammed shape changes upon mechanical loading [5, 92].

The ability to harness self-contact to switch a metamaterial's behavior is attractive because it enables discrete functionalities, like "if-then" responses, while also allowing for the careful design of the switching behavior. Sinusoidal lattice designs [32, 88] are especially well-suited because their curvy beam connections allow fine tuning of the onset of self-contact. While it is known that excessive compression of some auxetics can lead to lateral expansion [86], the unit cell's nonlinear response to deformation is more complex. Especially, the onset of expansion and its exploitation for a device remain largely unexplored. This forms a core motivation behind this work, also because such an approach can potentially be applied to other mechanical metamaterials, hence facilitating a more widespread application of them.

In the presented work, I exploit the self-contacting metamaterial based on a sinusoidal unit cell regarding its contraction-expansion behavior during compression, indicated by a change of Poisson's ratio. Because Poisson's ratio originates from the unit cell's geometry, it can not only take a wide range of initial values, but can also change during deformation. Engineering and instantaneous Poisson's ratio ν_{eng} and ν_{inst} capture the unit cell's nonlinear behavior: ν_{inst} switches from negative to positive at the onset of self-contact and ν_{eng} switches at expansion past initial width. By means of FEM simulations, I show that these switching points depend on the unit cell's geometry parameters, hence they can be finely tuned. This is further backed by good agreement with experiments ($R^2 > 0.9$), which indicates that the geometry robustly dictates the switch of auxeticity.

The metamaterial's unit cell can be designed to undergo lateral contraction first, switch auxeticity, and, finally, expand past its initial width during compression. By simultaneously deforming specimens of different switching points, their expansion occurs in a predefined sequence, which I exploit to close electrical circuits in the presented work. This sequence can be adjusted by the unit cell's geometry parameters and highlights a potential use case of the metamaterial: a discrete sensing element. This is especially interesting because the switching behavior is embedded into the unit cell's load-bearing core, which means reduced complexity due to functional integration. Furthermore, the presented approach of parametrically mapping and exploiting self-contact offers a versatile pathway that can be applied to other classes of mechanical metamaterials.

The presented approach is not only easily replicable, but also discloses an important aspect of metamaterial design: within a continuous parameter space, the resulting unit cell properties can vary drastically. During compression, most unit cells exhibit an auxetic contraction, followed by expansion after self-contact, while others do not switch their auxeticity beyond self-contact. This contrasts previous studies, which often introduced their unit cells only within the narrow parameter space where the expected behavior occurs [4, 31]. The presented systematic exploration shows that subtle geometric changes can either fine-tune or fundamentally alter the metamaterial's mechanical response. Furthermore, the direct implementation of the metamaterial as discrete sensing elements underscores its practical relevance. Since its publication, the characteristics of the presented unit cell have gained further interest in the field of mechanical metamaterials [93] and soft robotics [94]. In essence, this work establishes a replicable approach for designing self-contact-based nonlinearities into the response to deformation of mechanical metamaterials.

Materials & Design 236 (2023) 112468

Contents lists available at ScienceDirect

Materials & Design

journal homepage: www.elsevier.com/locate/matdes

Exploiting self-contact in mechanical metamaterials for new discrete functionalities

David Schwarz [a], Gerrit Felsch [a], Falk Tauber [a,b], Stefan Schiller [c], Viacheslav Slesarenko [a,*]

[a] Cluster of Excellence livMatS @ FIT – Freiburg Center for Interactive Materials and Bioinspired Technologies, Georges-Köhler-Allee 105, D-79110, Freiburg, Germany
[b] Plant Biomechanics Group (PBG) Freiburg @ Botanic Garden of the University of Freiburg, Freiburg, Germany
[c] Institute for Pharmaceutical Technology, Goethe University Frankfurt, Max-von-Laue-Str. 9, D-60438, Frankfurt, Germany

ARTICLE INFO

Keywords:
Metamaterials
Self-contact
Load-function systems
Logic
Tunability
Functionality

ABSTRACT

The rational geometric and topological organization of mechanical metamaterials allows for unconventional responses to external loads. These materials exhibit a coupling between deformation in orthogonal directions governed by Poisson's ratio, which, in turn, can be precisely adjusted through the deliberate selection of specific geometrical parameters within the metamaterial's structure. Although certain structural motifs may even enable a negative Poisson's ratio, it is conventionally assumed to remain constant or near-constant during deformation. In this study, we introduce a novel design concept that enables metamaterials to switch the sign of Poisson's ratio during loading, specifically at predetermined compressive strain levels, by harnessing self-contact between individual elements of the metamaterial. Through the integration of finite element simulations and experimental testing, we establish a direct correlation between the geometrical parameters of the unit cell and the mechanical response of the metamaterial. This correlation enables us to engineer samples with desired functionality and we present a discrete scales demonstrator that exploits this switchable behavior.

1. Introduction

The rational internal organization of mechanical metamaterials enables them to exhibit unconventional responses when subjected to mechanical loading. One of the most well-known manifestations of such unusual behavior can be observed in so-called auxetic materials [1]. Unlike conventional materials, which undergo lateral expansion when subjected to uniaxial compression, auxetic metamaterials exhibit simultaneous contraction in all directions, effectively exhibiting a negative Poisson's ratio [2]. Auxetic materials have garnered considerable attention as novel solutions for impact [3,4] or blast protection [5], sports equipment such as helmets [6] or shoes [7] and wearable electronics [8]. In biomedical applications, auxetic materials find utility in various areas [9], including coronary stents [10–12], bio-compatible porous implants [13–15], and scaffolds for tissue engineering [16–18]. The underlying internal organization responsible for the auxetic behavior has been replicated across multiple length scales, ranging from materials with nanoscale features [19,20], to materials with microscale dimensions [21], millimeter-sized features [22], and even structures spanning meters in one or two dimensions [23].

The global mechanical response of mechanical metamaterials is intrinsically linked to their internal periodic structure. Consequently, researchers primarily focus their attention on the design of the smallest building block - the unit cell [24]. Among auxetic metamaterials, one might distinguish several most common design motifs [1], such as honeycomb/reentrant cells [25,26], chiral patterns [27,28], and rotating rigid structures [29,30]. The reentrant unit cell, for example, consists of interconnected straight beams that fold inward upon compression, resulting in a negative Poisson's ratio. In this case, the Poisson's ratio value directly correlates with the geometrical characteristics of the unit cell, such as the length of the struts and the angle between them. The enduring popularity of the classical reentrant design stems from the clear deformation mechanism behind its negative Poisson's ratio [31]. Alternatively, for "intuitive" design, more direct methods can be employed in the search for new unit cells. For instance, Körner et al. [32] used eigenmode analysis to describe a family of lattices containing non-straight elements with auxetic behavior. Notably, a chiral lattice with sinusoidal curvy beam connections, as depicted in Fig. 1A, can exhibit auxetic behavior depending on the unit cell's geometry. Taking this concept further, Clausen et al. [33] utilized topology optimization to tune the Poisson's ratio of the lattice under tensile load, achieving

* Corresponding author.
E-mail address: viacheslav.slesarenko@livmats.uni-freiburg.de (V. Slesarenko).

https://doi.org/10.1016/j.matdes.2023.112468
Received 13 September 2023; Received in revised form 31 October 2023; Accepted 6 November 2023
Available online 13 November 2023
0264-1275/© 2023 The Author(s). Published by Elsevier Ltd. This is an open access article under the CC BY license (http://creativecommons.org/licenses/by/4.0/).

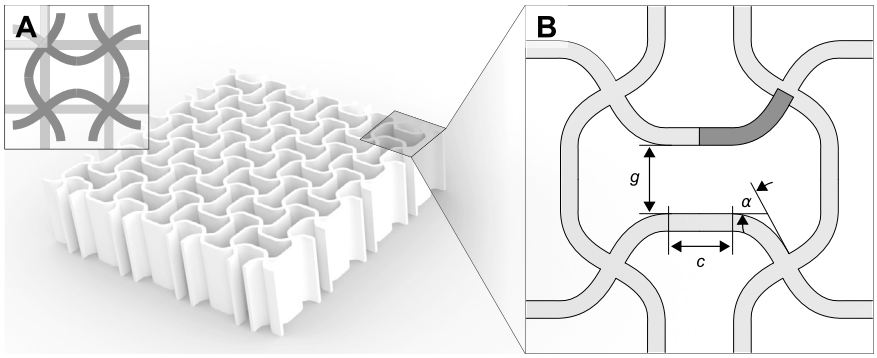


Fig. 1. Design of the unit cell and the resulting metamaterial. A: Base design is derived from a quadratic lattice (light grey), which is distorted to a sinusoidal lattice (dark grey) as described in [32]. B: Geometrical parameters g, and c defining the geometry of the unit cell.

values ranging from -0.8 to 0.8. It is worth noting that curved geometries have recently gained prominence for enriching the design space and expanding the range of admissible properties in mechanical metamaterials [34–36].

It has been observed that contact between the elements of metamaterials can occur under sufficiently large compressive strain [37]. Consequently, the response of the metamaterial suddenly becomes much stiffer as compared with the initial stage of compression [38]. Therefore, depending on the applied deformation, such a lattice may exhibit two distinctly different behaviors, effectively switching between them. In general, the ability to control the behavior of metamaterials by manipulating their internal architecture after fabrication is highly desirable. To achieve this, both mechanical and non-mechanical external stimuli can be harnessed. For instance, non-mechanical control through temperature changes has shown the potential to alter the Poisson's ratio of metamaterials containing active materials such as hydrogels [39], shape memory polymers [40], or liquid crystal elastomers [41]. The employment of magnetic interaction between the metamaterial's components enables another avenue for tuning their behavior [42–44]. Additionally, more exotic next-generation smart materials, capable of adapting and learning [45–47], might enable the attainment of more intelligent control over architectural changes in metamaterials, thus expanding their application scope. For already reported metamaterials, control via mechanical stimuli relies on intricate coupling between various loading sequences [48], instability-driven transformations [49,50], or self-contact between elements [51]. The latter approach relies solely on the internal geometry and, due to its relative simplicity, can open new avenues for introducing novel functionalities in metamaterials that emerge from changes in behavior during deformation. For example, the implementation of contact between unit cells has enabled the realization of 'if-then-else' functionality [52]. Similarly, alternating Poisson's ratios under load have been achieved through sequentially activated self-contacts [53] or sliding and locking mechanisms [54]. Helou et al. [55] utilized self-contact in a classical rotating-square design to embed electrical circuits that can close upon self-contact, demonstrating basic computational capabilities stemming from the rational architecture of metamaterials. These mechanisms for smart property switching are part of the emerging field of mechanical computing [56].

Self-contact presents a unique opportunity to facilitate functionalities based on discrete states and to achieve transitions resulting from abrupt changes in mechanical responses. In this context, the previously mentioned sinusoidal lattice [33,34,37] exhibits intriguing properties: when subjected to compression, we observe alterations in lattice connectivity due to self-contact, which can be harnessed to influence the resulting Poisson's ratio. In this study, we systematically evaluate the contact-induced changes in mechanical response concerning the unit cell's geometry. Furthermore, we apply these metamaterials in the design of scales-like devices, capitalizing on the anticipated auxeticity switches.

2. Unit cell and design space

2.1. Shape definition

Fig. 1 presents the mechanical metamaterial based on curvy connections. For parameterized scripting of the unit cell, we utilized the Grasshopper module of Rhino 7 (Robert McNeel & Associates, Seattle, USA). The unit cell of the metamaterial under consideration is uniquely defined by the shape of a single beam. By employing circular patterning around its bent end, followed by horizontal and vertical mirroring, we derived the unit cell depicted in Fig. 1B. We achieved a diverse range of unit cell geometries by manipulating two key geometric parameters: gap size (g) and contact length (c). It is worth noting that the angle α, as shown in Fig. 1B, is exclusively determined by g and c, both expressed as percentages of the unit cell's width/height. Additionally, we maintained a consistent beam cross-section by setting the curvy beams' widths to 5% of the unit cell's size.

2.2. Shape changes

We demonstrate the parameter space of the considered designs (Fig. 2), alongside two examples of the "most extreme" unit cells. This two-dimensional design space was probed in 15 equidistant steps per parameter. The range of values for contact length (c) spanned from 1% to 50% of the unit cell size, while gap sizes (g) ranged from 1% to 15%. The boundaries for the gap size were established to prevent initial contact at minimum value and ensure gap closure at a reasonable compression level when set to $g = 15\%$. This approach effectively captures the influence of gap size g and contact length c on the angle α and ensures the overall continuity of the parameter space, as depicted in Fig. 2.

3. Simulations for characterization

3.1. Simulation setup

With sufficient coverage of the parameter space, we conducted a detailed investigation into the mechanical behavior of selected metamaterials under compression using finite element (FE) analysis. This analysis was performed using COMSOL Multiphysics 6.0 (Comsol AB, Stockholm, Sweden), with a specific focus on studying the changes in properties induced by self-contact. Prior to importing the 2D representations of the unit cells, we applied a 25% shift in both the vertical and horizontal directions. This adjustment was made to ensure more reliable meshing and simplify the imposition of periodic boundary conditions. Additionally, we filleted sharp corners to prevent singularities during simulations. Each geometry was meshed with a minimum of five second-order quad elements spanning the width of the curvy beam structures.

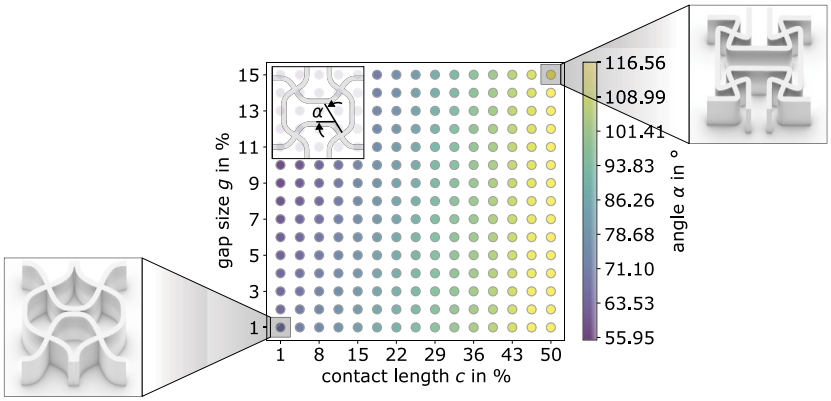


Fig. 2. Parameter space (g and c) coverage with angle α shown in color. Two extreme examples of the unit cells are shown in the corners.

We selected an incompressible neo-Hookean material model, with a Lamé parameter (μ) set to 2.93 MPa, to closely match the properties of the 3D-printable NinjaFlex thermoplastic polyurethane (TPU) filament, as reported in [57]. Furthermore, in Section 4, we employed experimental testing to assess the adequacy of this material model. To accurately capture the mechanical response of the unit cell, including self-contact, we incorporated geometric non-linearity and allowed contact between all boundaries. The application of strain and periodicity to the lattice was facilitated by a set of periodic boundary conditions.

$$v(T) - v(B) = -\varepsilon_y \cdot l_0 \tag{1}$$

$$u(T) - u(B) = 0 \tag{2}$$

$$v(L) - v(R) = 0 \tag{3}$$

$$u(L) - u(R) = u(p_1) - u(p_2), \tag{4}$$

with T, B, L and R being the top, bottom, left and right boundaries, respectively, and l_0 being the initial height of the unit cell. Here v and u are displacements in x and y direction. Note that further we assume that the height and width of the unit cell to be equal to 1 initially. In the boundary condition (1), we apply a compression strain ε_y. The maximum applied strain was set to $3.5g$ or 25% of the initial height, whichever was lower (see Fig. 3). This limit was chosen to ensure the convergence of the simulation by preventing extremely large deformations after self-contact was reached. By analyzing the evolution of the coordinates of two corner points, we obtained the engineering and instantaneous Poisson's ratios ν_{eng} and ν_{inst} of the lattice, as defined by [58]:

$$\nu_{eng} = -\frac{\varepsilon_x}{\varepsilon_y} \tag{5}$$

$$\nu_{inst} = -\frac{\varepsilon_{inst,x}}{\varepsilon_{inst,y}} \tag{6}$$

Here, ν_{eng} reflects the deformation of the metamaterial in relation to the initial undeformed configuration. For instance, if $\nu_{eng} < 0$, then it is guaranteed that the current width of the metamaterial under compression is smaller than the original one. In contrast, ν_{inst} compares current strains to strains at the previous moment in time. Therefore, it might occur that ν_{eng} is still negative while the metamaterial is in the process of expansion characterized by $\nu_{inst} > 0$. To be precise, each Poisson's definition relies on a differently defined strain ε_{eng} and ε_{inst}. Strains $\varepsilon_{eng,j}$ were calculated from the point coordinates, as depicted in Fig. 3. Specifically, they were calculated with respect to initial dimension values $l_{0,j}$, with $j = x, y$:

$$\varepsilon_{eng,j} = \frac{l_{i,j} - l_{0,j}}{l_{0,j}} \tag{7}$$

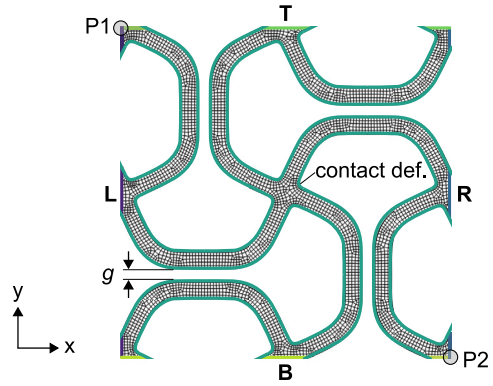


Fig. 3. Meshed lattice with evaluation points and contact definition boundaries shown in green.

For ε_{inst}, we used previous dimension values $l_{i-1,j}$:

$$\varepsilon_{inst,j} = \frac{l_{i,j} - l_{i-1,j}}{l_{i-1,j}} \tag{8}$$

$l_{i,j}$ being the current distance between the corner points p_1 and p_2 in x- and y-directions for $\varepsilon_{inst,x}$ and $\varepsilon_{inst,y}$, respectively.

3.2. Results and discussion

In Fig. 4, we present a typical response of the unit cell, which can be divided into three distinctive zones or regimes (I-III) with two transition points (P_S and P_E) that can be evaluated for each unit cell. In the initial phase of compressive loading, we observe auxetic behavior (regime I), characterized by a negative Poisson's ratio (both ν_{inst} and ν_{eng}). Subsequently, self-contact occurs at point P_S ($\varepsilon = \varepsilon^{cont}$), leading to a change in topology. This change results in a significant jump in the instantaneous Poisson's ratio (ν_{inst}), followed by a gradual increase in the value of the engineering Poisson's ratio (ν_{eng}) in regime II. As compression continues, the lattice may reach its initial width at point P_E, coinciding with $\nu_{eng} = 0$. Finally, the lattice continues to expand beyond its initial width, maintaining positive values for both ν_{eng} and ν_{inst} in regime III.

A similar observation can be made regarding the evolution of the metamaterial's stiffness during compression. Upon self-contact, the metamaterial undergoes a noticeable stiffening, which is visible on the stress-strain curve (Fig. 4B). In a similar fashion to ν_{inst}, the instantaneous Young's modulus E_{inst}, defined as the slope of the stress-strain curve at each specific point, exhibits a step-like jump upon contact (Fig. 4B). The difference in stiffness (E_{inst}) before and after self-contact can be attributed to the underlying deformation mechanisms. Prior to contact, deformation is mostly facilitated via the rotation in the lattice's

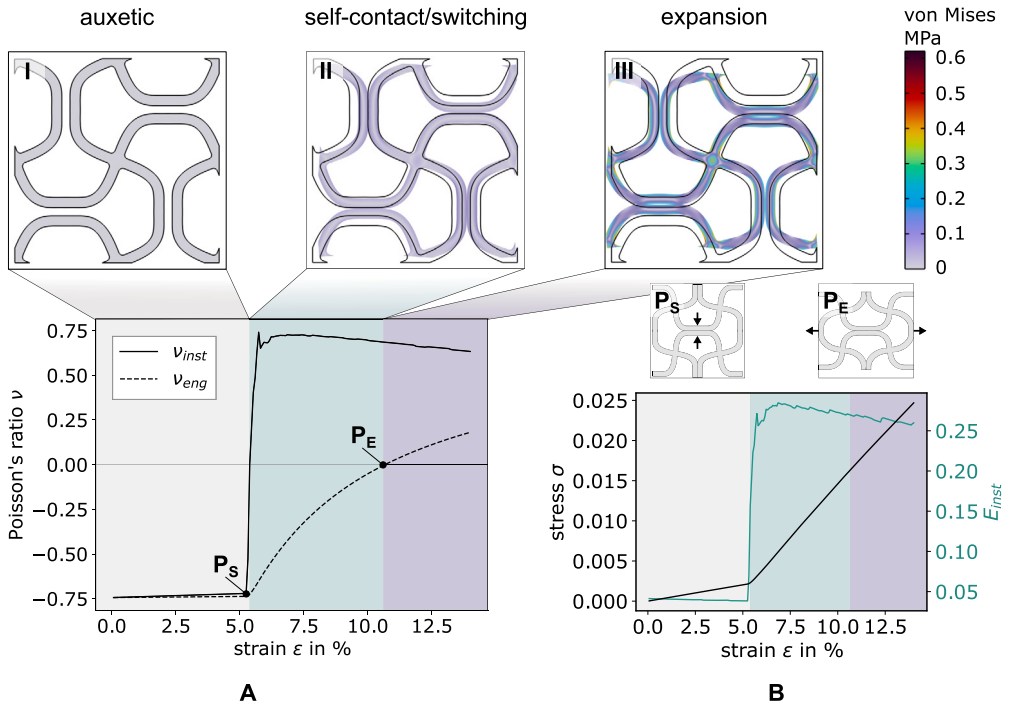


Fig. 4. Typical response of the metamaterial during compression. A: Poisson's ratio I: Auxetic behavior is seen ($\nu_{inst} < 0$ and $\nu_{eng} < 0$). II: After self-contact at strain ε^{cont} (point P_S), switching of instantaneous Poisson's ratio sign can be observed ($\nu_{inst} > 0$ and $\nu_{eng} < 0$). III: Expansion beyond initial width after reaching ε^{exp} (point P_E) corresponding to the case of $\nu_{inst} > 0$ and $\nu_{eng} > 0$. B: Stress σ and E_{inst} during compression.

nodes. However, this rotational motion becomes constrained upon self-contact, resulting in a deformation dominated by bending of the beams in regimes II and III (Fig. 4 and supplementary video 1). It is worth noting that stiffening of the metamaterial also leads to an increase in the level of internal stresses. The maximal stresses are usually observed in the lattice nodes and in contact zones; however, due to the length of such zones, there is no pronounced stress concentration after self-contact that might lead to crack initiation.

The strain at which self-contact occurs (ε^{cont}) is depicted for each geometry from the considered parameter space in Fig. 5A. Here we can observe the anticipated relation between ε^{cont} and g. Indeed, specimens with larger initial gap g require larger strain before self-contact takes place. Specifically, ε^{cont} spans from 1% to 21% for the minimum and maximum gap sizes g, respectively. In contrast, we observe a minimal influence of the contact length (c) on the strain ε^{cont} required for self-contact. This indifference can be attributed to the fact that during the initial stages of compression, deformation primarily occurs due to bending and rotation near the intersection nodes, while straight elements do not significantly contribute to ν_{inst} in stage I. However, the contact length (c) plays a crucial role in determining the height of the jump in the value of ν_{inst} upon reaching ε^{cont}.

While for all considered geometries ν_{inst} increases after self-contact, in some cases it does not reach 0 and continues to be negative. This behavior is typical for lattices with large contact lengths ($c > 40\%$), as indicated by the points marked with a cross in Fig. 5A. Consequently, these metamaterials do not undergo a switch in the sign of the instantaneous Poisson's ratio (ν_{inst}) and maintain their auxetic behavior after self-contact. The consequence of this behavior is an inability to return to the original width, as the lattice continues to shrink laterally during subsequent compression.

The distinction between designs that switch or don't switch their auxeticity due to self-contact visible in Fig. 5A can assist in selecting unit cells tailored for a specific use-case. For instance, if maintaining the auxeticity after self-contact is favorable for impact engineering, the lattices with large enough c are well-suited according to this criterion. These designs offer the dual benefit of maintaining auxeticity and the ability to significantly stiffen the material upon reaching a pre-programmed deformation level [38]. At the same time, the switch in the sign of instantaneous Poisson's ratio can be harnessed for novel use-cases, such as mechanical if-then switches activated upon achieving specific compressive strains. Since self-contact in such lattices only facilitates a change in the sign of ν_{inst} rather than ν_{eng}, it becomes essential to determine the strain value ε^{exp} at which the metamaterial expands beyond its initial width. Fig. 5B utilizes color coding to indicate the values of ε^{exp}. For points in the parameter space marked by a cross, no expansion occurs because the corresponding unit cells do not undergo a switch in auxeticity. For points marked by empty circles, expansion occurs; however, after reaching 25% compressive strain, the lattice's width is still smaller than the initial width. From a practical standpoint, we limit our focus to lattices that expand beyond their initial width at compressive strains less than 25%. This mapping of ε^{exp} onto the geometrical parameters defining unit cell design allows for the deliberate selection of geometries with specific sequences of lateral shrinking and expansion during compression. Since expansion occurs at larger values of strain than self-contact, we additionally utilize experimental testing to ensure accuracy of our model.

4. Experimental testing

4.1. Experimental setup

To confirm the observed non-trivial behavior and validate the obtained dependencies, we conducted compressive experiments on 3D-printed specimens. We carefully selected 10 different unit cell designs to ensure maximum representation of the parameter space, as illustrated in Fig. 6. These lattice specimens were fabricated using fused filament fabrication (FFF) with NinjaFlex TPU (NinjaTek, Lititz, USA). The specimens were composed of 20 mm unit cells arranged in a 3×3 pattern. We performed compression testing on a uniaxial testing machine (ZwickRoell, Ulm, Germany) equipped with a 10 kN loadcell. The load cycle was comprised of 15 mm vertical compression with subsequent unloading at a constant testing speed of 15 mm min^{-1}. Note that

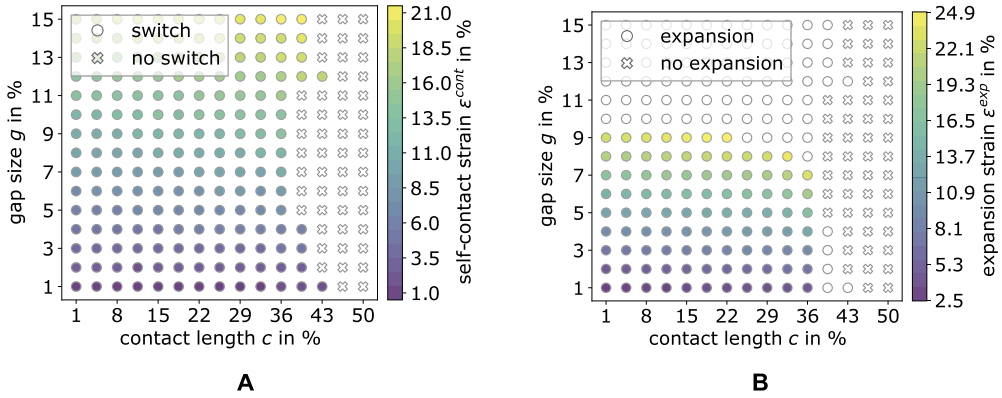


Fig. 5. A: Value of the self-contact strain ε^{cont} for different unit cells in the design space. Combinations marked by cross do not exhibit switch in the sign of the Poisson's ratio. B: Strain at the onset of expansion beyond the initial width ε^{exp} for different geometrical parameters c and g. Empty circles mark combinations of geometrical parameters for which the expansion happens for strains exceeding 25%. Cross sign marks geometrical parameters for which $\nu_{inst} < 0$ even after self-contact.

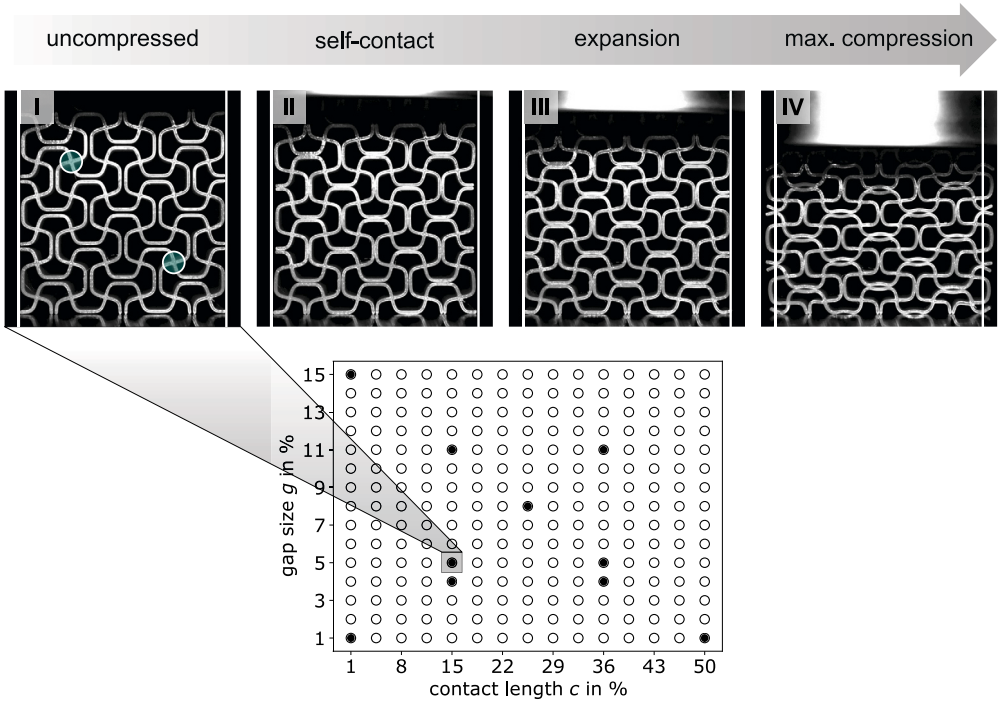


Fig. 6. Experimentally tested specimens are depicted as filled circles in the parameter space. The evolution of specimen shape throughout compression. I: uncompressed state ($\varepsilon = 0$), II: self-contact ($\varepsilon = \varepsilon^{cont}$), III: start of the expansion beyond initial width ($\varepsilon = \varepsilon^{exp}$), IV: maximum compression ($\varepsilon = 25\%$). Vertical lines indicate the initial width of 60 mm, tracked points are shown as filled circles in I.

15 mm vertical displacement on the considered specimens corresponds precisely to 25% strain. We used video recordings for characterization of the lattice's deformation under load. The positions of two points on the lattice (indicated by circles in Fig. 6) were automatically tracked to retrieve two values of interest: the strain of self-contact (ε^{cont}) and, if observable, the strain of expansion beyond initial width ε^{exp}.

Fig. 6I-IV provides a visual representation of the status of the tested specimen at various compression levels. The act of compressing the specimen results in the closure of the initial gap, introducing self-contact in predefined areas, as shown in Fig. 6II. Additionally, we observe lateral shrinkage of the specimen concerning the lines that indicate the initial width. This observation is indicative of the specimen's auxetic behavior before self-contact occurs. Upon self-contact that happens nearly simultaneously between all contact zones, the shrinking process halts, and the specimen begins to undergo lateral expansion. This expansion is evident as the specimen touches the white lines representing the initial width in Fig. 6III. Furthermore, it expands beyond these lines with an increase in applied compressive strain, as demonstrated in Fig. 6IV (for specimen compression, see supplementary video 1).

4.2. Validation and characterization

Qualitatively, we have confirmed the behavior previously observed in simulations, and we have identified the distinct phases of mechanical response, as depicted in Fig. 4. The validation of self-contact and expansion values for all tested specimens empowers us to harness these mechanical response phases for practical applications. For all 10 tested specimens, we extracted values of ε^{cont} and ε^{exp} where possible. When comparing experimentally obtained self-contact strain ε^{cont} with numerically predicted values, we find a substantial agreement with an R^2 value of 0.9401 (Fig. 7A). As applied strain increases, lattices with shorter contact lengths (c) undergo an auxeticity-switch. Consequently,

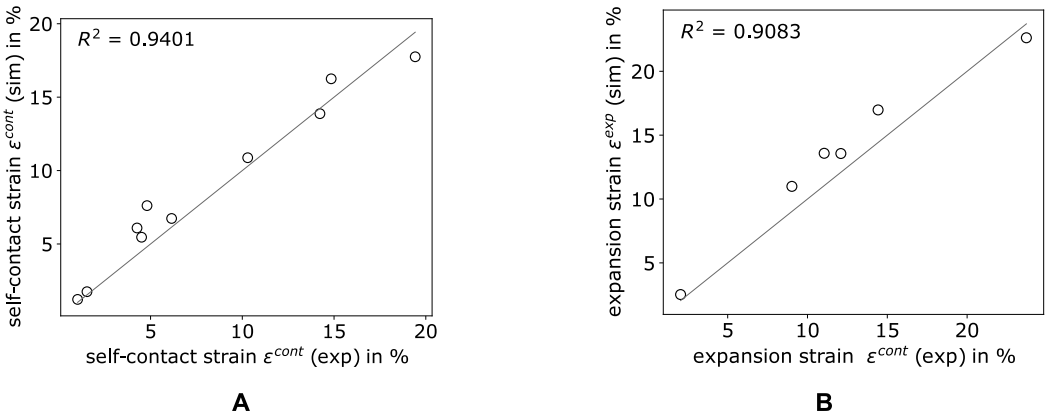


Fig. 7. Simulations vs experiments. A: Strain at observed self-contact ε^{cont}. B: Onset of expansion beyond the initial width ε^{exp}.

we compared numerically predicted and experimentally obtained expansion strains (ε^{exp}) for such lattices, as shown in Fig. 7B. Despite the need to exclude lattices that either do not expand at all or don't exhibit expansion beyond the initial width for applied strains less than 25%, we observe a strong agreement between experiments and simulations, with an R^2 value of 0.9083. It is worth noting that numerical simulations generally slightly overestimate strains associated with self-contact and expansion beyond the initial width as compared with experiments. This minor discrepancy may be attributed to geometric imperfections introduced by the 3D printing process. Specifically, the gap size in the printed samples might be smaller than designed due to finite value of extrusion width that cannot be arbitrary low, resulting in slightly thicker printed beams.

In summary, our performed numerical simulations not only capture the real auxeticity switch induced by self-contact in the considered metamaterials but also provide us with reliable estimates of the specific strain levels at which contact or expansion beyond the original boundaries occurs.

5. Scales demonstrator

To demonstrate the applicability of the introduced design framework, we developed a discrete scales demonstrator that relies on the switches in Poisson's ratio caused by self-contact in the metamaterial. We created four specimens with identical outer dimensions (as used in Section 4) but with different geometrical parameters (c and g). These specimens were 3D-printed using conductive Filaflex TPU filament (Recreus, Elda, Spain). Utilizing the information from Fig. 5B, we selected specimens with varying expansion strains (ε_i^{exp}), where $i = 1...4$. These strains amounted to $5.2\%, 13\%, 20.9\%$ and $>25\%$ respectively. The 3D-printed specimens were placed within an enclosure, as illustrated in Fig. 8A. In their undeformed state, each specimen made contact with corresponding electrodes integrated into the enclosure, which were connected to pairs of LEDs, as depicted in Fig. 8B. These LEDs were placed behind their corresponding specimens to illuminate them upon reaching pre-programmed strains that results in closure of the electric circuit. To ensure even load distribution during compression, we covered the assembled system with a lid. Subsequently, the system was positioned in a universal testing machine, with two perpendicular mirrors placed behind it to facilitate video capturing of three sides of the scale demonstrator.

In the initial uncompressed state, all metamaterials are illuminated from inside the scales, as shown in Fig. 8C. Almost immediately after the compression begins, the lattices lose contact with the electrodes due to their auxetic behavior, which facilitates lateral shrinking, resulting in all LEDs switching off. As compression continues, the LEDs gradually light up the connected lattices one by one. The side of the cube containing the metamaterial with the lowest expansion strain (ε_1^{exp}) is the first to illuminate. In a cascading manner, the specimens light up as their specified expansion strains (ε_i^{exp}) are reached. During unloading, the illumination on the sides of the specimens switches off in the opposite sequence until all LEDs are off when the applied strain drops below ε_1^{exp}. In addition, at the latest stage of unloading, when the metamaterials return to their initial undeformed state, all sides of the scales demonstrator are illuminated again, indicating that the scales are "self-calibrated" and ready for the next measurement. This behavior is proven to be repeatable during multiple consecutive loading-unloading cycles for applied strains less than 25% (for a scales demonstration, see supplementary video 2).

Since values of ε_i^{exp} are known and, moreover, purposefully selected, LED states enable us to deduct the applied strain, or at the least, place it within a specific range. If all LEDs are off, it indicates that the applied strain is lower than ε_1^{exp}. If only two LEDs are on, it suggests that the applied strain falls within the range between ε_2^{exp} and ε_3^{exp}. Moreover, this concept can be repurposed for measuring force instead of strain. Within the proposed design, the reaction force monotonically increases with an increase in applied compressive strain, as observed in load-cell data. This is because there are no snap-through transitions within the metamaterial. Consequently, a correspondence between force and strain, and thus between force and LED states, can be established. Additionally, within this concept, we can even detect faults in the electric circuitry. For example, if one of the LEDs fails to illuminate after complete unloading, it may indicate a faulty contact.

This approach can therefore be implemented for targeted applications of the presented lattice. Here, not only the expansion but also the sudden change of the sign of Poisson's ratio upon self-contact can be considered as a feature, with results from Fig. 5 serving as a lookup table to further enhance the utility of metamaterial.

6. Conclusion

In this study, we explored the concept of mechanical metamaterials capable of switching their Poisson's ratio at a pre-programmed strain level (ε^{cont}) by harnessing self-contact between metamaterial elements. For a selected design inspired by metamaterials with curvy beams, we assessed the relationship between the geometrical characteristics of unit cells and the resulting mechanical response through simulations and experimental testing. In the continuous design space, we identified geometry parameters that result in different shrinking-expansion sequences. We demonstrated, that for specific unit cells, self-contact immediately changes the instantaneous Poisson's ratio, but the metamaterial continues to shrink laterally upon subsequent compression. Meanwhile, for another class of unit cells, self-contact facilitates a change in the effective Poisson's ratio sign, leading to the expansion of the metamaterial and eventual expansion beyond its initial dimensions for larger compressive strain (ε^{exp}). We showed how these critical strains (ε^{cont} and

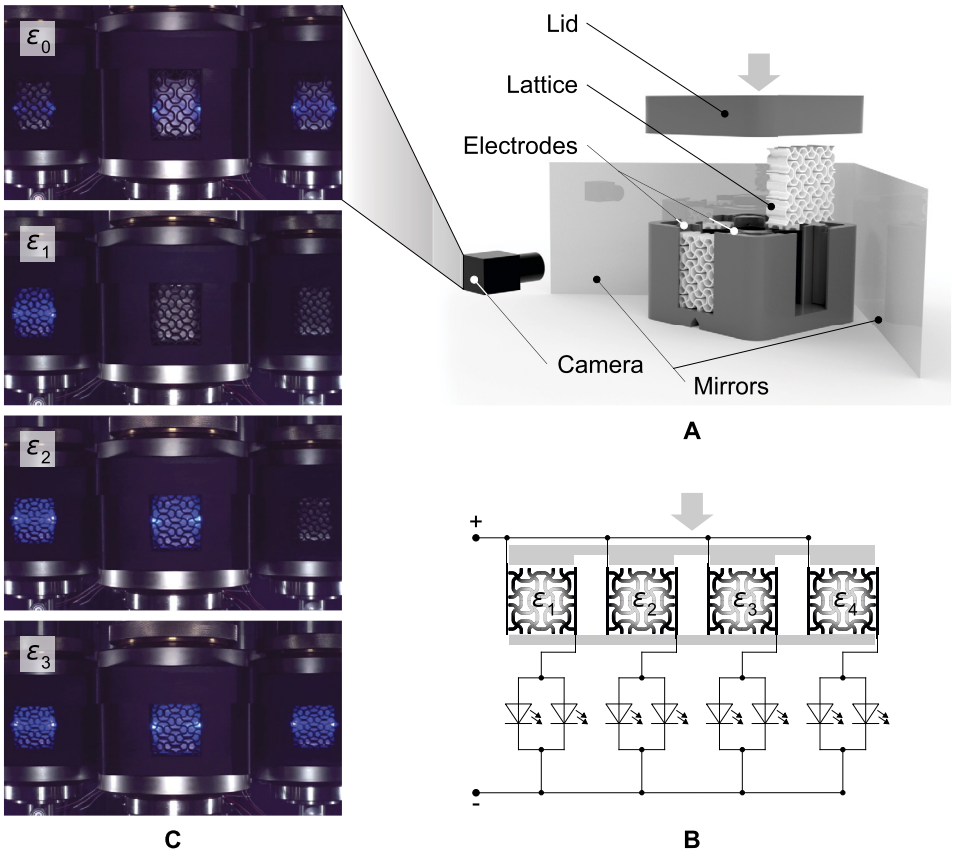


Fig. 8. Discrete scales demonstrator. A: Components of the demonstrator. B: Circuitry of the demonstrator containing two LEDs per lattice with pre-programmed expansion strain ε_{1-4}^{exp}. C: Scales during compression testing, mirrors allow observation of three sides at once. Initially all circuits are closed at $\varepsilon_0 = 0$. Subsequently, all LEDs switch off until the lattices close their circuits at individual expansion strains ε_i^{exp}.

ε^{exp}) can be tuned via the geometry of the unit cell to enable novel functionalities in the corresponding metamaterials. Utilizing numerical and experimental results, we created a demonstrator model of a discrete scales-like device capable of indicating the applied strain through the statuses of multiple LEDs. During compression, the sides of the demonstrator light up one by one upon reaching the selected critical strains, triggered by switches in the Poisson's ratio caused by self-contact. It is important to note that in this proposed concept the self-contact functionality is integral part of the metamaterial's load-bearing core, which significantly simplifies the design. The findings presented here can be applied to implement the lattice's switching capabilities in complex applications, such as soft robotics or lifelike stimuli-responsive material systems.

Declaration of competing interest

The authors declare that they have no known competing financial interests or personal relationships that could have appeared to influence the work reported in this paper.

Data availability

Data will be made available on request.

Acknowledgement

Funded by the Deutsche Forschungsgemeinschaft (DFG, German Research Foundation) under Germany's Excellence Strategy – EXC-2193/1 – 390951807. S. Schiller gratefully acknowledges the 'Alfons und Gertrud Kassel-Stiftung, Frankfurt am Main'. The authors acknowledge support by the state of Baden-Württemberg through bwHPC and the German Research Foundation (DFG) through grant no INST 39/963-1 FUGG (bwForCluster NEMO). The authors acknowledge support by the Open Access Publication Fund of the University of Freiburg.

Appendix A. Supplementary material

Supplementary material related to this article can be found online at https://doi.org/10.1016/j.matdes.2023.112468.

References

[1] H.M.A. Kolken, A.A. Zadpoor, Auxetic mechanical metamaterials, RSC Adv. 7 (9) (2017) 5111–5129.
[2] X. Ren, R. Das, P. Tran, T.D. Ngo, Y.M. Xie, Auxetic metamaterials and structures: a review, Smart Mater. Struct. 27 (2) (2018) 023001.
[3] F. Usta, H.S. Türkmen, F. Scarpa, Low-velocity impact resistance of composite sandwich panels with various types of auxetic and non-auxetic core structures, Thin-Walled Struct. 163 (2021) 107738.
[4] A. Bührig-Polaczek, C. Fleck, T. Speck, P. Schüler, S.F. Fischer, M. Caliaro, M. Thielen, Biomimetic cellular metals—using hierarchical structuring for energy absorption, Bioinspir. Biomim. 11 (4) (2016) 045002.
[5] R.P. Bohara, S. Linforth, T. Nguyen, A. Ghazlan, T. Ngo, Anti-blast and -impact performances of auxetic structures: a review of structures, materials, methods, and fabrications, Eng. Struct. 276 (2023) 115377.
[6] O. Duncan, T. Shepherd, C. Moroney, L. Foster, P. Venkatraman, K. Winwood, T. Allen, A. Alderson, Review of auxetic materials for sports applications: expanding options in comfort and protection, Appl. Sci. 8 (6) (2018) 941.
[7] A. Papadopoulou, J. Laucks, S. Tibbits, Auxetic materials in design and architecture, Nat. Rev. Mater. 2 (12) (2017).
[8] S. Han, E.J. Lee, B. Kim, S. Jung, S. Jeong, S.-W. Kim, Y. Choi, S.Y. Lee, High-performance dual-mode triboelectric nanogenerator based on hierarchical auxetic structure, ACS Energy Lett. 5 (11) (2020) 3507–3513.
[9] S. Shukla, B.K. Behera, Auxetic fibrous materials and structures in medical engineering – a review, J. Text. Inst. 114 (7) (2022) 1078–1089.

[10] F. Amin, M.N. Ali, U. Ansari, M. Mir, M.A. Minhas, W. Shahid, Auxetic coronary stent endoprosthesis: fabrication and structural analysis, J. Appl. Biomater. Funct. Mater. 13 (2) (2015) 127–135.
[11] R. Gatt, L. Mizzi, J.I. Azzopardi, K.M. Azzopardi, D. Attard, A. Casha, J. Briffa, J.N. Grima, Hierarchical auxetic mechanical metamaterials, Sci. Rep. 5 (1) (2015).
[12] H. Jiang, H. Ziegler, Z. Zhang, H. Zhang, L.L. Barbenchon, S. Atre, Y. Chen, 3d printed tubular lattice metamaterials for mechanically robust stents, Composites, Part B, Eng. 236 (2022) 109809.
[13] H.M.A. Kolken, S. Janbaz, S.M.A. Leeflang, K. Lietaert, H.H. Weinans, A.A. Zadpoor, Rationally designed meta-implants: a combination of auxetic and conventional meta-biomaterials, Mater. Horiz. 5 (1) (2018) 28–35.
[14] N. Ghavidelnia, M. Bodaghi, R. Hedayati, Femur auxetic meta-implants with tuned micromotion distribution, Materials 14 (1) (2020) 114.
[15] A. Sharipova, I. Gotman, S. Psakhie, E. Gutmanas, Biodegradable nanocomposite Fe–Ag load-bearing scaffolds for bone healing, J. Mech. Behav. Biomed. Mater. 98 (2019) 246–254.
[16] Y. Jin, C. Xie, Q. Gao, X. Zhou, G. Li, J. Du, Y. He, Fabrication of multi-scale and tunable auxetic scaffolds for tissue engineering, Mater. Des. 197 (2021) 109277.
[17] G. Flamourakis, I. Spanos, Z. Vangelatos, P. Manganas, L. Papadimitriou, C. Grigoropoulos, A. Ranella, M. Farsari, Laser-made 3d auxetic metamaterial scaffolds for tissue engineering applications, Macromol. Mater. Eng. 305 (7) (2020).
[18] Ó. Lecina-Tejero, M.Á. Pérez, E. García-Gareta, C. Borau, The rise of mechanical metamaterials: auxetic constructs for skin wound healing, J. Tissue Eng. 14 (2023).
[19] L. Mizzi, E. Salvati, A. Spaggiari, J.-C. Tan, A.M. Korsunsky, 2d auxetic metamaterials with tuneable micro-/nanoscale apertures, Appl. Mater. Today 20 (2020) 100780.
[20] J. Valente, E. Plum, I.J. Youngs, N.I. Zheludev, Nano- and micro-auxetic plasmonic materials, Adv. Mater. 28 (26) (2016) 5176–5180.
[21] K.K. Dudek, J.A.I. Martínez, G. Ulliac, M. Kadic, Micro-scale auxetic hierarchical mechanical metamaterials for shape morphing, Adv. Mater. 34 (14) (2022).
[22] L.Y.W. Loh, U. Gupta, Y. Wang, C.C. Foo, J. Zhu, W.F. Lu, 3d printed metamaterial capacitive sensing array for universal jamming gripper and human joint wearables, Adv. Eng. Mater. 23 (5) (2021).
[23] R.P. Bohara, S. Linforth, T. Nguyen, A. Ghazlan, T. Ngo, Dual-mechanism auxetic-core protective sandwich structure under blast loading, Compos. Struct. 299 (2022) 116088.
[24] X. Yu, J. Zhou, H. Liang, Z. Jiang, L. Wu, Mechanical metamaterials associated with stiffness, rigidity and compressibility: a brief review, Prog. Mater. Sci. 94 (2018) 114–173.
[25] U. Larsen, O. Signund, S. Bouwsta, Design and fabrication of compliant micromechanisms and structures with negative Poisson's ratio, J. Microelectromech. Syst. 6 (2) (1997) 99–106.
[26] Z. Chen, X. Wu, Y.M. Xie, Z. Wang, S. Zhou, Re-entrant auxetic lattices with enhanced stiffness: a numerical study, Int. J. Mech. Sci. 178 (2020) 105619.
[27] D. Mousanezhad, B. Haghpanah, R. Ghosh, A.M. Hamouda, H. Nayeb-Hashemi, A. Vaziri, Elastic properties of chiral, anti-chiral, and hierarchical honeycombs: a simple energy-based approach, Theor. Appl. Mech. Lett. 6 (2) (2016) 81–96.
[28] K.K. Dudek, New type of rotation of chiral mechanical metamaterials, Smart Mater. Struct. 29 (11) (2020) 115027.
[29] J.N. Grima, K.E. Evans, Auxetic behavior from rotating squares, J. Mater. Sci. Lett. 19 (17) (2000) 1563–1565.
[30] V. Slesarenko, Planar mechanical metamaterials with embedded permanent magnets, Materials 13 (6) (2020) 1313.
[31] R.F. Almgren, An isotropic three-dimensional structure with Poisson's ratio =-1, J. Elast. 15 (4) (1985) 427–430.
[32] C. Körner, Y. Liebold-Ribeiro, A systematic approach to identify cellular auxetic materials, Smart Mater. Struct. 24 (2) (2014) 025013.
[33] A. Clausen, F. Wang, J.S. Jensen, O. Sigmund, J.A. Lewis, Topology optimized architectures with programmable Poisson's ratio over large deformations, Adv. Mater. 27 (37) (2015) 5523–5527.
[34] J.C. McCaw, E. Cuan-Urquizo, Curved-layered additive manufacturing of non-planar, parametric lattice structures, Mater. Des. 160 (2018) 949–963.
[35] G. Felsch, N. Ghavidelnia, D. Schwarz, V. Slesarenko, Controlling auxeticity in curved-beam metamaterials via a deep generative model, Comput. Methods Appl. Mech. Eng. 410 (2023) 116032.
[36] V. Slesarenko, Bandgap structure in elastic metamaterials with curvy Bezier beams, Appl. Phys. Lett. 123 (8) (2023).
[37] J. Dong, G. Ye, Y. Wang, F. Jin, H. Fan, Design, manufacture and crushing behaviors of buckling-inspired auxetic meta-lattice structures, Int. J. Smart Nano Mater. 12 (4) (2021) 491–510.
[38] M.A. Wagner, F. Schwarz, N. Huber, L. Geistlich, H. Galinski, R. Spolenak, Deformation-induced topological transitions in mechanical metamaterials and their application to tunable non-linear stiffening, Mater. Des. 221 (2022) 110918.
[39] O. Skarsetz, V. Slesarenko, A. Walther, Programmable auxeticity in hydrogel metamaterials via shape-morphing unit cells, Adv. Sci. 9 (23) (2022) 2201867.
[40] M. Lei, W. Hong, Z. Zhao, C. Hamel, M. Chen, H. Lu, H.J. Qi, 3d printing of auxetic metamaterials with digitally reprogrammable shape, ACS Appl. Mater. Interfaces 11 (25) (2019) 22768–22776.
[41] Z. Wang, Z. Wang, Y. Zheng, Q. He, Y. Wang, S. Cai, Three-dimensional printing of functionally graded liquid crystal elastomer, Sci. Adv. 6 (39) (2020).
[42] K.K. Dudek, J.A.I. Martínez, G. Ulliac, L. Hirsinger, L. Wang, V. Laude, M. Kadic, Micro-scale mechanical metamaterial with a controllable transition in the Poisson's ratio and band gap formation, Adv. Mater. 35 (20) (2023).
[43] K.K. Dudek, R. Gatt, M.R. Dudek, J.N. Grima, Negative and positive stiffness in auxetic magneto-mechanical metamaterials, Proc. R. Soc. A, Math. Phys. Eng. Sci. 474 (2215) (2018) 20180003.
[44] T. Chen, M. Pauly, P.M. Reis, A reprogrammable mechanical metamaterial with stable memory, Nature 589 (7842) (2021) 386–390.
[45] A. Walther, Viewpoint: from responsive to adaptive and interactive materials and materials systems: a roadmap, Adv. Mater. 32 (20) (2019) 1905111.
[46] G. Fusi, D.D. Giudice, O. Skarsetz, S.D. Stefano, A. Walther, Autonomous soft robots empowered by chemical reaction networks, Adv. Mater. 35 (7) (2022) 2209870.
[47] M.C. Huber, U. Jonas, S.M. Schiller, An autonomous chemically fueled artificial protein muscle, Adv. Intell. Syst. 4 (4) (2022) 2100189.
[48] M.F. Berwind, A. Kamas, C. Eberl, A hierarchical programmable mechanical metamaterial unit cell showing metastable shape memory, Adv. Eng. Mater. 20 (11) (2018).
[49] J. Li, V. Slesarenko, S. Rudykh, Auxetic multiphase soft composite material design through instabilities with application for acoustic metamaterials, Soft Matter 14 (30) (2018) 6171–6180.
[50] J. Shim, S. Shan, A. Košmrlj, S.H. Kang, E.R. Chen, J.C. Weaver, K. Bertoldi, Harnessing instabilities for design of soft reconfigurable auxetic/chiral materials, Soft Matter 9 (34) (2013) 8198.
[51] S. Kamrava, D. Mousanezhad, H. Ebrahimi, R. Ghosh, A. Vaziri, Origami-based cellular metamaterial with auxetic, bistable, and self-locking properties, Sci. Rep. 7 (1) (2017).
[52] F. Wenz, I. Schmidt, A. Leichner, T. Lichti, S. Baumann, H. Andrae, C. Eberl, Designing shape morphing behavior through local programming of mechanical metamaterials, Adv. Mater. 33 (37) (2021) 2008617.
[53] A. Farzaneh, N. Pawar, C.M. Portela, J.B. Hopkins, Sequential metamaterials with alternating Poisson's ratios, Nat. Commun. 13 (1) (2022).
[54] T.-C. Lim, Metamaterials with Poisson's ratio sign toggling by means of microstructural duality, SN Appl. Sci. 1 (2) (2019).
[55] C.E. Helou, B. Grossmann, C.E. Tabor, P.R. Buskohl, R.L. Harne, Mechanical integrated circuit materials, Nature 608 (7924) (2022) 699–703.
[56] H. Yasuda, P.R. Buskohl, A. Gillman, T.D. Murphey, S. Stepney, R.A. Vaia, J.R. Raney, Mechanical computing, Nature 598 (7879) (2021) 39–48.
[57] T. Reppel, K. Weinberg, Experimental determination of elastic and rupture properties of printed ninjaflex, Tech. Mech. 38 (1) (2018).
[58] C.W. Smith, R.J. Wootton, K.E. Evans, Interpretation of experimental data for Poisson's ratio of highly nonlinear materials, Exp. Mech. 39 (4) (1999) 356–362.

3.2 Correlating Fluorescence and Residual Stiffness in Self-Reporting Microcapsule Composites with an Intact Soft Matrix

Authors: David Schwarz, Viacheslav Slesarenko
Journal: Composites Part C: Open Access
Date: 18.4.2025
DOI: https://doi.org/10.1016/j.jcomc.2025.100586

Author	Contributions
David Schwarz	Writing – original draft, methodology, investigation, formal analysis, conceptualization
Viacheslav Slesarenko	Writing – review & editing, validation, supervision, methodology, funding acquisition, conceptualization

The article is open access under the CC BY license (http://creativecommons.org/licenses/by/4.0/) and reprinted without changes.

Context and Personal Assessment

By elegantly engineering a response into a structured material, mechanical metamaterials go beyond common associations we have with conventional bulk materials. Their achievable responses span a wide range, from purely auxetic [3] to nonlinear responses, like the auxeticity switching geometry discussed in Section 3.1. Since their behavior is primarily geometry-driven, mechanical metamaterials are widely applicable [95, 96]. Moreover, their mechanical responses can be enhanced by altering their base material. Composite materials, which combine multiple components to achieve their superior mechanical properties [97], can also exhibit responses to external triggers when incorporating liquid-filled structures. Building on this concept, self-healing [16, 52, 98] and self-reporting [17, 99] composites respond autonomously to local damage. By engineering stress concentrations into a mechanical metamaterial, the deliberate release of the liquid content can trigger a secondary response, making solid-liquid composites attractive base materials.

Solid-liquid composites can be realized by embedding vascular networks or liquid-filled microcapsules within a solid matrix material [81]. When subjected to high stresses, these incorporated structures rupture, releasing their liquid content. Depending on the system, the liquid either polymerizes to enable self-healing [52] or visually reports damage [17]. While self-reporting is attractive for maintenance applications [81], it also allows for more advanced concepts utilizing local self-reporting to embed information. For instance, a mechanical metamaterial incorporating microcapsules could localize stresses in specific regions. Upon mechanical loading, the microcapsules in these locations would rupture and release their liquid content, revealing a predefined pattern.

However, realizing such a responsive mechanical metamaterial requires a thorough understanding of the composite's mechanical properties, both in the intact state and after capsule rupture. Moreover, a well established self-reporting mechanism, aggregation induced emission (AIE), relies on solvent evaporation to induce fluorescence under UV light [6]. The transient nature of visual self-reporting necessitates correlating fluorescence intensity to the extent of damage and the residual mechanical properties of the composite. This relationship is especially relevant when the capsules rupture during loading, but the surrounding matrix stays intact.

In the presented work, I establish the transient relation between the self-reporting fluorescence intensity and the change in mechanical properties in a microcapsule composite. The composite employs a flexible PDMS matrix with embedded, rigid

poly-(urea-formaldehyde) (PUF) microcapsules containing the dissolved AIE luminogen. Unlike previous works that have focused on local capsule breakage through incision [6, 17], I apply global tensile loading to probe the composite's properties. This approach reveals a unique response: as the microcapsules start to break and release their content, the matrix material remains intact, but Young's modulus drops. This reduction is immediate, yet it continues to change and only stabilizes after several hours. Similarly, the fluorescence signal immediately responds, but continues to rise, reaching its maximum after 15 h. Notably, at any given time, the brightness is linearly correlated to Young's modulus ($R^2 > 0.88$), but evolves over time and stabilizes only after many hours. Hence, if the time since loading is known, the recorded brightness provides a measure of residual stiffness of the microcapsule composite.

Previous studies have either demonstrated self-reporting in response to local damage [6, 17], or microcapsules have been introduced into fiber composites to enable more global structural health monitoring [81]. While the latter has been commercialized for self-healing purposes [85], the presented work introduces a new concept: microcapsules not only enable self-reporting, but also influence the composite's mechanical properties depending on their state. For the soft polymer matrix, the intact capsules initially increase stiffness, whereas their rupture leads to a significant stiffness reduction. These results can be used for several improvements in microcapsule composites. First, the composite's response can be fine-tuned to occur at a specific deformation level by ensuring consistent capsule size, for instance, through microfluidic fabrication [55]. Second, strategically placing capsules within regions of higher stress concentration, as those dictated by a metamaterial's design, enables a localized response. Finally, materials with a graded stiffness upon mechanical loading might be conceived: the drop in stiffness due to broken capsules can be harnessed to soften the composite progressively under load. As a result, the presented work lays the foundation for mechanical metamaterials that utilize a composite with microcapsules as base material to harness the transient, self-reporting stiffness drop behavior.

Composites Part C: Open Access 17 (2025) 100586

Contents lists available at ScienceDirect

Composites Part C: Open Access

journal homepage: www.elsevier.com/locate/composites-part-c-open-access

Correlating fluorescence and residual stiffness in self-reporting microcapsule composites with an intact soft matrix

David Schwarz [a], Viacheslav Slesarenko [a,b,*]

[a] Cluster of Excellence livMatS @ FIT – Freiburg Center for Interactive Materials and Bioinspired Technologies, University of Freiburg, Freiburg, 79110, Germany
[b] Department of Microsystems Engineering, University of Freiburg, Freiburg, 79110, Germany

ARTICLE INFO

MSC:
74E30
74A40

Keywords:
Self-reporting
Microcapsules
Composites
Damage
Soft materials
Stiffness

ABSTRACT

Self-reporting microcapsule-based systems are highly valuable for providing information about a composite's health, whether by indicating the location of damage or, in more advanced cases, reflecting the extent of damage through intensity of fluorescence. However, measuring such intensity alone is insufficient for evaluating the deterioration of a composite's mechanical properties. Using self-reporting stiff capsules containing tetraphenylethylene (TPE) and hexyl acetate embedded in a soft polymeric matrix, we observe that accurately assessing mechanical properties after damage in evaporation-based self-reporting systems requires not only measuring fluorescence brightness but also accounting for the time elapsed since the rupture of the capsules. While the fluorescence–stiffness correlation can be approximated by a linear fit at any given time, the proportionality coefficient gradually evolves, stabilizing only hours after capsule rupture. This study highlights the importance of considering the transient nature of fluorescence–stiffness relationships when leveraging self-reporting composites for advanced damage evaluation.

1. Introduction

Combining multiple materials into a single composite often pursues the aim of enhancing overall mechanical properties, such as stiffness or toughness [1]. However, it is also possible to introduce additional functionalities via the composite structure. One such functionality is self-healing — the material's ability to repair itself — which is often achieved by incorporating vascular networks [2,3] or filled capsules within the matrix material [4–6]. In the latter approach, a propagating crack in the composite ruptures the capsules along its path, releasing a healing agent that reacts with catalysts embedded in the matrix [7,8]. This reaction leads to in-situ polymerization, effectively repairing the mechanically induced damage [9,10]. Extensive research has investigated various matrix and capsule combinations, demonstrating a wide range of mechanical properties and chemical mechanisms that enable self-healing functionality [11–15].

Any degree of damage, including regions that have been allegedly healed, often results in inferior mechanical properties compared to the composite's original, intact state [9,10,16]. Therefore, identifying such damaged regions, whether healed or not, is crucial. Similar to self-healing, self-reporting can be achieved by embedding dye-filled capsules within the matrix material [17–19]. Upon rupture, the release of the capsule's contents can activate chemical processes that visually distinguish damaged areas from undamaged ones [20–22]. Of particular interest are self-reporting capsules that indicate damage through color changes or fluorescence [17,21,23,24]. Depending on the design and the loading conditions, two main scenarios might take place. In the case when capsule rupture happens simultaneously with the occurrence of damage in the matrix, as in incisions [17], self-reporting informs directly about the damage in the matrix. However, the capsules can be ruptured even when the matrix is still intact due to achieving locally the critical stress level [25]. Here, the visual self-reporting just highlights the reaching of some specific strain or stress level and partially resembles self-sensing when the overall strain state is acquired [26]. For the design of composites containing capsules, special attention should be directed to the assessment of the capsule's contribution to the composite's mechanical properties. The shape [27] and size [28] of capsules play a significant role in the overall mechanical behavior of the composite before and after their rupture. Depending on the goals, capsules can be deliberately designed before incorporation, since the existing fabrication processes allow them to be manufactured down to the nanometer range [29,30]. If the matrix is not getting damaged while some capsules break, one might tune the contrast between the stiffness of intact and damaged composites.

The partial recovery of mechanical properties in self-healing microcapsule composites is relatively slow due to the time required for

* Corresponding author.
E-mail address: viacheslav.slesarenko@livmats.uni-freiburg.de (V. Slesarenko).

https://doi.org/10.1016/j.jcomc.2025.100586
Received 16 January 2025; Received in revised form 15 March 2025; Accepted 4 April 2025
Available online 18 April 2025
2666-6820/© 2025 The Authors. Published by Elsevier B.V. This is an open access article under the CC BY license (http://creativecommons.org/licenses/by/4.0/).

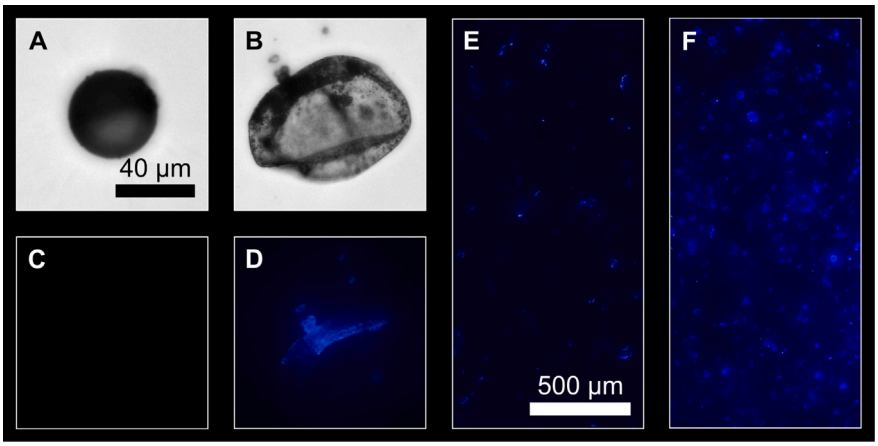


Fig. 1. (A, B): Micrograph of a single intact and ruptured microcapsule, respectively. (C, D): Fluorescence signal of a single intact and ruptured microcapsule, respectively. (E, F): Fluorescence of PDMS specimen with embedded microcapsules before (E) and after (F) rupture.

the chemical reactions involved in the healing process [10,31]. To prevent the use of materials after partial damage but before healing is complete, self-reporting systems are expected to respond more rapidly [32]. However, depending on the chemical mechanism underlying the reporting system, a delay between capsule rupture and damage detection may still occur, and this delay is particularly pronounced in evaporation-based fluorescent reporting systems [21,33,34]. Among the various mechanisms that rely on evaporation to trigger fluorescence, aggregation-induced emission (AIE) is one of the most commonly used for damage reporting. Initially, an AIE luminogen, such as tetraphenylethylene (TPE), is dispersed in a solvent and remains non-fluorescent. Upon rupture of the microcapsule containing the solution, the solvent evaporates, causing the luminogen to aggregate and fluoresce under UV light, thereby facilitating damage detection [21,35].

Notably, the intensity of the visual signal can be correlated to the extent of the damage or the number of ruptured capsules in the composite, as demonstrated in studies of localized impacts and incisions [21,34]. Given that fluorescence saturation may take hours, whereas the mechanical consequences of the capsules breaking are instantaneous [20], it raises the question of how reliably the extent of damage can be correlated with the fluorescence brightness at any given moment.

In this study, we address this using poly(dimethylsiloxane) (PDMS) with embedded poly(urea formaldehyde) (PUF) capsules. The widely used silicone-based elastomer PDMS, selected as a matrix material, exhibits excellent mechanical properties, including high elasticity and durability, while its relatively low viscosity facilitates easy molding and precise replication of fine structures [36]. Complementing other studies that focus on locally induced damage [10,12,17,25], here we subject the specimens to non-local tensile loading, causing capsule rupture throughout the entire volume of the specimen. This approach allows us to monitor the overall fluorescence brightness as well as mechanical properties over several hours following capsule rupture and correlate them to each other.

2. Materials and methods

Polyurethane/poly(urea-formaldehyde) (PU/UF)-based core–shell microcapsules containing a 1 wt% (8.7 $\mathrm{mg\,mL^{-1}}$, 26 mM) solution of TPE in hexyl acetate were prepared using a well-established single-batch in situ emulsification–condensation method, similar to that described in [21,33,37,38]. The capsules had a diameter of 41 ± 17 µm, similar to those used in the recently published work by Stamp et al. [39]. These microcapsules, containing the TPE/hexyl acetate solution, are colorless under visible light (Fig. 1A) and non-emissive under UV-A irradiation (λ = 365 nm) (Fig. 1C). When the microcapsule shells are ruptured by mechanical stress, the solution is released, leading to evaporation of the hexyl acetate (Fig. 1B). This evaporation causes the TPE to aggregate, emitting blue light under UV-A irradiation (Fig. 1D). After successfully fabricating the microcapsules, tensile specimens were prepared via molding. The specimens were produced by incorporating 10 wt% microcapsules into commercially available poly(dimethylsiloxane) (PDMS), Sylgard 184 (Dow, Midland, USA). The mixture was degassed, then poured into two-piece molds machined from poly(methyl methacrylate) (PMMA), and cured in an oven at 100 °C for 30 min. Each fabrication batch produced at least five specimens with dimensions closely resembling ISO 37 type 2, along with a reference disk-shaped specimen of 20 mm in diameter.

The PDMS-microcapsule composite with intact capsules initially exhibits negligible emission in the blue region of the visible spectrum (λ_{max} = 455 nm) under UV-A irradiation (λ = 365 nm) (Fig. 1E). When the shells of the microcapsules in the composite were ruptured by mechanical stress (e.g., stretching), fluorescence (λ_{max} = 455 nm) became observable (Fig. 1F). The intact specimens were then mechanically tested using a uniaxial testing machine (ZwickRoell, Ulm, Germany) equipped with a 500 N load cell (Fig. 2). To monitor changes in fluorescence, the specimens were continuously illuminated with UV-ring light (λ = 365–375 nm), and a video was recorded using a CMOS camera (IDS UI-3880CP, IDS Imaging Development Systems GmbH, Obersulm, Germany) synchronized with the testing machine. A reference disk (non-damaged) was included within the video frame, while the entire test setup was covered with light-tight fabric to minimize the influence of ambient light.

The mechanical testing procedure included two different types of loading, both conducted in displacement-controlled settings. During the so-called load cycle, the specimen was stretched to a predefined displacement, triggering the partial breaking of the embedded capsules, and then unloaded to zero force. While it is almost impossible to accurately count the number of broken capsules, their number positively correlates with the magnitude of the applied deformation. As will be shown later, larger applied deformation is associated with more pronounced changes in the composite's behavior. To evaluate Young's modulus, so-called probing cycles were used before (20 cycles) and after (880 cycles) the load cycle (Fig. 2B). Each probing cycle consisted of stretching up to 2 mm at a rate of 8 $\mathrm{mm\,min^{-1}}$, followed by unloading to zero force at the same rate and a subsequent hold time of 30 s. Preliminary tests indicated that such a small stretch does not cause capsule rupture but allows the assessment of Young's modulus from force–displacement data. Stress was calculated from the force by dividing it by the initial cross-section in the center of the specimen, while strain was obtained by referencing the initial length of the specimen (i.e., the distance between fixtures). A correction factor of 0.52, determined by

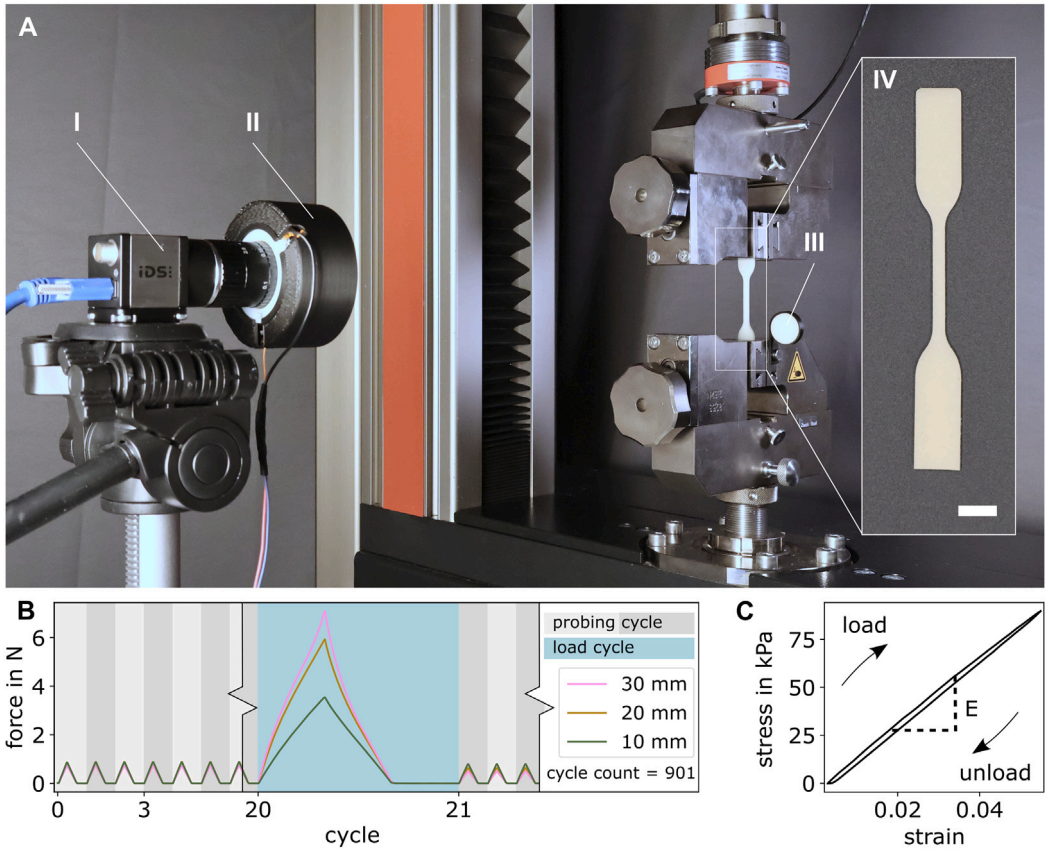


Fig. 2. (A): Test setup. I: Video camera, II: UV ring light (λ = 365–375 nm), III: Cylindrical reference specimen from the same batch as the tensile specimen, IV: Tensile specimen, scale bar = 10 mm. (B): Schematic of the testing procedure. Probing cycles are shown with light and dark gray backgrounds, while the load cycle is shown with a blue background. Each probing cycle includes a displacement-controlled load up to 2 mm, followed by unloading to zero force and a 30 s hold time. The force output in the load cycle is displayed for 30 mm, 20 mm, and 10 mm. Note that this cycle has different x-axis scaling for the three specimens. (C): Stress–strain curve of a single probing cycle, with the depiction of Young's modulus evaluation as the slope of the loading section. (For interpretation of the references to color in this figure legend, the reader is referred to the web version of this article.)

finite element simulations in COMSOL Multiphysics 6.0 (Comsol AB, Stockholm, Sweden), was applied to recalculate the strain occurring in the central gauge section, following the methodology described in [36]. Young's modulus was subsequently calculated as the slope of the linear section of the curve, as shown in Fig. 2C, and was approximately 30% higher for intact specimens as compared to pure PDMS.

To evaluate the fluorescent response due to broken microcapsules at each moment in time, the recorded video was analyzed. Pixel values were averaged over the central region of the specimen, referenced to the brightness of the non-damaged disk captured in each frame, and normalized to the initial value. This method demonstrated good correlation with spectrographic measurements (see Appendix) while offering the advantage of capturing a larger area. Similarly, Diekmann et al. demonstrated that CMOS-equipped cameras are suitable for fluorescence detection [40]. For each strain level during the loading cycle, at least three specimens were tested to ensure statistically robust conclusions.

3. Results and discussion

As-fabricated specimens exhibit a certain level of fluorescence, possibly due to initially broken capsules or damage introduced during de-molding. However, the first probing cycles confirm that no further capsule rupture occurs during testing (Fig. 3, left). Immediately after the loading cycle, the central section of the specimen begins to fluoresce, indicating the rupture of some microcapsules within the matrix and the subsequent release of their contents (Fig. 3, middle). Over time, the fluorescence intensity increases, and after 15 h, the specimen appears visibly brighter (Fig. 3, right) compared to its state immediately after the loading cycle. This observation highlights the transient nature of the self-reporting mechanism.

Fig. 4 illustrates the evolution of Young's modulus and fluorescence response following the loading cycle for specimens subjected to different strain levels. A noticeable increase in fluorescence response is observed immediately after the loading cycle, attributed to the release of contents from ruptured capsules. This increase is minimal for an applied displacement of 5 mm but becomes evident starting at 10 mm, with the magnitude of the increase growing as the displacement rises. The most pronounced fluorescence response is observed at a displacement of 30 mm (Fig. 4A). Since all other conditions were kept constant, we conclude that the increased brightness immediately after the loading cycle at higher strain levels is due to a larger number of broken capsules. While a single capsule can provide limited information about its state, the presence of multiple capsules significantly enhances the reporting capabilities. Under global deformation, such as uniaxial tension, capsules embedded in a soft matrix do not rupture simultaneously. Since directly counting the number of broken capsules is nearly impossible, indirect measures, such as changes in fluorescence or stiffness, can serve as proxies. In this case, larger changes correspond to a higher number of ruptured capsules, indicating greater achieved stresses and more significant damage. A similar approach has been shown to be effective even for relatively localized loading in microcapsule-based composites [21,34]. Simultaneously, our experiments show that for all specimens, the brightness does not remain constant but continues to

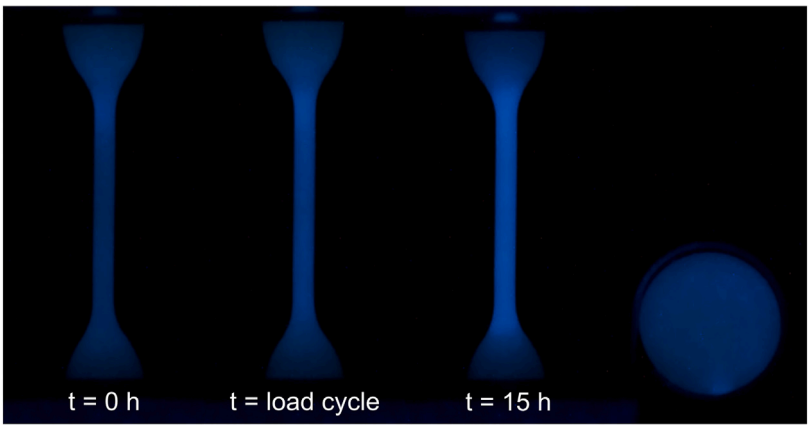


Fig. 3. Fluorescence of the tensile specimen before start of the test, immediately after loading cycle, and after 15 h (left to right). Reference cylindrical sample is shown as well. The brightness has been uniformly enhanced for visualization purposes.

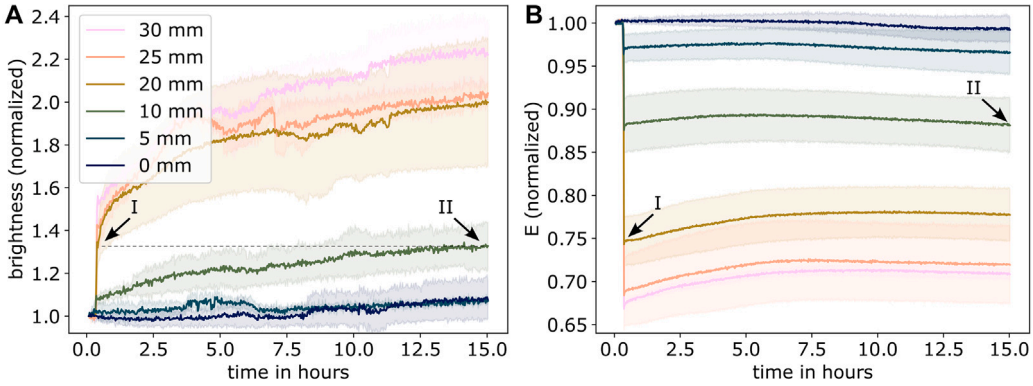


Fig. 4. Normalized brightness (A) and normalized Young's modulus (B) over time after loading to different displacements, with solid lines representing the mean and shaded areas indicating the standard deviation.

increase over the 15-hour period following the loading cycle (Fig. 4A). This effect is particularly evident for the 30 mm loading, which exhibits a 1.5-fold increase in brightness immediately after capsule rupture, with the final brightness recorded after 15 h reaching 2.2 times the initial value. The final brightness (after 15 h) follows a trend similar to the immediate post-load brightness, being higher for specimens subjected to larger displacements. Transient brightness changes after the loading cycle and capsule rupture make it difficult to correlate absolute brightness with the amount of damage unless sufficient time has passed.

As depicted in Fig. 4B, the rupture of microcapsules during loading significantly affects the composite's Young's modulus. Upon capsule breaking, we observe an immediate drop in Young's modulus of over 30% for larger displacements, such as 25 or 30 mm. At the same time, similar to the absence of immediate changes in brightness, there is no change in Young's modulus for specimens loaded only up to 2 mm, confirming that no capsules are ruptured in this case. With increasing applied displacement, the drop in Young's modulus becomes more pronounced immediately after the loading cycle. Simultaneously, a slight but gradual increase in Young's modulus is observed for specimens subjected to higher loads. This effect, though much less pronounced than the brightness changes, is primarily associated with the evaporation of solvent from the ruptured capsules and possible interaction between solvent and PDMS matrix. By combining observations of brightness and mechanical performance, we can conclude that relying solely on increase in brightness to assess damage, without considering time, can be misleading. For instance, a 30% increase in brightness might correspond to a drop in Young's modulus to 75% of its initial value if measured immediately after loading (Fig. 4, arrow I). However, if measurements are taken 15 h later, the same brightness increase may correspond to a smaller drop, down to 90% of the initial modulus (Fig. 4, arrow II).

Since both mechanical properties and fluorescence depend on the degree of damage — determined by the applied displacement during the loading cycle — it seems possible to establish a correlation by factoring in time. When the time after the loading cycle is fixed, specimens subjected to higher strains are expected to show greater changes in elastic modulus and brighter fluorescence due to the rupture of more capsules. To investigate this relationship, we plotted brightness against Young's modulus for individual specimens at three different points in time: immediately after loading (Fig. 5A), 5 hours after the start (Fig. 5B), and at the end of the observation period (Fig. 5C). Simplifying, we took the data from Fig. 4 and sliced for each selected time point.

Figs. 5A-C display a linear fit with the corresponding R^2 values, while the color represents the applied displacement during the loading cycle. Previous studies have suggested that the relationship between fluorescence and damage is generally linear, with saturation occurring when most capsules have ruptured [34]. This saturation is evident, for example, in Fig. 4B, where the properties of samples stretched to 25 mm and 30 mm are nearly identical. Our experiments further revealed that for displacements exceeding 30 mm, the PDMS matrix itself begins to fail. For the three selected times shown in Figs. 5A-C, the linear fit provides a good approximation of the dependency of Young's modulus on brightness, with R^2 values ranging from 0.9 at $t = 0$ h to 0.88 at $t = 15$ h. The data clearly shows that larger displacements result in brighter specimens and lower relative Young's modulus after capsule rupture. However, our findings also highlight an intrinsic feature of

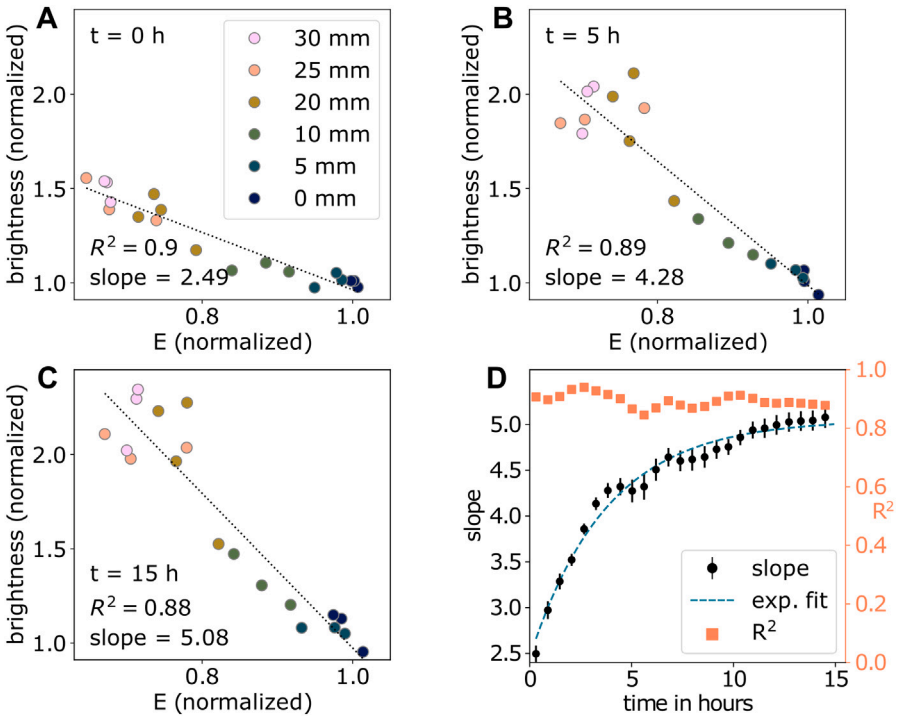


Fig. 5. Normalized brightness and normalized Young's modulus immediately after loading cycle (A), after 5 h (B), after 15 h (C). (D): Slope of the linear fit (black circles), exponential decay fit (blue line) and correlation coefficient R^2 (orange squares) over time.

self-reporting microcapsule composites: while the relationship between brightness and Young's modulus is close to linear, it evolves over time.

By performing a similar analysis and linear fitting for all available times up to 15 h, we observe that the assumption of a near-linear dependency between changes in Young's modulus and fluorescence holds true. The orange curve in Fig. 5D shows that the R^2 value for the linear fit (orange squares) remains consistently around 0.9 over time. The coefficient of proportionality m (black circles) increases over the course of the experiment, and eventually stabilizes (Fig. 5D). The coefficient m for brightness–stiffness correlation can be approximated as exponential decay function $m = m_\infty + (m_0 - m_\infty)e^{-t/\tau}$ (blue dashed line), where m_0, m_∞ and τ are fitting parameters, well-aligned with the kinetics of the evaporation process. Over time, the relationship between brightness and Young's modulus becomes more consistent as transient effects diminish and the system reaches equilibrium. This observed time-dependent evolution of the fluorescence-mechanics relationship may extend to other self-reporting composite systems, emphasizing the importance of considering temporal dynamics when interpreting damage indications.

4. Conclusions

By tracking and analyzing changes in Young's modulus and fluorescence over 15 h following the rupture of microcapsules embedded in PDMS matrix, we observed a clear correlation between fluorescence intensity and residual mechanical properties. However, the transient nature of this relationship must be considered. Fluorescence self-reporting occurs immediately after loading in the central section of the specimen, provided the applied load is sufficiently high. In this study, stretching up to 2 mm did not cause capsule rupture, while already a 5 mm displacement triggered fluorescence and a drop in Young's modulus. Both the fluorescence intensity and the decrease in Young's modulus were more pronounced for specimens subjected to higher loading, reflecting the extent of damage and the amount of ruptured capsules. While this behavior is somehow expected [13,34], the visible brightness continues to increase long after capsule rupture due to the gradual solvent evaporation process required for fluorescence. This highlights the importance of accounting for the time elapsed since the damaging event when correlating fluorescence with mechanical properties, as the transient nature of this relationship affects its accuracy. While the qualitative rule of "more damage — brighter fluorescence — lower stiffness" holds true, the exact relationship is time-dependent.

Our results demonstrate that the property–brightness relationship in the studied PDMS-microcapsule composite can be approximated as linear at any given moment, though the slope of this linear fit evolves over time and stabilizes several hours after capsule rupture. This aspect may not be critical when self-reporting is primarily used to locate damage within the matrix. In such cases, both the capsules and the load-bearing matrix material are often damaged simultaneously [14,17,21], particularly when cracks propagate through the material [9,12,13,31]. However, self-reporting can also be valuable in scenarios where capsule rupture occurs before significant matrix damage, as observed in the present study. Here, even after capsule rupture, the specimen retains its structural integrity and can withstand a slightly reduced load. Potentially, this mechanism enables the release of a self-healing agent while the matrix remains intact. Depending on the system's design, fluorescence-based self-reporting can complement self-healing in different ways. If the same capsules contain both the reporting and healing agents, fluorescence serves not only as a direct indicator of healing agent release but also as a measure of damage severity. Additionally, in the considered composites, where the elastic matrix remains intact, it becomes possible to preemptively release specific functional additives before the composite reaches total failure. In this case, fluorescence highlights the locations where specific criteria, such as reaching a critical stress level, have been met, facilitating localized changes through an additional chemical process. In general, the fluorescence of a self-reporting composite can indicate not only the extent of a specimen's property deterioration but also how close it has come to failure during previous loading. However, to achieve accurate assessments, we have shown that it is important to consider the time-dependent nature of the brightness–property relationship.

CRediT authorship contribution statement

David Schwarz: Writing – original draft, Methodology, Investigation, Formal analysis, Conceptualization. **Viacheslav Slesarenko:** Writing – review & editing, Validation, Supervision, Methodology, Funding acquisition, Conceptualization.

Declaration of Generative AI and AI-assisted technologies in the writing process

During the preparation of this work the authors used ChatGPT in order to check the grammar and slightly improve readability. After using this tool/service, the authors reviewed and edited the content as needed and take full responsibility for the content of the publication.

Declaration of competing interest

The authors declare that they have no known competing financial interests or personal relationships that could have appeared to influence the work reported in this paper.

Acknowledgments

The authors thank Dr. Celine Calvino and Dr. Claas-Hendrik Stamp for preparing the capsules and engaging in fruitful discussions. Funded by the Deutsche Forschungsgemeinschaft (DFG, German Research Foundation) under Germany's Excellence Strategy - EXC-2193/1 - 390951807. Open access funding enabled and organized by Projekt DEAL.

Appendix. Comparison of CMOS camera and spectrometer

To validate the use of the camera for fluorescence evaluation, we measured the specimens before and after the tests using a blue-wave spectrometer (StellarNet Inc., Tampa, FL, USA) and a 365 nm light source (Ocean Optics, Orlando, FL, USA). The measurements showed strong agreement, with $R^2 = 0.97$ (Fig. A.6), confirming the camera's suitability for our purposes.

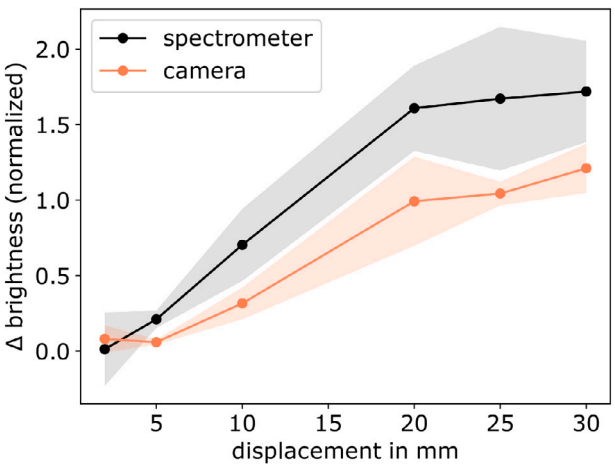


Fig. A.6. Relative change in brightness between intact specimen and after testing completion. Comparison between camera-based evaluation and spectrometer measurements, with solid points representing the mean and shaded areas indicating the standard deviation.

Data availability

Data will be made available on request.

References

[1] D.K. Rajak, D.D. Pagar, R. Kumar, C.I. Pruncu, Recent progress of reinforcement materials: a comprehensive overview of composite materials, J. Mater. Res. Technol. 8 (6) (2019) 6354–6374, http://dx.doi.org/10.1016/j.jmrt.2019.09.068.
[2] J. Pang, I. Bond, Bleeding composites—damage detection and self-repair using a biomimetic approach, Compos. Part A: Appl. Sci. Manuf. 36 (2) (2005) 183–188, http://dx.doi.org/10.1016/s1359-835x(04)00166-6.
[3] J.W. Pang, I.P. Bond, A hollow fibre reinforced polymer composite encompassing self-healing and enhanced damage visibility, Compos. Sci. Technol. 65 (11–12) (2005) 1791–1799, http://dx.doi.org/10.1016/j.compscitech.2005.03.008.
[4] H. Chang, Z. Guo, C. Chen, H. Zhang, Z. Li, X. Wang, J. Liu, Mechanical properties, durability and self-healing performance of mortar containing double-layers capsules, Mater. Today Commun. 38 (2024) 107880, http://dx.doi.org/10.1016/j.mtcomm.2023.107880.
[5] M.M. Caruso, B.J. Blaiszik, S.R. White, N.R. Sottos, J.S. Moore, Full recovery of fracture toughness using a nontoxic solvent-based self-healing system, Adv. Funct. Mater. 18 (13) (2008) 1898–1904, http://dx.doi.org/10.1002/adfm.200800300.
[6] C.E. Diesendruck, N.R. Sottos, J.S. Moore, S.R. White, Biomimetic self-healing, Angew. Chem. Int. Ed. 54 (36) (2015) 10428–10447, http://dx.doi.org/10.1002/anie.201500484.
[7] S.A. McDonald, S.B. Coban, N.R. Sottos, P.J. Withers, Tracking capsule activation and crack healing in a microcapsule-based self-healing polymer, Sci. Rep. 9 (1) (2019) http://dx.doi.org/10.1038/s41598-019-54242-7.
[8] H. Yuan, H. Chen, M.I. Khan, Z. Lv, J. Lin, Analytical models for crack-hitting probability and crack-healing efficiency by linear capsules in a material with parallelogram crack network, Mater. Today Commun. 41 (2024) 111048, http://dx.doi.org/10.1016/j.mtcomm.2024.111048.
[9] S.R. White, N.R. Sottos, P.H. Geubelle, J.S. Moore, M.R. Kessler, S.R. Sriram, E.N. Brown, S. Viswanathan, Autonomic healing of polymer composites, Nature 409 (6822) (2001) 794–797, http://dx.doi.org/10.1038/35057232.
[10] E.N. Brown, N.R. Sottos, S.R. White, Fracture testing of a self-healing polymer composite, Exp. Mech. 42 (4) (2002) 372–379, http://dx.doi.org/10.1007/bf02412141.
[11] D.Y. Zhu, M.Z. Rong, M.Q. Zhang, Self-healing polymeric materials based on microencapsulated healing agents: From design to preparation, Prog. Polym. Sci. 49–50 (2015) 175–220, http://dx.doi.org/10.1016/j.progpolymsci.2015.07.002.
[12] M. Kosarli, D.G. Bekas, K. Tsirka, D. Baltzis, D.T. Vaimakis-Tsogkas, S. Orfanidis, G. Papavassiliou, A.S. Paipetis, Microcapsule-based self-healing materials: Healing efficiency and toughness reduction vs. capsule size, Compos. Part B: Eng. 171 (2019) 78–86, http://dx.doi.org/10.1016/j.compositesb.2019.04.030.
[13] V.K. Mohonee, K.L. Goh, L. Mishnaevsky, P. Pasbakhsh, Capsule based self-healing composites: New insights on mechanical behaviour based on finite element analysis, Comput. Mater. Sci. 192 (2021) 110203, http://dx.doi.org/10.1016/j.commatsci.2020.110203.
[14] Y. Wang, W. Tan, X. Luo, X. Rao, Y. Wang, J. Wang, W. Suphamitmongkol, T. Chowwanonthapunya, L. Ma, D. Zhang, A novel self-healing coating with mechanically-triggered self-reporting properties: Color and fluorescence dual damage indications, Prog. Org. Coatings 187 (2024) 108147, http://dx.doi.org/10.1016/j.porgcoat.2023.108147.
[15] V.H. de Souza Rodrigues, A. Estêvão Carrara, S.S. Rossi, L. Mattos Silva, R. de Cássia Lazzarini Dutra, J.C.N. Dutra, Synthesis, characterization and qualitative assessment of self-healing capacity of PU microcapsules containing TDI and IPDI as a core agent, Mater. Today Commun. 21 (2019) 100698, http://dx.doi.org/10.1016/j.mtcomm.2019.100698.
[16] Z. Yin, J. Guo, J. Qiao, X. Chen, Improved self-healing properties and crack growth resistance of polydimethylsiloxane elastomers with dual-capsule room-temperature healing systems, Colloid Polym. Sci. 298 (1) (2019) 67–77, http://dx.doi.org/10.1007/s00396-019-04587-2.
[17] E.T.A. van den Dungen, B. Loos, B. Klumperman, Use of a profluorophore for visualization of the rupture of capsules in self-healing coatings, Macromol. Rapid Commun. 31 (7) (2010) 625–628, http://dx.doi.org/10.1002/marc.200900728.
[18] S.A. Odom, A.C. Jackson, A.M. Prokup, S. Chayanupatkul, N.R. Sottos, S.R. White, J.S. Moore, Visual indication of mechanical damage using core–shell microcapsules, ACS Appl. Mater. Interfaces 3 (12) (2011) 4547–4551, http://dx.doi.org/10.1021/am201048a.
[19] S. Vidinejevs, O. Strekalova, A. Aniskevich, S. Gaidukov, Development of a composite with an inherent function of visualization of a mechanical action, Mech. Compos. Mater. 49 (1) (2013) 77–84, http://dx.doi.org/10.1007/s11029-013-9323-9.
[20] J.F. Patrick, M.J. Robb, N.R. Sottos, J.S. Moore, S.R. White, Polymers with autonomous life-cycle control, Nature 540 (7633) (2016) 363–370, http://dx.doi.org/10.1038/nature21002.
[21] M.J. Robb, W. Li, R.C.R. Gergely, C.C. Matthews, S.R. White, N.R. Sottos, J.S. Moore, A robust damage-reporting strategy for polymeric materials enabled by aggregation-induced emission, ACS Central Sci. 2 (9) (2016) 598–603, http://dx.doi.org/10.1021/acscentsci.6b00198.
[22] Y. Yoo, C. Martinez, J.P. Youngblood, Sustained dye release using Poly(urea–urethane)/cellulose nanocrystal composite microcapsules, Langmuir 33 (6) (2017) 1521–1532, http://dx.doi.org/10.1021/acs.langmuir.6b04628.

[23] R. Rajamanickam, K. Kwon, G. Tae, Soft and elastic hollow microcapsules embedded silicone elastomer films with enhanced water uptake and permeability for mechanical stimuli responsive drug delivery applications, Mater. Sci. Eng.: C 111 (2020) 110789, http://dx.doi.org/10.1016/j.msec.2020.110789.
[24] C. Calvino, E. Henriet, L.F. Muff, S. Schrettl, C. Weder, Mechanochromic polymers based on microencapsulated solvatochromic dyes, Macromol. Rapid Commun. 41 (7) (2020) http://dx.doi.org/10.1002/marc.201900654.
[25] M. Hu, Z. Ma, M. Kim, D. Kim, S. Ye, S. Pané, Y. Bao, R.W. Style, L. Isa, Self-reporting multiple microscopic stresses through tunable microcapsule arrays, Adv. Mater. (2024) http://dx.doi.org/10.1002/adma.202410945.
[26] P. Scholle, M. Sinapius, Influence of the electrical anisotropy of unidirectional carbon fiber reinforced plastics on their self strain sensing properties, Compos. Part C: Open Access 8 (2022) 100256, http://dx.doi.org/10.1016/j.jcomc.2022.100256.
[27] H. Ono, Micromechanical analysis for effective elastic moduli and thermal expansion coefficient of composite materials containing ellipsoidal fillers oriented randomly, Compos. Part C: Open Access 14 (2024) 100482, http://dx.doi.org/10.1016/j.jcomc.2024.100482.
[28] A. Teimouri, R. Barbaz Isfahani, S. Saber-Samandari, M. Salehi, Experimental and numerical investigation on the effect of core-shell microcapsule sizes on mechanical properties of microcapsule-based polymers, J. Compos. Mater. 56 (18) (2022) 2879–2894, http://dx.doi.org/10.1177/00219983221107831.
[29] W. Meier, Polymer nanocapsules, Chem. Soc. Rev. 29 (5) (2000) 295–303, http://dx.doi.org/10.1039/a809106d.
[30] M. Hu, S. Peil, Y. Xing, D. Döhler, L.C. da Silva, W.H. Binder, M. Kappl, M.B. Bannwarth, Monitoring crack appearance and healing in coatings with damage self-reporting nanocapsules, Mater. Horizons 5 (1) (2018) 51–58, http://dx.doi.org/10.1039/c7mh00676d.
[31] M. Keller, S. White, N. Sottos, A self-healing Poly(Dimethyl Siloxane) elastomer, Adv. Funct. Mater. 17 (14) (2007) 2399–2404, http://dx.doi.org/10.1002/adfm.200700086.
[32] A. Tabatabaeian, S. Liu, P. Harrison, E. Schlangen, M. Fotouhi, A review on self-reporting mechanochromic composites: An emerging technology for structural health monitoring, Compos. Part A: Appl. Sci. Manuf. 163 (2022) 107236, http://dx.doi.org/10.1016/j.compositesa.2022.107236.
[33] C. Calvino, A. Guha, C. Weder, S. Schrettl, Self-calibrating mechanochromic fluorescent polymers based on encapsulated excimer-forming dyes, Adv. Mater. 30 (19) (2018) 1704603, http://dx.doi.org/10.1002/adma.201704603.
[34] C. Calvino, C. Weder, Microcapsule-containing self-reporting polymers, Small 14 (46) (2018) 1802489, http://dx.doi.org/10.1002/smll.201802489.
[35] C. Calvino, Polymer-based mechanochromic composite material using encapsulated systems, Macromol. Rapid Commun. 42 (1) (2020) 2000549, http://dx.doi.org/10.1002/marc.202000549.
[36] F. Schneider, T. Fellner, J. Wilde, U. Wallrabe, Mechanical properties of silicones for MEMS, J. Micromech. Microeng. 18 (6) (2008) 065008, http://dx.doi.org/10.1088/0960-1317/18/6/065008.
[37] M.M. Caruso, B.J. Blaiszik, H. Jin, S.R. Schelkopf, D.S. Stradley, N.R. Sottos, S.R. White, J.S. Moore, Robust, double-walled microcapsules for self-healing polymeric materials, ACS Appl. Mater. Interfaces 2 (4) (2010) 1195–1199, http://dx.doi.org/10.1021/am100084k.
[38] M.W. Keller, N.R. Sottos, Mechanical properties of microcapsules used in a self-healing polymer, Exp. Mech. 46 (6) (2006) 725–733, http://dx.doi.org/10.1007/s11340-006-9659-3.
[39] C.-H. Stamp, J. Stumpp, C. Calvino, Adhesives with debonding-on-demand capability: Leveraging responsive microcapsules for mechanically-induced debonding, Adv. Mater. (2025) e2414308, http://dx.doi.org/10.1002/adma.202414308.
[40] R. Diekmann, K. Till, M. Müller, M. Simonis, M. Schüttpelz, T. Huser, Characterization of an industry-grade CMOS camera well suited for single molecule localization microscopy – high performance super-resolution at low cost, Sci. Rep. 7 (1) (2017) http://dx.doi.org/10.1038/s41598-017-14762-6.

3.3 Light Induced Training Enabled by Crosslinking in 3D Printed Mechanical Metamaterials

Authors: David Schwarz (equal), Johan Liotier (equal), Viacheslav Slesarenko, Jürgen Rühe
Journal: Advanced Materials Technologies
Date: 17.10.2025
DOI: https://doi.org/10.1002/admt.202501416

Author	Contributions
David Schwarz	Designed, printed, tested and evaluated the specimens and built the training system, writing – original draft
Johan Liotier	Synthesized the crosslinker and prepared the filament, conceived and supervised the research, writing – original draft
Viacheslav Slesarenko	Writing – review & editing, validation, supervision, methodology, funding acquisition, conceptualization
Jürgen Rühe	Writing – review & editing, validation, supervision, methodology, funding acquisition, conceptualization

The article is open access under the CC BY license (http://creativecommons.org/licenses/by/4.0/) and reprinted without changes.

Context and Personal Assessment

The unconventional responses of mechanical metamaterials to deformation arise from their geometric features. Hence, they can be precisely tuned, as demonstrated in Section 3.1. Another strategy for designing a response into a material involves composites. One example is the self-reporting material in Section 3.2, which combines a matrix and microcapsules. To create an adaptive, trainable material that goes beyond these approaches, it is possible to establish a connection between the response of the geometry and the base material.

A variety of artificial materials have achieved stimuli-responsiveness. Hydrogels swell in response to humidity [100], liquid crystal elastomers are responsive to light or temperature [101], and shape memory alloys exhibit programmable shape-morphing [102]. Yet, such materials lack the ability to accumulate changes in response to repeated stimuli, unlike biological systems such as muscles that grow under repeated loading [103] or leafs that adapt their morphology to environmental conditions [104]. To expand the achievable shapes and responses in artificial systems, recent efforts have focused on using stimuli-responsive materials in additive manufacturing [11]. This enabled an artificial flower that opens and closes with changing temperatures [105]. However, in these examples, there is no accumulated change of the response. Hence, to obtain life-like material systems resembling natural adaptation, coupling and retention between stimulus and response must be established.

In the presented work, we set out to combine two types of responses: the geometry's ability to respond to deformation (Section 3.1) and the base material's ability to change its stiffness (Section 3.2). The resulting closed-loop system allows for a response that changes with repeated stimuli, thereby enabling trainable mechanical behavior. A commercially available TPU filament for FFF 3D printing is functionalized by C,H-insertion chemistry, as described by Liotier et al. [18]. The molecule, covalently attached to the polymer chains, enables UV-induced crosslinking, which in turn impacts the material's mechanical properties. Subsequently, I successfully print and test tensile specimens, which reveal four crucial properties of the novel material. First, upon irradiation in a UV chamber, the stiffness can be increased to 300%. However, prolonged exposure causes material degradation, limiting further stiffening. Second, an immediate onset of the stiffening occurs when irradiated during stiffness-probing, though it is less pronounced due to the reduced intensity of the UV lights attached to the test setup. Third, intermittent irradiation shows that stiffening is instant and persistent after the lights are turned off. Finally, specimens irradiated under larger deformations exhibit a permanent elongation. When the

specimen is irradiated while stretched, its length increases compared with irradiation during smaller deformations.

Building on the material's properties, I subsequently apply it to responsive mechanical structures. The structure with circular cutouts (Table 2.1), adapted from Bertoldi et al. [9], serves to visualize local stiffening. Under sufficient compression, the circular holes collapse into elliptical shapes, driven by instabilities. Selective irradiation of one half of the specimen leads to an asymmetry during loading: the non-irradiated side collapses, whereas the irradiated side remains stiff, showcasing the localized stiffness-tunability. To close the loop between mechanical deformation and irradiation, I integrate the mechanical metamaterial from Section 3.1 in a setup with an optical switch to control UV lights. When compressed beyond its designed expansion strain, the metamaterial triggers the UV irradiation, causing its base material to stiffen. Repeated loading cycles lead to saturation of the response, effectively adapting the system to the loading condition. Finally, by introducing two types of forces, I demonstrate threshold training. Utilizing the metamaterial's expansion under compression, the larger force triggers an irradiation event during a subsequent unloaded hold, while the smaller force is not sufficient to trigger the event. When the forces are applied in a training schedule, the metamaterial is stiffened when the larger force occurs. After several training cycles, the metamaterial stiffens enough so that the larger force no longer induces irradiation, and the system is successfully trained to resist the stimulus.

The presented work highlights that responses can be engineered on two interconnected levels: the structural (metamaterial) level and the base material (polymer) level. This coupling enables local stiffening, as shown by the tilted block with holes. Previous works achieved local or graded mechanical properties in mechanical metamaterials by varying the geometry of the unit cell at the design stage [38]. Our approach achieves local stiffness changes dynamically, post-fabrication, through controlled crosslinking. The demonstration of a trainable, closed-loop system shows how metamaterial structures might become capable of adapting to their environment. Finally, the concept of threshold training provides a foundation for more intelligent material systems, in which scheduled stiffening acts as a form of memory, reminiscent of learning concepts proposed by Zhang et al. [106].

Check for updates

RESEARCH ARTICLE

Editor's Choice

ADVANCED MATERIALS TECHNOLOGIES

www.advmattechnol.de

Light Induced Training of 3D Printed Mechanical Metamaterials

David Schwarz, Johan Liotier, Viacheslav Slesarenko,* and Jürgen Rühe*

Stimuli-responsive materials often react to changes in environmental conditions by altering their shape. Here, it is shown that even changes in materials that are not directly observable, such as local stiffening, can be exploited to introduce the concept of trainable materials. A fully 3D-printable filament based on thermoplastic polyurethane (TPU) functionalized with a bivalent crosslinker capable of undergoing a C,H insertion reaction under UV irradiation was developed. Specimens printed from this filament demonstrate a gradual increase in stiffness, reaching almost 300% of their initial stiffness after 50 hours of irradiation. To exploit this tunability, mechanical metamaterials incorporating the developed material are engineered. By utilizing an instability-driven transformation under compression, it is demonstrated how local stiffening can be amplified through rational design. Moreover, by exploiting the unusual mechanical behavior of metamaterials arising from their internal architecture, a closed-loop system is presented in which, under compressive load, the metamaterial closes an electric circuit that activates UV light, which in turn modifies the properties of the base material. Through this approach, two trainable systems are realized: one that progressively conforms its shape to mechanical compression, and another that gradually increases its resistance to an applied force, mimicking the physical training of biological tissues.

1. Introduction

Nature offers a wide variety of examples of adaptation: upon repeated stimuli, muscles grow,[1] bones become stronger,[2,3] and leaf petioles change shape.[4] In engineering practice, we still often rely on materials with persistent properties, which is reasonable for many applications. At the same time, materials such as shape memory alloys,[5,6] polymers,[7,8] liquid crystal elastomers,[9,10] and hydrogels[11,12] alter their shape and behavior in response to temperature,[13] humidity,[14] or pH.[15] This allows their use as components of larger systems, usually as actuators. Materials may also undergo changes that do not directly manifest as a change in shape, for example, through color variation in self-reporting systems[16–18] or through stiffening.[19–21] The ability to store or even accumulate such changes is associated with the phenomenon of memory, which has been conceptually realized and observed on both the material[22] and structural level.[23] If changes in mechanical properties (e.g., stiffening) are not accompanied by a shape change, they can still be revealed under specific conditions, for example, when an external load is applied. Noticeably, even small variations can be amplified if the structure is rationally designed, as in the case of mechanical metamaterials.

Mechanical metamaterials are often defined as materials with rationally and purposefully designed internal architectures that give rise to a desired set of unorthodox mechanical properties.[24] Such architectures enable the realization of metamaterials that exhibit negative effective stiffness,[25] close-to-zero shear modulus,[26] or coupling between different deformation modes.[27,28] Among the most common manifestations of these unusual properties is a negative Poisson's ratio in so-called auxetic metamaterials.[29] Auxetic behavior can be found in some biological materials,[30] but more often it is engineered in artificial metamaterials via the rational design of the elementary building block, the unit cell, which periodically repeats throughout the metamaterial.[31] Within the unit cell, intricate connections of beams allow the engineering of the material's overall response to mechanical load. Elegantly, this design is geometric and therefore less sensitive to the unit cell's dimensions and base material. Hence, their functionality can be achieved over multiple length scales and base materials, ranging from nano- and micrometers[27,32,33] for micro-electromechanical systems (MEMS) to meters[34] for seismic shields. By further

D. Schwarz, J. Liotier, V. Slesarenko, J. Rühe
Cluster of Excellence livMatS@FIT - Freiburg Center for Interactive Materials and Bioinspired Technologies
University of Freiburg
79110 Freiburg, Germany
E-mail: johan.liotier@livmats.uni-freiburg.de; viacheslav.slesarenko@livmats.uni-freiburg.de

J. Liotier, J. Rühe
Department of Microsystems Engineering (IMTEK)
Laboratory for Chemistry and Physics of Interfaces
Albert-Ludwigs-Universität Freiburg
79110 Freiburg, Germany

The ORCID identification number(s) for the author(s) of this article can be found under https://doi.org/10.1002/admt.202501416

© 2025 The Author(s). Advanced Materials Technologies published by Wiley-VCH GmbH. This is an open access article under the terms of the Creative Commons Attribution License, which permits use, distribution and reproduction in any medium, provided the original work is properly cited.

DOI: 10.1002/admt.202501416

modifying the internal connections within the unit cell, more advanced functionalities such as logic gates or memory[23,35] are achievable. By carefully designing the elements to allow for self-contact, switching the sign of Poisson's ratio during deformation seems possible. For instance, initially auxetic metamaterials can, upon sufficient compression, expand beyond their initial width.[36] At the same time, even such complex mechanical responses are fixed at the design stage and normally cannot be changed after fabrication. To add new functionalities and enable changes in the mechanical behavior of already fabricated metamaterials, stimuli-responsive materials can be integrated into the metamaterial architecture.[37]

There are several possible approaches that can add stimuli sensitivity to existing polymers. Among them, C,H insertion crosslinking (CHic) is a chemical strategy to achieve a crosslinked polymer network. With this method, it is possible to crosslink polymers without catalysis in the solid state using only heat or UV-irradiation.[38–42] Upon triggering, reactive moieties are activated and react with neighboring C–H bonds to create crosslink points. The resulting covalent C–C bonds create a strongly bonded network. In addition, the reaction is non-specific, allowing to be used regardless of the polymer backbones and even to link additives in the network such as fluorescent dyes or biological molecules.[43] After crosslinking, the properties of the material changes drastically, notably regarding mechanical properties, solvent resistance and heat resistance.[44,45] These moieties are usually incorporated into the desired precursor polymer by copolymerization with the desired comonomer, thus limiting polymer usage. To avoid that, we recently developed a bivalent crosslinker able to be inserted into the polymer chain post polymerization.[46] This methodology is interesting as it does not require to know the exact structure of the polymer, only C–H bonds must be present, a requirement fulfilled for practically any polymer. This method allows the use of commercial polymers and to an extent also commercial 3D printable materials.

Being able to treat commercially available 3D printable materials opens new possibilities. Treating a commercial filament allows to easily obtain large amounts of polymer, omitting elaborate synthesis. Indeed, the necessary amount of crosslinker needed to obtain a then crosslinkable material is comparatively low, thus reducing the synthetic effort needed.[46] Here we set out to introduce CHic chemistry into a 3D printed structure to achieve a novel, trainable material system. The main goal is to exploit the ability of a CHic-treated polymer to change its stiffness upon UV irradiation and to transform such changes into unconventional, trainable behavior through the rational architecture of a mechanical metamaterial (**Figure 1**). The realization of a metamaterial capable of accumulating information about previous mechanical and non-mechanical stimuli and changing its behavior accordingly can open new approaches in emerging fields such as soft robotics.

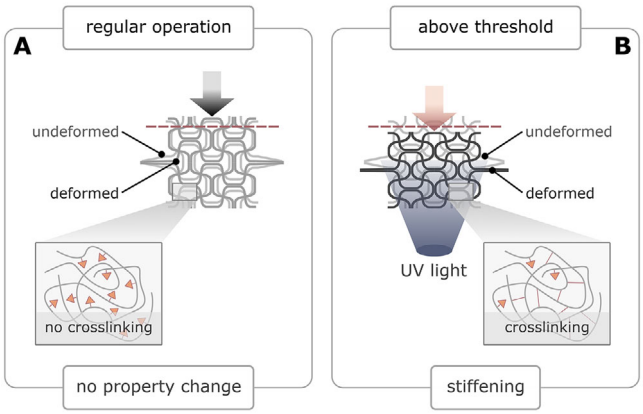


Figure 1. Schematic of the trainable material system utilizing the properties of the mechanical metamaterial and UV crosslinking. A) The metamaterial does not pass the threshold during loading, therefore no changes in mechanical properties happen. B) The metamaterial is loaded above threshold, therefore a UV light is triggered and crosslinking of the base-material is induced. The metamaterial itself becomes stiffer.

2. Results and Discussion

2.1. Material Design

In order to obtain a UV-crosslinkable and printable TPU, it is required to add a UV-reactive unit to the material. This might raise the idea to use an additive mixed into the material. However, this additive could be lost during the printing process due to high shear and elevated temperatures. To avoid that, the UV-reactive unit should be covalently linked to the polymer chain. This idea is derived from our previously published work where we developed a small molecule bearing a diazo compound and a benzophenone unit that can be easily mixed into a polymer.[46] Upon elevated temperature, the diazo compound is converted to a carbene that inserts in the closest neighboring C,H bond, covalently attaching the small molecule to the polymer chain. The second benzophenone part is then untouched and ready to be used to crosslink the polymer using UV-light. This strategy was proven successful with many polymers regardless of their structure and even with polyurethane of unknown chemical structure. The use of benzophenone is good on thin film because of its high reactivity under irradiation at 254 nm. However, while still reactive at 365 nm, its reactivity is slowed significantly. This would make its use on larger objects more difficult as the penetration depth of light at 254 nm is much lower than at 365 nm and typically only some hundred nanometers to a few microns. To avoid that, we decided to develop a new crosslinker, combining a 2-(2-diazo-2-phenylacetoxy) ethyl methacrylate (PEDAz) and an anthraquinone moiety noted PA, using the same concept while substituting the benzophenone unit by an anthraquinone unit. Anthraquinone units exhibit a higher absorption at 365 nm than benzophenone while still being able to undergo C,H insertion crosslinking.[47] The new molecule is obtained in a three-step synthesis (**Figure 2A**). The first step, leading to compound 1, is a Steglich esterification between phenylacetic acid and ethylene glycol. Compound 1 is then coupled to 2-hydroxyanthraquinone through a Mitsunobu reaction yielding compound 2. Finally, PA is obtained by adding a diazo compound through Regitz transfer. The global yield of this 3 step synthesis is 66%, allowing us to easily obtain several grams of the crosslinker.

The material production is described in Figure 2B,C. The TPU filament is insoluble in most solvents, which makes the C,H insertion of the filament more difficult. However, this filament swells strongly in solvents such as dichloromethane (DCM).

© 2025 The Author(s). Advanced Materials Technologies published by Wiley-VCH GmbH

2365709x, 0, Downloaded from https://advanced.onlinelibrary.wiley.com/doi/10.1002/admt.202501416 by Albert-Ludwigs-Universitat, Wiley Online Library on [20/10/2025]. See the Terms and Conditions (https://onlinelibrary.wiley.com/terms-and-conditions) on Wiley Online Library for rules of use; OA articles are governed by the applicable Creative Commons License

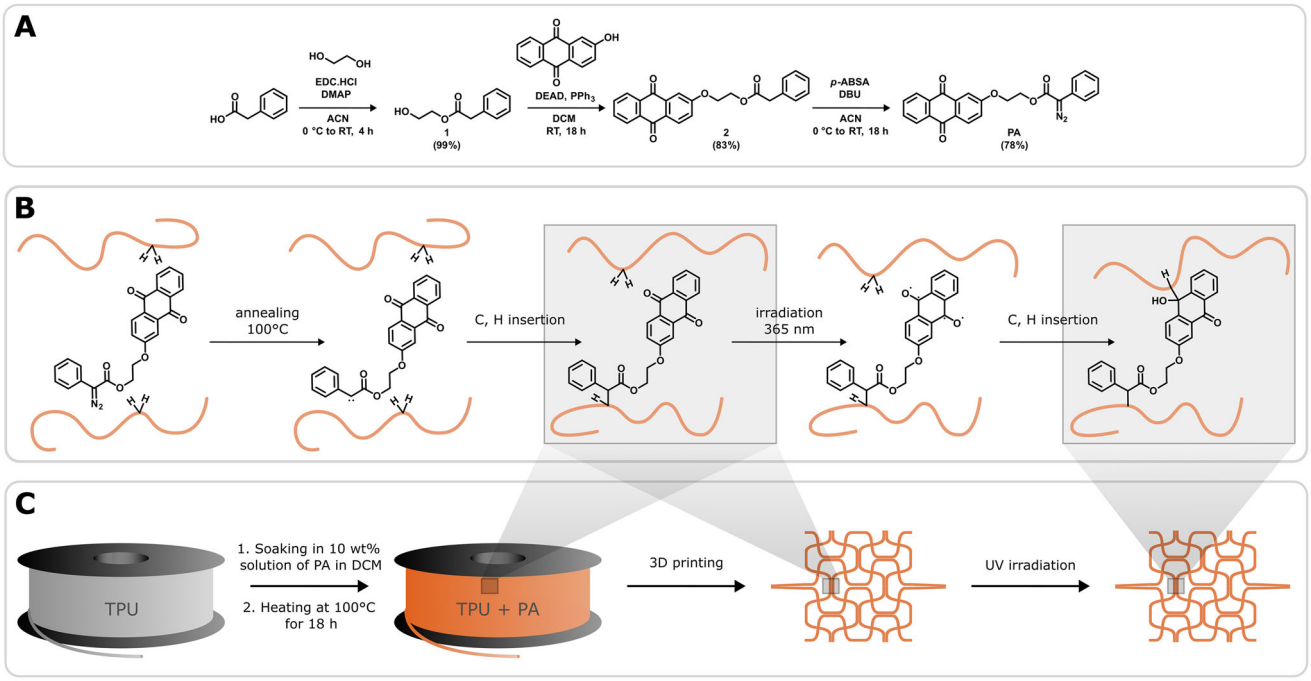


Figure 2. A) Schematic of the synthesis of PA. B) Molecular reaction of PA crosslinker with the polymer chains during the modification of the polymer and the crosslinking. C) Process-schematic of modification and printing of the filament.

Using this property, it is possible to make the PA molecule penetrate the filament. We used a solution of PA in DCM using 10 *wt*% of the crosslinker compared to the polymer. This low crosslinker content was selected to conserve most of the properties of the base-material. Then annealing at 100 °C for 18 h is performed to activate the diazo compound and link the crosslinker to the polymer chain. Using UV-vis measurements of the modified and unmodified filaments, the final crosslinker content is found to be 5 *wt*% (see experimental section). This base-material is then printable using similar parameters compared to the unmodified filament.

2.2. Property Change Induced by UV Irradiation

Crosslinkable PA mixed into TPU filament for fused filament fabrication (FFF) 3D printing enables a UV induced change in properties, which ultimately allows us to design a trainable material system. To assess the base-material's properties, we printed tensile specimens from the new material. These specimens were then exposed to UV light (λ = 365 nm) and we subsequently probed their stiffness. The process was repeated multiple times to reach an accumulated irradiation time of 55.4 h. After an initially steep (1.5×) increase in stiffness over 5 h of irradiation, we subsequently observe a proportional increase in stiffness with irradiation time (**Figure** 3A). Ultimately, a three-fold increase in stiffness was achieved during this process. One might assume, that more irradiation would eventually saturate the number of crosslinks formed as we would activate more crosslinkers until they are consumed completely.[48] Consequently the stiffness will increase and asymptotically reach a maximum value. In contrast, after this irradiation time we rather observe some cracking of the base TPU-material. UV degradation in the form of microcracking in PU and TPU materials is a well-known process.[49,50] However, the proportionality of irradiation and mechanical properties at times up to two days yields a well defined base-material for our trainable material system.

With the prior testing procedure, we obtain the ideal potential crosslinking of the modified TPU. Additionally, we also want to assess the properties with higher time-resolution and make sure stiffening happens solely due to UV-irradiation. Therefore, we tested a tensile-specimen continuously irradiated with custom UV-lamps mounted to the tensile-testing setup. As a control, we repeated the experiment with a not yet irradiated specimen and UV-lights turned off during testing. We can observe the aforementioned stiffening only if the UV-lamps are turned on, as depicted in Figure 3B. It should be noted, that when we use a lower intensity light source and smaller part of the geometry irradiated, we also see a reduced stiffening effect compared with Figure 3A. Boubarki et al.[49] observe an initial drop of stiffness upon irradiation of pure TPU, which is not happening for the PA treated TPU as depicted by the blue curve in Figure 3B. This indicates, that only the conjunction of PA's presence and UV exposure yield significant stiffening.

Additionally, we examine the material's response time to UV irradiation and its stiffness retention after irradiation is turned off. To accomplish this, we used UV-lights during stiffness probing in the tensile testing machine. This enabled us to intermittently turn the light source on or off during tensile-testing as depicted in Figure 3C. Here, we observe an immediate onset of stiffening upon UV irradiation and retention of reached stiffness when lights are off.

© 2025 The Author(s). Advanced Materials Technologies published by Wiley-VCH GmbH

2365709x, 0, Downloaded from https://advanced.onlinelibrary.wiley.com/doi/10.1002/admt.202501416 by Albert-Ludwigs-Universitat, Wiley Online Library on [20/10/2025]. See the Terms and Conditions (https://onlinelibrary.wiley.com/terms-and-conditions) on Wiley Online Library for rules of use; OA articles are governed by the applicable Creative Commons License

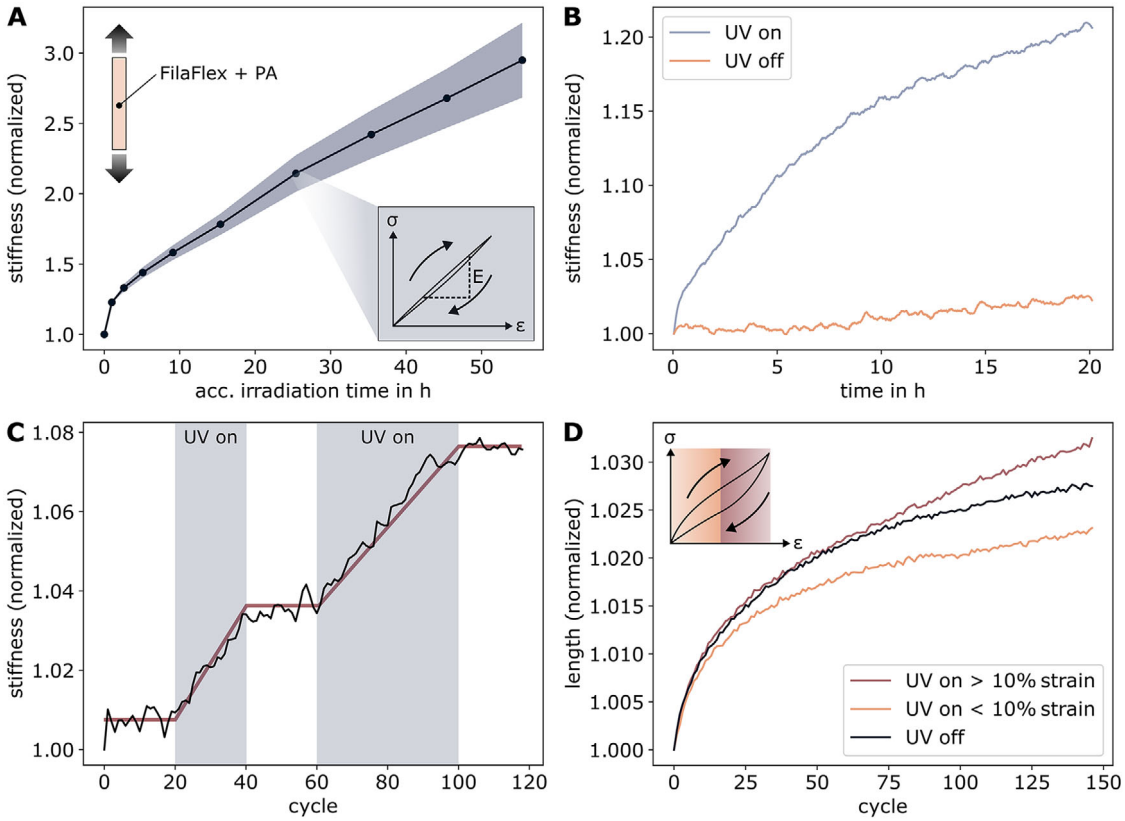


Figure 3. UV induced property changes of TPU + PA. A) Intermittent stiffness probing of single-side irradiated specimens in UV chamber. Insert: Assessment of Young's modulus from the stress-strain curve. Black line: mean, shaded area: standard deviation (n = 4). B) Tensile testing during irradiation with UV-lights turned on or off. C) Intermittent UV irradiation during tensile testing. UV on in shaded areas, red line as visual guidance. C: Assessment of specimen's length if irradiated at strains $\varepsilon < 10\%$, $\varepsilon > 10\%$ or UV off during cyclic loading to 20% strain.

Finally, we find the specimen's length to change according to its irradiated state during loading. We tested this by switching the UV-lights with respect to the applied strain. We loaded the tensile specimens up to 20% strain and varied the light switching, so we irradiate either during strains $\varepsilon < 10\%$ or $\varepsilon > 10\%$. We then compared it to a non-irradiated specimen for the same testing procedure. In Figure 3D we see a change in length of all specimens during testing. However, the specimen irradiated during strains $\varepsilon < 10\%$ is shortest and the specimen irradiated during strains $\varepsilon > 10\%$ is longest. From these results we can conclude, that irradiation also induces a change in the shape of the specimen. When irradiated in the strained state, the specimens tend to elongate compared with lights turned off. In turn, they tend to resist deformation more when irradiated in the relaxed state.

The ability to shift our material's properties by means of UV irradiation while being easily manufacturable is especially intriguing, because we can employ 3D printing to create complex structures. This sets our material system apart from other crosslinkable polymer systems, especially systems involving heat to trigger property changes. Kim and Lee[51] introduced a crosslinkable thermoplastic urethane which contains azide functional groups on the side chain. This allows a wide span of achievable mechanical properties, triggered by temperatures 80–120 °C. However, this temperature range prohibits extrusion based 3D printing, because the process involves printing temperatures exceeding 200 °C, effectively surpassing the activation temperature prematurely. Even lower activation temperatures of ca. 70 °C are achieved by trainable hydrogel systems.[52,53] Their inherently more complex manufacturing makes these systems harder to apply to metamaterial structures but are very intriguing because of their wide span of mechanical properties, as Nonoyama et al.[52] report a 1800× stiffness increase for their proposed material.

Our system yields a reduced but significant stiffening effect, which is especially interesting for metamaterial applications because of the locally controllable stiffening by irradiation. Here, instability driven mechanical metamaterials are especially intriguing. Bertoldi et al.[54] reported on such an instability-driven material with holes collapsing upon compression. During loading, as soon as a critical stress is reached, the holes collapse into an elliptic shape, resulting in an overall negative Poisson's ratio of the metamaterial. We utilized the metamaterial's sensitivity to its base-material's stiffness, to contrast the stiffness differences before and after irradiation (**Figure 4A**). We first tested the metamaterial under compression, where we displace its top with a crossbeam allowed to tilt about its center (Figure 4B). The metamaterial homogeneously deformed upon compression, indicated by the horizontal orientation of the crossbeam. Subsequently, we placed the block in a UV chamber at $\lambda = 365$ nm but covered the left half to prevent irradiation in this region. We retested the specimen and found the crossbar tilted upon compression. This

© 2025 The Author(s). Advanced Materials Technologies published by Wiley-VCH GmbH

2365709x, 0, Downloaded from https://advanced.onlinelibrary.wiley.com/doi/10.1002/admt.202501416 by Albert-Ludwigs-Universitat, Wiley Online Library on [20/10/2025]. See the Terms and Conditions (https://onlinelibrary.wiley.com/terms-and-conditions) on Wiley Online Library for rules of use; OA articles are governed by the applicable Creative Commons License

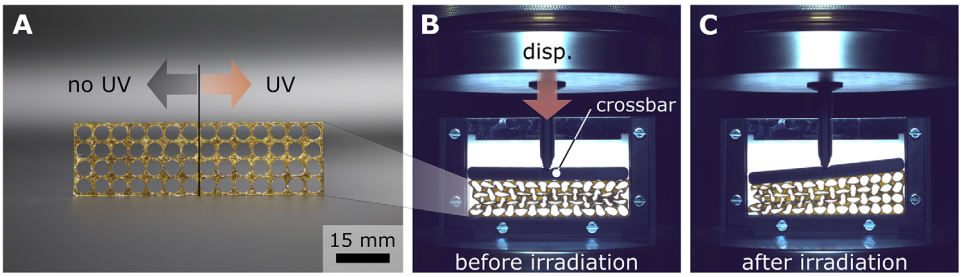


Figure 4. Metamaterial with instabilities. A) Unloaded, 3D printed specimen from TPU + PA. B) 4.5 mm compression of the specimen before irradiation. C) 4.5 mm compression of the specimen after 20 h irradiation of the right side: tilting indicates stiffness difference.

originates in the different stiffnesses in the left and right side, which is amplified by the instability-driven mechanism. The crossbar tilted toward the less stiff left side, as the metamaterial's holes collapsed there first (Figure 4C). This showcases a crucial benefit of the base-material: by targeted irradiation, local stiffness changes are achievable even after manufacturing of the structure. Especially intriguing is the fact, that we can control the stiffness of the region by the irradiation dose, potentially even allowing for graded material stiffness. This feature has the potential to become relevant for soft-robotics. Conrad and Teichmann et al.[55] have successfully 3D printed soft pneumatic logic and even a single input walking robot using the same TPU FilaFlex 70A base-material. Here, we would not only utilize 3D printing for manufacturing of complex hollow structures, but also tailor the stiffness locally afterwards. Locally stiffened structures can allow for increased load capacity or even change in behavior if the logic gates are treated. Furthermore, by locally changing the stiffness of the material, even switching of Poisson's ratio might be possible, dependent on a metamaterial's structure. Zhao et al.[56] report this ability for their multimaterial metamaterial, albeit for a globally increased temperature. Both approaches would result in 4D-printed systems, as Walker et al.[57] defined it, because an external, non mechanical stimulus yields a change in mechanical properties.

2.3. Harnessing Property Change for Training

The TPU + PA base-material gives us the potential to harness UV induced property changes in a trainable material system. For this, we employed a mechanical metamaterial with a distinct feature: switching lateral expansion upon vertical compression. As we described in a previous work,[36] we can tune the metamaterial's expansion behavior by its geometric features. Upon compression, the metamaterial initially exhibits lateral contraction, but when a critical deformation is reached, it starts expanding past its initial width: it effectively switches Poisson's ratio from negative to positive by closing internal gaps. By means of FFF 3D printing, we successfully manufactured the metamaterial as the core of the trainable material system. The metamaterial's arms can subsequently switch an optical light barrier (**Figure 5A**) in the test setup to trigger UV-irradiation upon compression (Figure 5B and 6A). Over the course of multiple compression cycles we expect the metamaterial's properties to change. Hence the fraction of the load-cycle with lights on alters due to the metamaterial's arms interacting with the optical light barrier. This is expected because of to the aforementioned characteristics of the base-material: modified shape and stiffening.

In Figure 6B,C, we clearly observe this behavior, derived from the material's crosslinking abilities. Here, only the metamaterial which employed PA and was subjected to UV irradiation showed an increased fraction of the load cycle with activated UV lights. In contrast, if unmodified TPU is used, or the UV-lights are turned off, we see a constant percentage of light-on time (Figure 6B,C). Because the testing was conducted using displacement controlled testing, we can assume that the change in light-on time is due to a shape change of the specimen: the metamaterial's internal gaps close immediately upon compression hence expansion (and therefore light-on time) happens during a larger fraction of the load-cycle.

This is further emphasized by the height of the specimen. While all specimens seem to conform to compression, only the specimen utilizing PA and UV changes its height significantly throughout the testing, as depicted in **Figure 7A**. This change in height is accompanied by a change of the specimen's stiffness. We see a sharp stiffness-increase for the metamaterial with PA and UV light, while the other specimens do not undergo a comparable stiffness increase (Figure 7B). This change in stiffness can be explained by two factors. First, the base-material becomes stiffer by UV activated crosslinking, similar to the results in Figure 3B. Second, the specimen's significant change in height results in closed internal gaps even upon unloading of the specimen. This results in an overall stiffer metamaterial compared

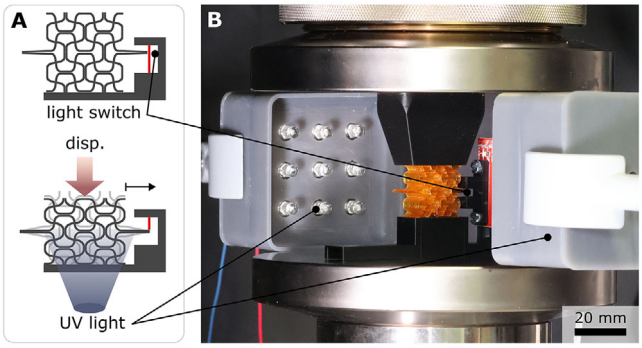


Figure 5. Test setup and working principle of the training process. A: The metamaterial is placed next to a light switch (top). Upon compression, the metamaterial expands and breaks the light switch, which triggers the UV lights. B: UV lights are placed front and rear of the specimen. The specimen is placed between the compression plates of the testing machine.

© 2025 The Author(s). Advanced Materials Technologies published by Wiley-VCH GmbH

2365709x, 0, Downloaded from https://advanced.onlinelibrary.wiley.com/doi/10.1002/admt.202501416 by Albert-Ludwigs-Universitat, Wiley Online Library on [20/10/2025]. See the Terms and Conditions (https://onlinelibrary.wiley.com/terms-and-conditions) on Wiley Online Library for rules of use; OA articles are governed by the applicable Creative Commons License

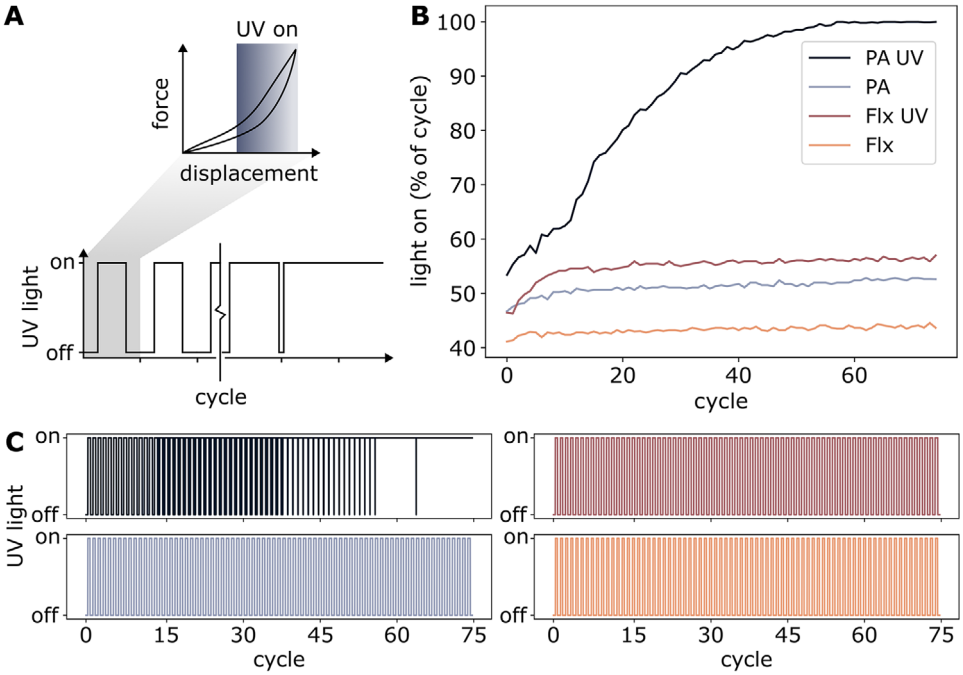


Figure 6. Displacement controlled training of the metamaterial system. A) The UV lights are activated by the metamaterial's expansion upon a specific displacement. This governs the percentage of light-on time during the testing cycle. B) Light-on percentage per test-cycle. PA with UV-lights activated saturates during testing. C) Light switching duty cycles per specimen and test. For clarity, switching times shorter than 10 s are not plotted.

to its initial state, independent of the base-material's property changes. In this case, the material adapts its height in order to keep the light on and gets a slightly deformed geometry.

Additionally, the metamaterial system allows for another mode of stimulus adaption. To independently assess the stiffening of the base-material, we designed a testing procedure comprised of two types of compression forces. The first compression force (F_{probe} = 1 N) was not sufficient to trigger the UV-lights by the metamaterial's lateral expansion (**Figure** 8A top). The compression was followed by 15 min uncompressed hold. After a repetition of the cycle, the second compression force followed. This force (F_{max} = 1.7 N) was sufficient to trigger a 15 min UV irradiation event (Figure 8A bottom). After 23 cycles we found the UV-lights not being triggered by F_{max} anymore. This originates form the base-material being sufficiently stiffened by UV-irradiation, resulting in a successfully trained metamaterial system, able to resist the compression force (Figure 8B,C).

The observed stiffening upon compression resembles adaptation or training mechanisms we find in nature. Muscles grow due to repeated weight training, ultimately they are able to lift a heavier weight.[1] Compared to that, our system becomes stiffer upon repeated compression, ultimately it is able to resist a higher force. Fitness enhancing properties of biological tissues have inspired works that similarly resemble training on a material level. Matsuda et al.[58] have introduced a hydrogel capable of "self-growing" upon a mechanical stimulus, resulting in a stretching induced stiffening. While the system elegantly trains upon the single mechanical stimulus, it relies on a hydrogel system, which limits its applicability and deployable environment. Pavlovian materials further elaborate on the aspect of training, were

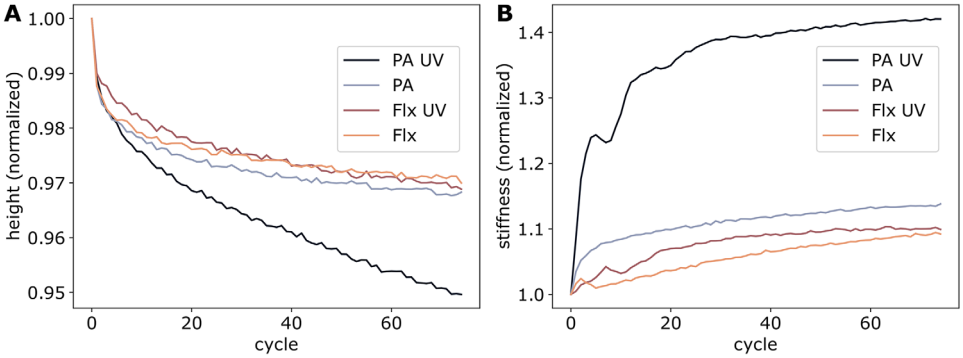


Figure 7. Mechanical evaluation of the metamaterial during testing. A) Height of the specimen (no mechanical load applied). B) Stiffness per metamaterial during cycled compression.

© 2025 The Author(s). Advanced Materials Technologies published by Wiley-VCH GmbH

2365709x, 0, Downloaded from https://advanced.onlinelibrary.wiley.com/doi/10.1002/admt.202501416 by Albert-Ludwigs-Universitat, Wiley Online Library on [20/10/2025]. See the Terms and Conditions (https://onlinelibrary.wiley.com/terms-and-conditions) on Wiley Online Library for rules of use; OA articles are governed by the applicable Creative Commons License

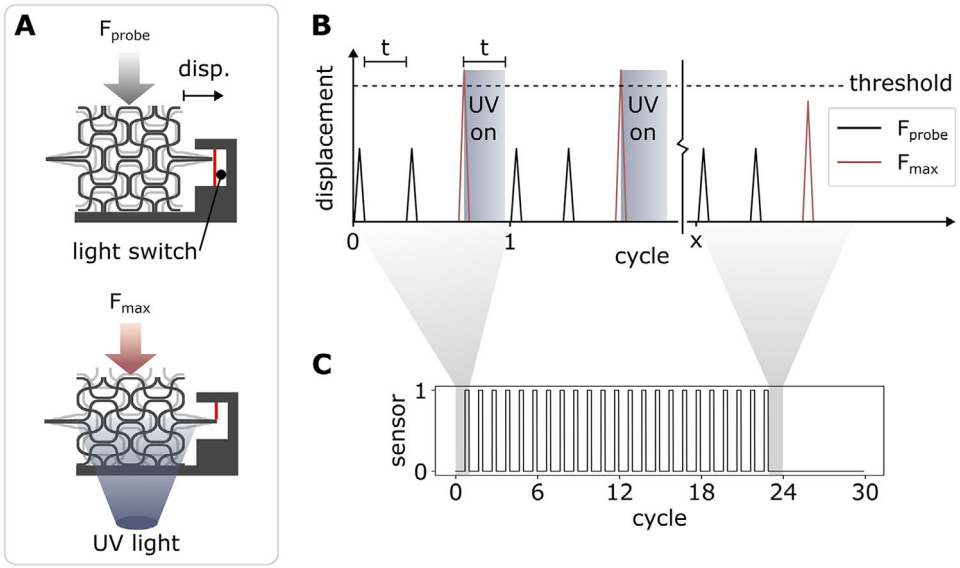


Figure 8. Threshold training. A) Top: F_{probe} is not sufficient to trigger the light by lateral expansion. Bottom: F_{max} triggers UV-lights by activating the light-switch. B) Testing procedure: F_{probe}, t = 15 min wait, F_{probe}, wait (t), F_{max}, wait (t). After x-cycles, the metamaterial is sufficiently stiff to resist F_{max}. C) Results from the test show no UV activation after about x = 23 testing-cycles.

the conjunction of two stimuli allow for a seemingly more intelligent system, capable of information processing, surpassing the sole reaction to mechanical loading.[59,60]

Here, we combine both abilities in one system: stiffening as reaction to a mechanical stimulus, facilitated by a secondary UV-stimulus. Furthermore, we open up the possibility to manufacture more complex geometries by means of 3D printing, effectively overcoming the limitations of previously discussed hydrogel-systems. This means that the metamaterial comprised of TPU + PA can achieve two types of behavior: it can be directly stiffened by an external UV-stimulus or its complex deformation can be harnessed in a system with sensors to make it adaptable or trainable toward mechanical loading.

3. Conclusion

Stimuli-responsive materials are crucial for the development of trainable systems, exhibiting life-like behavior. Here we present a 3D printable TPU at the core of a material system capable of adapting to a mechanical stimulus. We successfully incorporated CHic-able groups into 3D printable TPU filament, fabricated tensile specimens and mechanical metamaterials to assess and showcase its capabilities. By testing tensile specimens, we showed an up to 300% increase in stiffness upon irradiation. The changes in stiffness are rapid and can be introduced in an intermittent manner, carefully tailoring the specimens stiffness by accumulating stiffness. The change in stiffness is also accompanied by a change in the specimen's dimensions, if the specimen is irradiated in a deformed state. Additionally, we show the local effects of the irradiation driven crosslinking by harnessing an instability driven metamaterial with holes. We clearly see, that irradiation of one half leads to a collapse of the structure's other half under compression. Tilting of the specimen's top surface clearly indicates locally higher base-material stiffness.

Finally, we utilized both change in dimensions and change in stiffness to create a trainable material system, with a 3D printed metamaterial at its core. Upon compression, the specimen activates its own UV irradiation by means of a geometrically designed point of expansion. After a sufficient number of loading cycles the material becomes adapted to the compression and shows an increased stiffness. Furthermore, we employed the metamaterial's tailored point of expansion to create a system capable of threshold sensitive training. Only if the applied force results in a minimum expansion, the UV irradiation is turned on. We could successfully show that initially the applied force was large enough to trigger the light source, but eventually the metamaterial's increased stiffness prohibited the triggering event. This can be interpreted as the material system training to resist the triggering force.

The metamaterial comprised of TPU + PA can achieve two types of behavior. It can be directly stiffened by an external UV-stimulus or its complex deformation can be harnessed in a system with sensors to make it trainable toward mechanical loading. The observed stimulus stiffening of our complex 3D printed objects resembles adaptation or training mechanisms we find in nature, like growing muscles due to repeated training. The developed fitness enhancing properties on a material level closely resemble these biological tissues. The here described material system has the potential to improve soft robotics by locally tuning material properties after manufacturing, but it can also be deployed in other trainable materials leading to life-like, stimuli-responsive systems.

4. Experimental Section

Synthesis—Synthesis of Compound 1: In a dried three-neck-round-bottom flask equipped with magnetic stirring bar, a solution of Ethylene glycol (16.43 mL, 293.8 mmol, 4.00 eq) and

© 2025 The Author(s). Advanced Materials Technologies published by Wiley-VCH GmbH

2365709x, 0, Downloaded from https://advanced.onlinelibrary.wiley.com/doi/10.1002/admt.202501416 by Albert-Ludwigs-Universitat, Wiley Online Library on [20/10/2025]. See the Terms and Conditions (https://onlinelibrary.wiley.com/terms-and-conditions) on Wiley Online Library for rules of use; OA articles are governed by the applicable Creative Commons License

4-dimethylaminopyridine (2.96 g, 24.24 mmol, 0.33 eq) in acetonitrile (100 mL) was prepared under nitrogen and cooled to 0 °C. 1-Ethyl-3-(3-dimethylaminopropyl)carbodiimide hydrochloride (9.32 g, 48.62 mmol, 1.10 eq) was then added slowly. Phenyl acetic acid (15.49 g, 80.79 mmol, 1.00 eq) was dissolved in acetonitrile (100 mL) and added dropwise to the above mentioned solution. The reaction mixture was stirred at 0 °C for 1 h.

The reaction was then stopped with water (150 mL). The aqueous phase was then extracted thrice with ethyl acetate (3 times 100 mL). The organic phases were then combined, dried over Na_2SO_4 and the solvent was removed under reduced pressure. 12.75 g of Compound 1 was obtained as a liquid (96%).

^{1}H NMR (250 MHz, Chloroform-d) δ 7.43 – 7.23 (m, 5H), 4.31 (s, 1H), 4.23 (t, J = 4.7 Hz, 2H), 3.80 (t, J = 5.6 Hz, 2H), 3.68 (d, J = 2.2 Hz, 2H). ^{13}C NMR (63 MHz, CDCl3) δ 172.05, 147.73, 127.24, 78.81, 77.24, 75.66, 41.25.

Synthesis—Synthesis of Compound 2: In a 500 mL three-necked flask with septum, 2-hydroxyantraquinone (5.47 g, 24.42 mmol, 1.1 eq) was dissolved in tetrahydrofuran (200 mL) under nitrogen. Then triphenylphosphine (17.47 g, 66.59 mmol, 3 eq) and diethyl azodicarboxylate (11.26 mL, 66.59 mmol, 3.00 eq) were added and the reaction mixture was stirred for 1 h at room temperature. Compound 1 (4 g, 22.2 mmol, 1 eq) was then added in tetrahydrofuran (50 mL) and the reaction solution was stirred overnight at room temperature.

The reaction was then stopped with water (150 mL). The aqueous phase is then extracted thrice with ethyl acetate (3 times 100 mL). The organic phases are then combined, dried over Na_2SO_4 and the solvent was removed under reduced pressure.

The crude product was then purified by silica gel column chromatography (eluant Hexane/Ethyl acetate: 60/40) to afford 7.16 g of Compound 2 as a yellow solid was obtained (83%).

^{1}H NMR (250 MHz, Chloroform-d) δ 8.47 – 8.16 (m, 4H), 8.01 – 7.61 (m, 3H), 7.46 – 7.05 (m, 5H), 4.57 (t, J = 3.1, 2.5 Hz, 2H), 4.42 (t, J = 3.1, 2.5 Hz, 2H), 3.73 (s, 2H). ^{13}C NMR (63 MHz, CDCl3) δ 150.29, 140.34, 134.27, 133.80, 133.65, 129.87, 129.28, 128.67, 127.23, 124.53, 123.81, 121.60, 110.57, 66.50, 62.76, 41.22

Synthesis—Synthesis of PA: In a brown, dried three-neck-round-bottom flask equipped with magnetic stirring bar, a solution of compound 2 (2 g, 5.18 mmol, 1.00 eq) in acetonitrile (20 mL) was prepared under nitrogen and cooled to 0 °C. 4-Acetamidobenzenesulfonyl azide (1.52 g, 6.31 mmol, 1.22 eq) was added and the reaction mixture was degassed under argon bubbling for 15 min. 1,8-Diazabicyclo[5.4.0]undec-7-ene (1.55 mL, 10.35 mmol, 2.00 eq) was added at 0 °C and the solution was allowed to warm up to room temperature. The reaction mixture was stirred overnight.

The reaction was then stopped with water (150 mL). The aqueous phase is then extracted thrice with ethyl acetate (3 times 100 mL). The organic phases are then combined, dried over Na_2SO_4 and the solvent was removed under reduced pressure.

The crude product was then purified by silica gel column chromatography (eluant Hexane/Ethyl acetate: 80/20) to afford 4.16 g of PA were obtained as a yellow solid (78% yield).

^{1}H NMR (250 MHz, Chloroform-d) δ 8.34 (td, J = 6.5, 6.1, 3.3 Hz, 3H), 7.89 – 7.76 (m, 3H), 7.52 (d, J = 7.8 Hz, 2H), 7.48 – 7.28 (m, 3H), 7.23 (t, J = 7.1 Hz, 1H), 4.74 (t, J = 4.4 Hz, 2H), 4.50 (t, J = 4.4 Hz, 2H). ^{13}C NMR (63 MHz, CDCl3) δ 163.21, 142.18, 134.29, 133.80, 133.55, 129.87, 128.93, 127.14, 124.06, 121.51, 119.46, 110.62, 78.69, 77.11, 75.52, 50.35. UV-Vis (DCM, 2.10^{-5} mol L^{-1}): $\varepsilon_{265\ nm}$ = 31,000 L mol^{-1} cm^{-1}; $\varepsilon_{330\ nm}$ = 2,500 L mol^{-1} cm^{-1}; $\varepsilon_{365\ nm}$ = 1,900 L mol^{-1} cm^{-1}; $\varepsilon_{400\ nm}$ = 587 L mol^{-1} cm^{-1}.

Synthesis—Filament modification: 9.86 g of filament was immersed in 197 mL of a 5 mg mL^{-1} solution of PA in dichloromethane (DCM) (986 mg of PA in 197 mL of DCM). The solution was then agitated until the filament absorbed the whole solution by swelling. The filament was then dried at room temperature for 1 h before being heated at 100 °C for 18 h.

To quantify the inserted crosslinker, the modified filament was melted and spread on a glass slide until the layer is 0.07 mm thick. The layer was then analysed with a UV-Vis spectrometer (Agilent, Cary 60) and compared to a similar layer of Filaflex 70A (**Figure 9**). The absorbtion of Filaflex was null at 400 nm while the modified filament exhibit an absorption of 0.513. Using the Beer-Lambert law, 5 wt% of the crosslinker was obtained in the final filament.

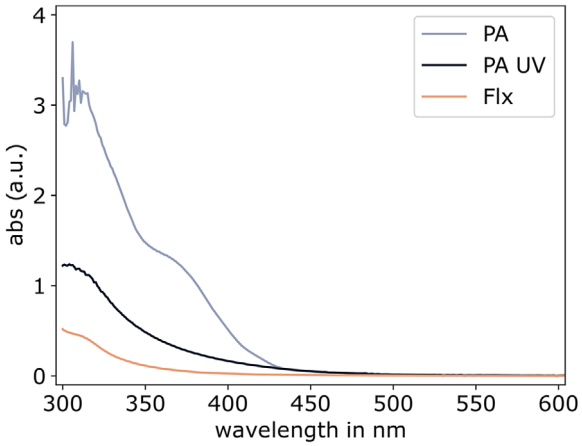


Figure 9. UV-Vis spectrum of FilaFlex TPU, FilaFlex + PA and FilaFlex + PA after irradiation at 365 nm for 1 h (solid state, 0.07 mm thickness).

To demonstrate the crosslinking spectroscopically, a layer of PA-containing filament was irradiated for 1 h at 365 nm. After this time, the absorption band around 365 nm disappears. The absorption around 300 nm was also reduced but remains higher than that of the pure filament, thus providing UV protection.

Printing: The filament was subsequently used to print the specimens for testing. We printed with standard and PA modified transparent Filaflex 70A TPU (Recreus, Alicante, Spain) with 0.4 mm nozzle on a standard Prusa MK4 3D printer (Prusa, Prague, Czech Republic). The chosen printing settings were as follows: print temperature = 220 °C, bed temperature = 60 °C, layer height = 0.1 mm (initial layer height = 0.2 mm), print speed = 10 mm s^{-1}, infill = 100% and "avoid crossing perimeters" activated. Tensile specimens were printed in a single layer with following dimensions: 0.2 × 4 × 40 mm (**Figure 10**A). The metamaterial specimens consist of 2 × 2 unit cells with 5 mm arms (Figure 10B), internal dimensions are specified in Figure 10C.

Tensile Testing: The tensile test results depicted in Figure 3 were conducted on a universal testing machine (ZwickRoell, Ulm, Germany) equipped with a 500 N load cell. For all testing depicted in Figure 3A, 4 specimens were each tested 10 times to a displacement of 2 mm at a testing speed of 4 mm min^{-1}. The obtained force-displacement data was converted to stress-strain and Young's modulus was evaluated in the region of 80-100% of the load cycle. The average of 4 central cycles was used per specimen, mean ± standard deviation was calculated across the tested specimens. Subsequently, the specimens were placed on electrical tape (to ensure one-sided irradiation) and irradiated in the UV-chamber Bio-Link 365 (Vilber, Marne La Vallée, France). Irradiation time was determined by Renard R5 series, meaning the irradiation cycles lasted: 1 h, 1.6 h, 2.5 h, 4 h, 6.3 h and 4 × 10 h.

Tensile tests shown in Figure 3B employed a tensile specimen with FilaFlex 70A + PA per curve. However, here two UV lamps were used during tensile testing, one placed in front and one behind the specimen. We used custom lamps, which were comprised of 3 × 3 arrays of LEDs (λ = 365–375 nm) (Figure 5B). The same setup was used for intermittent irradiation in Figure 3C, with the lamps only switched on for 20 min after 20 cycles and for 40 min after 60 cycles.

To test the specimen's length dependent on the irradiated state, the aforementioned setup was modified. Here, it was tested 150 times to a displacement of 5 mm (20% strain) at a testing speed of 10 mm min^{-1}. We tested three specimens, one with UV lights off, one with UV activated for displacements < 2.5 mm and another one with UV activated for displacements > 2.5 mm. To accomplish this in a repeatable way, we tracked the testing machine's cross-head with a laser distance sensor (Baumer OADK

© 2025 The Author(s). Advanced Materials Technologies published by Wiley-VCH GmbH

2365709x, 0, Downloaded from https://advanced.onlinelibrary.wiley.com/doi/10.1002/admt.202501416 by Albert-Ludwigs-Universitat, Wiley Online Library on [20/10/2025]. See the Terms and Conditions (https://onlinelibrary.wiley.com/terms-and-conditions) on Wiley Online Library for rules of use; OA articles are governed by the applicable Creative Commons License

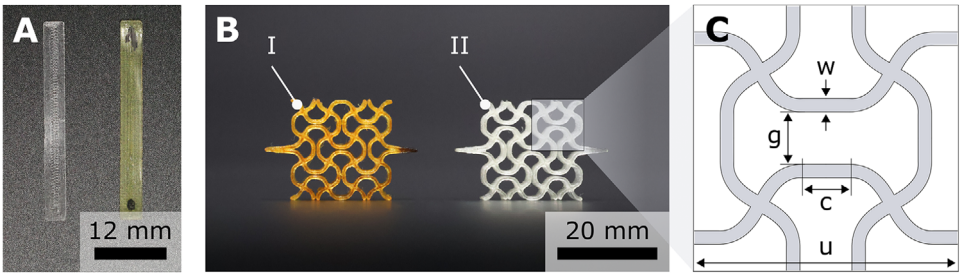


Figure 10. A) Tensile specimens with dimensions 0.2 × 4 × 40 mm. Left: transparent FilaFlex 70A, right: Filaflex 70A + PA. B) Printed metamaterials, with a thickness of 10 mm. I: Filaflex 70A + PA, II: Unmodified, transparent FilaFlex 70A. C) Size of unit cell u = 10 mm, gap size g = 0.5 mm, contact length c = 0.45 mm, beam width w = 0.4 mm.

2517480/S14C, Frauenfeld, Switzerland) and switched the UV-lamps automatically with a relay and a microcontroller (sparkfun Artemis, Niwot, USA). The specimen's length was determined at the end of each load cycle, when returned to the preload force of 0.05 N. This made sure, the specimen was flat and not buckled out of plane.

Compression Testing of Metamaterial with Holes: The metamaterial with holes resembled the shape proposed by Bertoldi et al.[54] The holes had a diameter of 4.6 mm and a wall thickness of 0.6 mm between them, forming the metamaterial block with a thickness of 1.5 mm in a 4 × 14 array (Figure 4A). They were printed on the aforementioned Prusa 3D printer from FilaFlex 70A + PA. Subsequently, the metamaterial was placed in the test-setup. The test-setup was comprised of two clear plexiglas-windows, preventing out of plane buckling, a crossbar for even load application and a compression-pin (Figure 4B). The compression pin was pushed in 6 mm at 18 mm min^{-1} by the ZwickRoell universal testing machine. After this initial testing, the left half of the specimen was covered in aluminum foil and then placed in the Bio-Link 365 UV chamber for 10 h for irradiation from the top. The specimen was then flipped and irradiated for another 10 h from the bottom. Finally, the specimen is retested in the compression setup, were the notched crossbar allowed for rotation and therefore visualization of the different stiffnesses across the specimen.

Compression Testing of Metamaterial with Arms: For compression testing of the metamaterial with arms, the setup displayed in Figure 5 was used. Four metamaterials were tested with arms, as depicted in Figure 10. They were placed on a 3D printed fixture with central needles to mitigate lateral movement and an optical end-switch. The end-switch was triggered by the specimen's arm, reaching into its optical pathway upon sufficient compression due to lateral expansion. The light-switch was connected to an Arduino uno microcontroller (Monza, Italy). The microcontroller subsequently switched on the UV lights by a relay upon detected expansion. It was tested with the same universal testing machine, equipped with the aforementioned 500 N load cell up to a compression of 5 mm at a testing speed of 5 mm min^{-1}. The testing was recorded with a synchronized CMOS camera (IDS UI-3880CP, Imaging Development Systems, Obersulm, Germany) and the end-switch data was logged. The testing was done with UV lights connected or disconnected from power per tested material, as described in **Table 1**.

For force controlled threshold testing, a single metamaterial printed from FilaFlex 70A + PA was used. The setup remained similar to the aforementioned, with a difference in the testing procedure, comprised of three steps: First, the metamaterial was compressed to F_{probe} = 1 N at a testing speed of 3 mm min^{-1} followed by a t = 15 min pause, this was repeated a second time. Third, the metamaterial was compressed to F_{max} = 1.7 N, followed by another pause of duration t (Figure 8). The third loading had the aim of triggering the optical end-switch, after which the UV lights were turned on for 15 min, facilitated by the Arduino microcontroller. The testing was repeated 30 times with the goal of reaching sufficient resistance of the metamaterial against the applied force, so the lights would not be turned on.

Table 1. Metamaterials with their material composition and testing condition.

Material	Testing condition
FilaFlex 70A	no UV
FilaFlex 70A	UV
FilaFlex 70A + PA	no UV
FilaFlex 70A + PA	UV

Acknowledgements

This research was funded by the Deutsche Forschungsgemeinschaft (DFG, German Research Foundation) under Germany's Excellence Strategy: EXC-2193/1-390951807.

Open access funding enabled and organized by Projekt DEAL.

Conflict of Interest

The authors declare no conflict of interest.

Author Contributions

D.S. and J.L. contributed equally to the work. J.L. synthesized the crosslinker and prepared the filament. D.S. designed, printed, tested and evaluated the specimens and built the training system. V.S. and J.L. conceived and supervised the research. J.R. advised and helped with the conceptualization of the experiments. D.S. and J.L. wrote the original draft. All authors discussed the results and wrote the manuscript. All authors reviewed the manuscript.

Data Availability Statement

The data that support the findings of this study are available from the corresponding author upon reasonable request.

Keywords

C,H-insertion crosslinking, materials training, mechanical metamaterial, stimuli responsive

Received: July 3, 2025
Revised: September 12, 2025
Published online:

© 2025 The Author(s). Advanced Materials Technologies published by Wiley-VCH GmbH

2365709x, 0, Downloaded from https://advanced.onlinelibrary.wiley.com/doi/10.1002/admt.202501416 by Albert-Ludwigs-Universitat, Wiley Online Library on [20/10/2025]. See the Terms and Conditions (https://onlinelibrary.wiley.com/terms-and-conditions) on Wiley Online Library for rules of use; OA articles are governed by the applicable Creative Commons License

[1] D. C. Hughes, S. Ellefsen, K. Baar, *Cold Spring Harbor Perspect. Med.* **2017**, *8*, a029769.
[2] P. D. Chilibeck, D. G. Sale, C. E. Webber, *Sports Medicine* **1995**, *19*, 103.
[3] P. Fratzl, *J. R. Soc., Interface* **2007**, *4*, 637.
[4] N. P. R. Anten, R. Alcalá-Herrera, F. Schieving, Y. Onoda, *New Phytologist* **2010**, *188*, 554.
[5] K. Otsuka, X. Ren, *Intermetallics* **1999**, *7*, 511.
[6] A. Amadi, M. Mohyaldinn, S. Ridha, V. Ola, *J. Alloys Compd.* **2024**, *976*, 173227.
[7] H. E. Meijer, L. E. Govaert, *Prog. Polym. Sci.* **2005**, *30*, 915.
[8] C. Ni, D. Chen, Y. Yin, X. Wen, X. Chen, C. Yang, G. Chen, Z. Sun, J. Wen, Y. Jiao, C. Wang, N. Wang, X. Kong, S. Deng, Y. Shen, R. Xiao, X. Jin, J. Li, X. Kong, Q. Zhao, T. Xie, *Nature* **2023**, *622*, 748.
[9] E. M. Terentjev, *J. Phys.: Condens. Matter* **1999**, *11*, R239.
[10] M. Chen, M. Gao, L. Bai, H. Zheng, H. J. Qi, K. Zhou, *Adv. Mater.* **2023**, *35*, 23.
[11] Y. S. Zhang, A. Khademhosseini, *Science* **2017**, *356*, 6337.
[12] O. Skarsetz, V. Slesarenko, A. Walther, *Adv. Sci.* **2022**, *9*, 2201867.
[13] O. Skarsetz, P. J. Swinkels, J. Figueiredo da Silva, G. Vozzolo, M. Masukawa, G. Fusi, B. Dúzs, Y. Lassiat, C. Drees, V. Slesarenko, A. Walther, *Adv. Mater.* **2025**.
[14] W. Pu, F. Wei, L. Yao, S. Xie, *J. Mater. Sci.* **2022**, *57*, 12202.
[15] J. Wang, F. Jin, X. Dong, J. Liu, M. Zheng, *Adv. Mater. Technol.* **2022**, *7*, 8.
[16] A. Tabatabaeian, S. Liu, P. Harrison, E. Schlangen, M. Fotouhi, *Composites, Part A* **2022**, *163*, 107236.
[17] C. M. Geiselhart, H. Mutlu, C. Barner-Kowollik, *Angew. Chem., Int. Ed.* **2021**, *60*, 17290.
[18] D. Schwarz, V. Slesarenko, *Composites Part C: Open Access* **2025**, 100586.
[19] P. Testa, R. W. Style, J. Cui, C. Donnelly, E. Borisova, P. M. Derlet, E. R. Dufresne, L. J. Heyderman, *Adv. Mater.* **2019**, *31*, 29.
[20] O. Skarsetz, R. Mathes, R. S. Schmidt, M. Simon, V. Slesarenko, A. Walther, *ACS Appl. Mater. Interfaces* **2024**, *16*, 38511.
[21] T. Mai, T. Yasui, R. Tanaka, H. Masunaga, T. Kabe, K. Tsunoda, S. Sakurai, K. Urayama, *Adv. Sci.* **2024**, *11*, 12.
[22] J. Diani, B. Fayolle, P. Gilormini, *Eur. Polym. J.* **2009**, *45*, 601.
[23] T. Chen, M. Pauly, P. M. Reis, *Nature* **2021**, *589*, 386.
[24] A. A. Zadpoor, *Mater. Horiz.* **2016**, *3*, 371.
[25] K. Che, C. Yuan, J. Wu, H. Jerry Qi, J. Meaud, *J. Appl. Mech.* **2016**, *84*, 1.
[26] M. Kadic, T. Bückmann, R. Schittny, P. Gumbsch, M. Wegener, *Phys. Rev. Appl.* **2014**, *2*, 054007.
[27] T. Frenzel, M. Kadic, M. Wegener, *Science* **2017**, *358*, 1072.
[28] X. Fang, D. Yu, J. Wen, Y. Dai, M. R. Begley, H. Gao, P. Gumbsch, *Nature* **2025**.
[29] H. M. A. Kolken, A. A. Zadpoor, *RSC Adv.* **2017**, *7*, 5111.
[30] R. Gatt, M. Vella Wood, A. Gatt, F. Zarb, C. Formosa, K. M. Azzopardi, A. Casha, T. P. Agius, P. Schembri-Wismayer, L. Attard, N. Chockalingam, J. N. Grima, *Acta Biomater.* **2015**, *24*, 201.
[31] J. U. Surjadi, L. Gao, H. Du, X. Li, X. Xiong, N. X. Fang, Y. Lu, *Adv. Eng. Mater.* **2019**, *21*, 3.
[32] J. Valente, E. Plum, I. J. Youngs, N. I. Zheludev, *Adv. Mater.* **2016**, *28*, 5176.
[33] K. K. Dudek, J. A. I. Martínez, G. Ulliac, M. Kadic, *Adv. Mater.* **2022**, *34*, 14.
[34] M. Miniaci, A. Krushynska, F. Bosia, N. M. Pugno, *New J. Phys.* **2016**, *18*, 083041.
[35] T.-C. Lim, *Oxford Open Materials Science* **2022**, *2*, 1.
[36] D. Schwarz, G. Felsch, F. Tauber, S. Schiller, V. Slesarenko, *Mater. Des.* **2023**, *236*, 112468.
[37] P. Jiao, J. Mueller, J. R. Raney, X. Zheng, A. H. Alavi, *Nat. Commun.* **2023**, *14*, 1.
[38] J. Kost, A. Bleiziffer, D. Rusitov, J. Rühe, *J. Am. Chem. Soc.* **2021**, *143*, 10108.
[39] M. Liu, C. Xu, H. Zhao, T. Jiang, S. Chen, J. Xuan, *Adv. Funct. Mater.* **2025**.
[40] R. Toomey, D. Freidank, J. Rühe, *Macromolecules* **2004**, *37*, 882.
[41] D. Rusitov, F. Deussen, J. Rühe, *Adv. Mater. Interfaces* **2023**, *10*, 26.
[42] P. F. Kotrade, J. Rühe, *Angew. Chem., Int. Ed.* **2017**, *56*, 14405.
[43] T. A. Weber, L. Metzler, P. L. Fosso Tene, T. Brandstetter, J. Rühe, *ACS Appl. Mater. Interfaces* **2022**, *14*, 25147.
[44] M. Akiba, *Prog. Polym. Sci.* **1997**, *22*, 475.
[45] Q. Guo, *Thermosets Structure Properties And Applications*, Woodhead Publishing **2012**.
[46] J. Liotier, T. Piock, J. Rühe, *Macromolecules* **2024**, *58*, 1859.
[47] A. J. Straub, F. D. Scherag, H. I. Kim, M.-S. Steiner, T. Brandstetter, J. Rühe, *Langmuir* **2021**, *37*, 6510.
[48] T. Kanokwijitsilp, M. Körner, O. Prucker, A. Anton, J. Lübke, J. Rühe, *Macromolecules* **2021**, *54*, 6238.
[49] A. Boubakri, N. Guermazi, K. Elleuch, H. Ayedi, *Mater. Sci. Eng., A* **2010**, *527*, 1649.
[50] L. Rosu, C. Cascaval, C. Ciobanu, D. Rosu, E. Ion, C. Morosanu, M. Enachescu, *J. Photochemistry Photobiology A: Chemistry* **2005**, *169*, 177.
[51] H. Kim, K. J. Lee, *Polymer* **2021**, *236*, 124350.
[52] T. Nonoyama, Y. W. Lee, K. Ota, K. Fujioka, W. Hong, J. P. Gong, *Adv. Mater.* **2019**, *32*, 4.
[53] S. Hu, Y. Fang, C. Liang, M. Turunen, O. Ikkala, H. Zhang, *Nat. Commun.* **2023**, *14*, 1.
[54] K. Bertoldi, P. M. Reis, S. Willshaw, T. Mullin, *Adv. Mater.* **2010**, *22*, 361.
[55] S. Conrad, J. Teichmann, P. Auth, N. Knorr, K. Ulrich, D. Bellin, T. Speck, F. J. Tauber, *Sci. Rob.* **2024**, *9*, 86.
[56] Z. Zhao, C. Yuan, M. Lei, L. Yang, Q. Zhang, H. Chen, H. J. Qi, D. Fang, *Phys. Rev. Appl.* **2019**, *11*, 044074.
[57] A. Walker, K. Shea, *Smart Mater. Struct.* **2024**, *33*, 115047.
[58] T. Matsuda, R. Kawakami, R. Namba, T. Nakajima, J. P. Gong, *Science* **2019**, *363*, 504.
[59] H. Zhang, H. Zeng, A. Priimagi, O. Ikkala, *Adv. Mater.* **2020**, *32*, 20.
[60] H. Zeng, H. Zhang, O. Ikkala, A. Priimagi, *Matter* **2020**, *2*, 194.

© 2025 The Author(s). Advanced Materials Technologies published by Wiley-VCH GmbH

2365709x, 0, Downloaded from https://advanced.onlinelibrary.wiley.com/doi/10.1002/admt.202501416 by Albert-Ludwigs-Universitat, Wiley Online Library on [20/10/2025]. See the Terms and Conditions (https://onlinelibrary.wiley.com/terms-and-conditions) on Wiley Online Library for rules of use; OA articles are governed by the applicable Creative Commons License

4 Conclusion

To conclude the findings of this thesis, the following chapter progresses in two steps. First, it summarizes the main findings of the thesis, focusing on the three works that contribute to the field of mechanical metamaterials. Second, it outlines future directions and continuations to overcome current limitations and advance the development of stimuli-responsive material systems.

4.1 Summary

This thesis advances the field of mechanical metamaterials through three consecutive contributions toward engineered material responses. The used methodologies, which include mechanical fundamentals, mechanical metamaterial design motifs, and manufacturing techniques, were introduced first. Building on this foundation, the three contributions followed on geometry, composition, and combined geometry-composition based responses in mechanical metamaterials.

The first work on a self-contacting mechanical metamaterial revealed the relationship between the geometric features of its unit cell and its nonlinear response under compression. The material exhibits a contact-driven switch of auxeticity upon sufficient compression, which ultimately leads to expansion past initial width. This "if-then" mechanical behavior, indicated by a changing Poisson's ratio, was quantitatively analyzed, experimentally validated, and functionally demonstrated in a discrete scales device. These results highlight how self-contact can be harnessed and controlled by geometric design for practical applications in soft robotics or other life-like structures. This is especially enabled by the replicable framework established in this work, which provides a versatile approach to designing nonlinear mechanical responses.

The second work approached an engineered response on the material's composition level. Specifically, it examined the relationship between the fluorescence response

and the accompanying change in stiffness in a soft matrix microcapsule composite. While the intact microcapsules contribute to the composite's stiffness, their rupture and subsequent release of their self-reporting liquid leads to a significant stiffness reduction. Consequently, larger deformations lead to more broken capsules and a brighter self-reporting signal, accompanied by a greater decrease in Young's modulus. This relationship was shown to be linearly correlated but transient over time, which connects the self-reported degree of loading to the actual mechanical properties. These insights provide a foundation to apply this composite in mechanical metamaterials that locally break embedded capsules due to geometric features that deliberately concentrate stresses.

Finally, by combining a metamaterial's mechanical response with a responsive base material, a trainable material system was realized. By fabricating the mechanical metamaterial from a novel, UV-crosslinkable TPU and coupling its expansion behavior to a UV light source, a closed-loop, trainable system was created, capable of adapting to repeated mechanical stimuli through conforming or threshold-resisting behavior. This is especially intriguing because it enables the material system to change its response based on its loading history, going beyond previous works in which the response to mechanical deformation is fixed after manufacturing. While the system already exhibits life-like trainable properties, it also establishes a foundation for more intelligent material systems and can enhance the field of soft-robotics.

Together, these works present three interconnected levels for engineering responses into materials. The first response is purely geometric and can be achieved by fabricating the metamaterial from a wide variety of base materials. The second response is based on composition and can be applied to more complex geometries, triggering the response locally. The final response connects both geometry and base material in a closed-loop system that enables training. Collectively, these responses lay a conceptual basis for future developments toward stimuli-responsive materials that exhibit life-like behavior through interaction of structure and composition.

4.2 Limitations and Outlook

Mechanical metamaterials hold great potential beyond traditional structural applications, as responses can be engineered directly into their structure. This work accomplished such engineered responses in three consecutive approaches, collectively providing a foundation for functional integration using mechanical metamaterials.

While the responses in Section 3.1 - Section 3.3 worked well in isolation, they also show potential for implementation in more complex systems. Realizing this potential, however, requires overcoming limitations of each engineered response and addressing application-specific challenges.

The first work, highlighted in Section 3.1, exploited the self-contacting properties of the unit cell to accomplish a switch in Poisson's ratio. However, this self-contact could also be utilized to close electric circuits. In the presented scales demonstrator, a circuit was closed by expansion of the metamaterial, contacting two electrodes. While this served as a proof of concept, future works could attach electrodes directly to the self-contacting features of the unit cell. This would increase accuracy and sensitivity, because self-contact occurs at lower levels of compression than expansion. Another approach could exploit a drop in resistivity upon self-contact, if the metamaterial is made from a conductive base material, as in the works of Utzeri et al. [107]. A further direction lies in harnessing the instantaneous increase in Young's modulus upon self-contact. While this phenomenon was described in Section 3.1, its possible applications can range from adaptive load-bearing structures to impact protection systems.

The second work provided a clear understanding of the relation between self-reporting and mechanical properties in the PDMS-microcapsule composite (Section 3.2). This establishes a foundation for applications, in which the composite's behavior can be harnessed for new functionalities. In future works, this material could be integrated into mechanical metamaterials, where microcapsules would rupture in specific locations of high stress. This could yield preprogrammed self-reporting patterns, or a different response enabled by an alternative encapsulated liquid. The latter would open up the possibility to change the metamaterial's subsequent mechanical response. This could be achieved either by chemical abscission of certain unit cell features or adhesion of self-contacting elements, which would allow the lattice described in Section 3.1 to permanently change its Poisson's ratio.

The third work, introduced in Section 3.3, accomplished trainability in a closed-loop metamaterial system by coupling the expansion response of the metamaterial to a stiffness change in the UV-crosslinkable base material. However, the metamaterial does not only exhibit expansion, but also the "if-then" behavior described in the first work (Section 3.1). In future works, self-contact and expansion might each be used as separate triggers for UV irradiation. This would allow for a more nuanced control of the training behavior, distinguishing two different levels of compression or stimuli. Furthermore, embedding the UV light into enclosed cavities of the metama-

terial would allow for a UV protective coating on the outside, while maintaining its training capabilities internally for outdoor use. Beyond this, the system can be used as a sensing element in soft robotics. Similar to the work of Auth et al. [108], the material could respond to deformation by on-board irradiation, changing behavior of the robot or increasing its load-bearing capacity. Also, UV-triggered stiffening holds great potential beyond the trainable system presented in Section 3.3. Spatial control of UV exposure, through masking or projection of a UV pattern, could lead to three-dimensional geometries emerging from initially flat pieces. UV patterning can introduce locally stiffened features, which can act like a frame. By subsequent stretching or inflation, these features would restrict a uniform deformation, resulting in a 3D-folded geometry. Such approaches enable mechanical metamaterials with adaptive stiffness, embedded sensing, and complex shapes after manufacturing, exceeding the possibilities of current additive manufacturing or molding techniques.

Looking forward, material systems of the future are set out to enable autonomous behavior and, therefore, exhibit life-like responses to operate safely and robustly [14, 109]. Mechanical metamaterials exhibit such responses upon deformation, which is further enhanced by combining them with responsive base materials. The presented works overcome crucial challenges posed by Pishvar and Harne [14]: the first advances optimization and design for the self-contacting metamaterial, the second exploits the change in material properties, and the third harnesses stiffness changes by a 3D printable, UV-responsive base material applied in a metamaterial structure. Together, these contributions set a basis for future developments that enable safe autonomous systems.

5 Publications

5.1 Publications as First Author

D. Schwarz, J. Liotier, V. Slesarenko, and J. Rühe, “Light induced training of 3d printed mechanical metamaterials”, *Advanced Materials Technologies*, e01416, 2025. DOI: 10.1002/admt.202501416

D. Schwarz and V. Slesarenko, “Correlating fluorescence and residual stiffness in self-reporting microcapsule composites with an intact soft matrix”, *Composites Part C: Open Access*, p. 100 586, 2025. DOI: 10.1016/j.jcomc.2025.100586

D. Schwarz, G. Felsch, F. Tauber, S. Schiller, and V. Slesarenko, “Exploiting self-contact in mechanical metamaterials for new discrete functionalities”, *Materials & Design*, vol. 236, p. 112 468, 2023. DOI: 10.1016/j.matdes.2023.112468

5.2 Publication as Co-Author

G. Felsch, N. Ghavidelnia, D. Schwarz, and V. Slesarenko, “Controlling auxeticity in curved-beam metamaterials via a deep generative model”, *Computer Methods in Applied Mechanics and Engineering*, vol. 410, p. 116 032, 2023. DOI: 10.1016/j.cma.2023.116032

5.3 Presentations at Conferences

9th International Conference on Self-Healing Materials, Madrid, 24.-26.06.2024, "Delayed Reporting of Mechanical Changes in Self-Sensing Microcapsule Composites"

1st International Conference and Scientific Exhibition on Living Materials Systems, Freiburg, 21.-24.03.2023, "Mechanical metamaterials switch auxeticity during compression"

6 Scientific Curriculum Vitae

David Niels Schwarz

*12.12.1994 in Weingarten

Education

PhD Student *University of Freiburg*	since 2022
Mechanical Engineering: Digital Product Development & Simulation (M.Sc.) *FH Technikum Wien*	2019 – 2021
International Degree Course in Biomimetics (B.Sc.) *HS Bremen*	2015 – 2019
Material Design Bionics and Photonics *HS Hamm-Lippstadt*	2014 – 2015
Abitur *Gymnasium Weingarten*	2013

Publications

Schwarz, D., Liotier, J., Slesarenko, V. & Rühe, J. Light induced training of 3D printed mechanical metamaterials. *Advanced Materials Technologies*, e01416 (2025)

Schwarz, D. & Slesarenko, V. Correlating fluorescence and residual stiffness in self-reporting microcapsule composites with an intact soft matrix. *Composites Part C: Open Access*, 100586 (2025)

Schwarz, D., Felsch, G., Tauber, F., Schiller, S. & Slesarenko, V. Exploiting self-contact in mechanical metamaterials for new discrete functionalities. *Materials & Design* 236, 112468 (2023)

Felsch, G., Ghavidelnia, N., **Schwarz, D.** & Slesarenko, V. Controlling auxeticity in curved-beam metamaterials via a deep generative model. *Computer Methods in Applied Mechanics and Engineering* 410, 116032 (2023)

Ringel, B., **Schwarz, D.**, Vu, H. M., Meiniger, S., Schlick, G., Seidel, C. & Oechsner, M. Investigation on a predetermined point of failure for stainless steel 316L pressure loaded components made by laser powder bed fusion through stress analysis and experimental testing. *Progress in Additive Manufacturing* 8, 27–35 (2023)

Patents

Thurmeier, M., Dockhorn, M., Dirisamer, F., **Schwarz, D.** Sicherungselement für eine Abschlussplatte einer Batterieanordnung, *Pat. DE 10 2022 126 444 B3*, 2023

Thurmeier, M., Dockhorn, M., Dirisamer, F., **Schwarz, D.** Blechbauteil zum Umlenken eines Fluidstroms aus einer Batteriezelle, Herstellungsverfahren für ein solchen Blechbauteil, Batterieanordnung mit einem solchen Blechbauteil und Kraftfahrzeug mit einer solchen Batterieanordnung, *Pat. DE 10 2023 106 478 B3*, 2024

Thurmeier, M., Dirisamer, F., **Schwarz, D.** Verfahren, Kraftfahrzeug und Crashanordnung zum Schutz eines Batteriemoduls des Kraftfahrzeuges, *Pat. DE 10 2023 105 324 A1*, 2024
(patent application)

Thurmeier, M., Dirisamer, F., **Schwarz, D.** Kühlplattenanordnung mit integrierter Spanneinrichtung, Energiespeicher, Kraftfahrzeug und Verfahren zum Herstellen einer Kühlplattenanordnung, *Pat. DE 10 2023 103 578 A1*, 2024
(patent application)

Thurmeier, M., Dockhorn, M., Dirisamer, F., **Schwarz, D.** Batterie für ein Kraftfahrzeug und Verfahren zum Ableiten eines aus der Batteriezelle austretenden Gases, *Pat. DE 10 2023 100 761 A1*, 2024
(patent application)

Thurmeier, M., Dockhorn, M., Dirisamer, F., **Schwarz, D.** Temperieranordnung für eine Batterieanordnung, *Pat. DE 10 2022 128 309 A1*, 2024
(patent application)

Thurmeier, M., Dirisamer, F., **Schwarz, D.** Kraftfahrzeug, *Pat. DE 10 2022 121 515 A1*, 2024
(patent application)

Teaching

Micromechanics - Assistance, Tutoring — Winter term 2023/24
University of Freiburg

Professional Experience

Doctoral Researcher — since 2022
University of Freiburg

Simulation Engineer — 2021 – 2022
Digital Physics AI GmbH

Conferences & Research Stays

Presentation: Delayed Reporting of Mechanical Changes in Self-Sensing Microcapsule Composites — 06/2024
9th International Conference on Self-Healing Materials, Madrid

Research Stay & Invited Talk — 04/2023
Czech Technical University CVUT, Prague

Presentation: Mechanical Metamaterials Switch Auxeticity During Compression — 03/2023
1st International Conference and Scientific Exhibition on Living Materials Systems, Freiburg

First, I would like to thank my supervisor, Dr. Viacheslav Slesarenko. Without him, I would never have had the opportunity to come to Freiburg and pursue a PhD. His guidance was invaluable throughout my time here, helping me to stay on track and successfully navigate the peer review process. His honest feedback helped me grow as a scientist. I would also like to thank my second supervisor, Prof. Dr. Bastian Rapp, for his valuable feedback, especially regarding the writing of this thesis.

Furthermore, I would like to thank all the collaborators and co-authors of the publications in this thesis. In particular, I would like to thank Dr. Claas Stamp for his valuable contributions to the second publication. I would also like to thank Dr. Johan Liotier for the great collaboration on the third publication. It was a pleasure working with all of you.

I would also like to thank the rest of our group: Gerrit Felsch and Michael Somr. They both helped me push through the inevitable struggles, be it with technical details, gummy bears, or coffee. I would also like to thank the great second floor FIT people: Swathi, Maria, Esther, Hari, Stefano, and Christoph.

I would like to thank my family for their great support. Without them, I would not have had the opportunity to pursue this career, nor the help to get through the inevitable struggles I faced. Having great friends who supported and distracted me also helped immensely.

Moreover, I would like to thank the Deutsche Forschungsgemeinschaft (DFG) for funding my position and all of my research. I conducted my research in the Cluster of Excellence livMatS, which was enabled by the DFG under the grant EXC-2193/1 – 390951807. I am grateful for the colleagues I met, the workshops I attended, and the colloquia I listened to, all of which were provided by the cluster.

Finally, I would like to thank my proofreaders, Christoph, Swathi, Hari, and Jonathan, for their valuable feedback. Additionally, I used ChatGPT and DeepL to get improvement suggestions on the readability and grammar of this thesis. All changes to my original draft were applied by me, and I take full responsibility for the content.

Bibliography

[1] K. Michielsen and D. Stavenga, "Gyroid cuticular structures in butterfly wing scales: Biological photonic crystals", *Journal of The Royal Society Interface*, vol. 5, no. 18, pp. 85–94, 2007. DOI: 10.1098/rsif.2007.1065.

[2] I. Maskery, L. Sturm, A. Aremu, A. Panesar, C. Williams, C. Tuck, R. Wildman, I. Ashcroft, and R. Hague, "Insights into the mechanical properties of several triply periodic minimal surface lattice structures made by polymer additive manufacturing", *Polymer*, vol. 152, pp. 62–71, 2018. DOI: 10.1016/j.polymer.2017.11.049.

[3] R. F. Almgren, "An isotropic three-dimensional structure with poisson's ratio =-1", *Journal of Elasticity*, vol. 15, no. 4, pp. 427–430, 1985. DOI: 10.1007/bf00042531.

[4] T. Frenzel, M. Kadic, and M. Wegener, "Three-dimensional mechanical metamaterials with a twist", *Science*, vol. 358, no. 6366, pp. 1072–1074, 2017. DOI: 10.1126/science.aao4640.

[5] F. Wenz, I. Schmidt, A. Leichner, T. Lichti, S. Baumann, H. Andrae, and C. Eberl, "Designing shape morphing behavior through local programming of mechanical metamaterials", *Advanced Materials*, vol. 33, no. 37, p. 2 008 617, 2021. DOI: 10.1002/adma.202008617.

[6] M. J. Robb, W. Li, R. C. R. Gergely, C. C. Matthews, S. R. White, N. R. Sottos, and J. S. Moore, "A robust damage-reporting strategy for polymeric materials enabled by aggregation-induced emission", *ACS Central Science*, vol. 2, no. 9, pp. 598–603, 2016. DOI: 10.1021/acscentsci.6b00198.

[7] M. F. Ashby, *Materials selection in mechanical design*. Butterworth-Heinemann, 2011, ISBN: 9781856176637. DOI: 10.1016/C2009-0-25539-5.

[8] R. Lakes, "Foam structures with a negative poisson's ratio", *Science*, vol. 235, no. 4792, pp. 1038–1040, 1987. DOI: 10.1126/science.235.4792.1038.

[9] K. Bertoldi, P. M. Reis, S. Willshaw, and T. Mullin, "Negative poisson's ratio behavior induced by an elastic instability", *Advanced Materials*, vol. 22, no. 3, pp. 361–366, 2010. DOI: 10.1002/adma.200901956.

[10] A. Walther, "Viewpoint: From responsive to adaptive and interactive materials and materials systems: A roadmap", *Advanced Materials*, vol. 32, no. 20, p. 1 905 111, 2019. DOI: 10.1002/adma.201905111.

[11] R. T. Shafranek, S. C. Millik, P. T. Smith, C.-U. Lee, A. J. Boydston, and A. Nelson, "Stimuli-responsive materials in additive manufacturing", *Progress in Polymer Science*, vol. 93, pp. 36–67, 2019. DOI: 10.1016/j.progpolymsci.2019.03.002.

[12] P. Jiao, J. Mueller, J. R. Raney, X. Zheng, and A. H. Alavi, "Mechanical metamaterials and beyond", *Nature Communications*, vol. 14, no. 1, p. 6004, 2023. DOI: 10.1038/s41467-023-41679-8.

[13] J. U. Surjadi, L. Gao, H. Du, X. Li, X. Xiong, N. X. Fang, and Y. Lu, "Mechanical metamaterials and their engineering applications", *Advanced Engineering Materials*, vol. 21, no. 3, p. 1 800 864, 2019. DOI: 10.1002/adem.201800864.

[14] M. Pishvar and R. L. Harne, "Foundations for soft, smart matter by active mechanical metamaterials", *Advanced Science*, vol. 7, no. 18, p. 2 001 384, 2020. DOI: 10.1002/advs.202001384.

[15] Y. Chen, T. Li, F. Scarpa, and L. Wang, "Lattice metamaterials with mechanically tunable poisson's ratio for vibration control", *Physical Review Applied*, vol. 7, no. 2, p. 024 012, 2017. DOI: 10.1103/physrevapplied.7.024012.

[16] V. K. Mohonee, K. L. Goh, L. Mishnaevsky, and P. Pasbakhsh, "Capsule based self-healing composites: New insights on mechanical behaviour based on finite element analysis", *Computational Materials Science*, vol. 192, p. 110 203, 2021. DOI: 10.1016/j.commatsci.2020.110203.

[17] C. Calvino and C. Weder, "Microcapsule-containing self-reporting polymers", *Small*, vol. 14, no. 46, p. 1 802 489, 2018. DOI: 10.1002/smll.201802489.

[18] J. Liotier, T. Piock, and J. Rühe, "Universal cross-linking of nonfunctional polymers through c,h-insertion reactions", *Macromolecules*, vol. 58, no. 4, pp. 1859–1866, 2024. DOI: 10.1021/acs.macromol.4c02184.

[19] D. Gross, W. Hauger, and P. Wriggers, *Technische Mechanik 4*. Springer-Verlag GmbH, 2018, ISBN: 9783662556948. DOI: 10.1007/978-3-662-55694-8.

[20] H. A. Mang and G. Hofstetter, *Festigkeitslehre*. Springer Berlin Heidelberg, 2018, ISBN: 978-3-662-57564-2. DOI: 10.1007/978-3-662-57564-2.

[21] C. W. Smith, R. J. Wootton, and K. E. Evans, "Interpretation of experimental data for poisson's ratio of highly nonlinear materials", *Experimental Mechanics*, vol. 39, no. 4, pp. 356–362, 1999. DOI: 10.1007/bf02329817.

[22] D. Gross, W. Hauger, J. Schröder, and W. A. Wall, *Technische Mechanik 2: Elastostatik*. Springer Berlin Heidelberg, 2024, ISBN: 9783662684238. DOI: 10.1007/978-3-662-68423-8.

[23] T.-C. Lim, *Mechanics of Metamaterials with Negative Parameters*. Springer Singapore, 2020, ISBN: 978-981-15-6446-8. DOI: 10.1007/978-981-15-6446-8.

[24] H. M. A. Kolken and A. A. Zadpoor, "Auxetic mechanical metamaterials", *RSC Advances*, vol. 7, no. 9, pp. 5111–5129, 2017. DOI: 10.1039/c6ra27333e.

[25] J.-H. Lee, J. P. Singer, and E. L. Thomas, "Micro-/nanostructured mechanical metamaterials", *Advanced Materials*, vol. 24, no. 36, pp. 4782–4810, 2012. DOI: 10.1002/adma.201201644.

[26] W. Yang, Z.-M. Li, W. Shi, B.-H. Xie, and M.-B. Yang, "Review on auxetic materials", *Journal of Materials Science*, vol. 39, no. 10, pp. 3269–3279, 2004. DOI: 10.1023/b:jmsc.0000026928.93231.e0.

[27] K. L. Alderson, R. S. Webber, and K. E. Evans, "Novel variations in the microstructure of auxetic ultra-high molecular weight polyethylene. part 2: Mechanical properties", *Polymer Engineering & Science*, vol. 40, no. 8, pp. 1906–1914, 2000. DOI: 10.1002/pen.11322.

[28] F. Amin, M. N. Ali, U. Ansari, M. Mir, M. A. Minhas, and W. Shahid, "Auxetic coronary stent endoprosthesis: Fabrication and structural analysis", *Journal of Applied Biomaterials & Functional Materials*, vol. 13, no. 2, pp. 127–135, 2015. DOI: 10.5301/jabfm.5000213.

[29] A. Bührig-Polaczek, C. Fleck, T. Speck, P. Schüler, S. F. Fischer, M. Caliaro, and M. Thielen, "Biomimetic cellular metals—using hierarchical structuring for energy absorption", *Bioinspiration & Biomimetics*, vol. 11, no. 4, p. 045 002, 2016. DOI: 10.1088/1748-3190/11/4/045002.

[30] U. Larsen, O. Signund, and S. Bouwsta, "Design and fabrication of compliant micromechanisms and structures with negative poisson's ratio", *Journal of Microelectromechanical Systems*, vol. 6, no. 2, pp. 99–106, 1997. DOI: 10.1109/84.585787.

[31] A. Alderson, K. Alderson, G. Chirima, N. Ravirala, and K. Zied, "The in-plane linear elastic constants and out-of-plane bending of 3-coordinated ligament and cylinder-ligament honeycombs", *Composites Science and Technology*, vol. 70, no. 7, pp. 1034–1041, 2010. DOI: 10.1016/j.compscitech.2009.07.010.

[32] C. Körner and Y. Liebold-Ribeiro, "A systematic approach to identify cellular auxetic materials", *Smart Materials and Structures*, vol. 24, no. 2, p. 025 013, 2014. DOI: 10.1088/0964-1726/24/2/025013.

[33] J. N. Grima and K. E. Evans, "Auxetic behavior from rotating squares", *Journal of Materials Science Letters*, vol. 19, no. 17, pp. 1563–1565, 2000. DOI: 10.1023/a:1006781224002.

[34] R. Gatt, L. Mizzi, J. I. Azzopardi, K. M. Azzopardi, D. Attard, A. Casha, J. Briffa, and J. N. Grima, "Hierarchical auxetic mechanical metamaterials", *Scientific Reports*, vol. 5, no. 1, p. 8395, 2015. DOI: 10.1038/srep08395.

[35] J. N. Grima and R. Gatt, "Perforated sheets exhibiting negative poisson's ratios", *Advanced Engineering Materials*, vol. 12, no. 6, pp. 460–464, 2010. DOI: 10.1002/adem.201000005.

[36] J. N. Grima, L. Mizzi, K. M. Azzopardi, and R. Gatt, "Auxetic perforated mechanical metamaterials with randomly oriented cuts", *Advanced Materials*, vol. 28, no. 2, pp. 385–389, 2015. DOI: 10.1002/adma.201503653.

[37] G. Felsch and V. Slesarenko, "Generative models struggle with kirigami metamaterials", *Scientific Reports*, vol. 14, no. 1, p. 19 397, 2024. DOI: 10.1038/s41598-024-70364-z.

[38] J. K. Wilt, C. Yang, and G. X. Gu, "Accelerating auxetic metamaterial design with deep learning", *Advanced Engineering Materials*, vol. 22, no. 5, p. 1 901 266, 2020. DOI: 10.1002/adem.201901266.

[39] K. Che, C. Yuan, J. Wu, H. Jerry Qi, and J. Meaud, "Three-dimensional-printed multistable mechanical metamaterials with a deterministic deformation sequence", *Journal of Applied Mechanics*, vol. 84, no. 1, p. 011 004, 2016. DOI: 10.1115/1.4034706.

[40] P. Jiao, H. Zhang, and W. Li, "Origami tribo-metamaterials with mechano-electrical multistability", *ACS Applied Materials & Interfaces*, vol. 15, no. 2, pp. 2873–2880, 2023. DOI: 10.1021/acsami.2c16681.

[41] C. Lv, D. Krishnaraju, G. Konjevod, H. Yu, and H. Jiang, "Origami based mechanical metamaterials", *Scientific Reports*, vol. 4, no. 1, p. 5979, 2014. DOI: 10.1038/srep05979.

[42] M. Kadic, T. Bückmann, R. Schittny, P. Gumbsch, and M. Wegener, "Pentamode metamaterials with independently tailored bulk modulus and mass density", *Physical Review Applied*, vol. 2, no. 5, p. 054 007, 2014. DOI: 10.1103/physrevapplied.2.054007.

[43] G. W. Milton and A. V. Cherkaev, "Which elasticity tensors are realizable?", *Journal of Engineering Materials and Technology*, vol. 117, no. 4, pp. 483–493, 1995. DOI: 10.1115/1.2804743.

[44] M. Kadic, G. W. Milton, M. van Hecke, and M. Wegener, "3d metamaterials", *Nature Reviews Physics*, vol. 1, no. 3, pp. 198–210, 2019. DOI: 10.1038/s42254-018-0018-y.

[45] Z. Li, Z. Luo, L.-C. Zhang, and C.-H. Wang, "Topological design of pentamode lattice metamaterials using a ground structure method", *Materials & Design*, vol. 202, p. 109 523, 2021. DOI: 10.1016/j.matdes.2021.109523.

[46] C. Beinert, G. Burkhardt, U. Hüsgen, M. Kalwa, G. Pötsch, and C. Schwenzer, *Plastics Processing, 1. Processing of Thermoplastics*. Wiley, 2022, pp. 1–48, ISBN: 9783527306732. DOI: 10.1002/14356007.a20_663.pub3.

[47] M. W. Keller, S. R. White, and N. R. Sottos, "A self-healing poly(dimethyl siloxane) elastomer", *Advanced Functional Materials*, vol. 17, no. 14, pp. 2399–2404, 2007. DOI: 10.1002/adfm.200700086.

[48] M. F. Alexandre-Franco, R. Kouider, R. Kassir Al-Karany, E. M. Cuerda-Correa, and A. Al-Kassir, "Recent advances in polymer science and fabrication processes for enhanced microfluidic applications: An overview", *Micromachines*, vol. 15, no. 9, p. 1137, 2024. DOI: 10.3390/mi15091137.

[49] W. Li, F. Wang, O. Sigmund, and X. S. Zhang, "Digital synthesis of free-form multimaterial structures for realization of arbitrary programmed mechanical responses", *Proceedings of the National Academy of Sciences*, vol. 119, no. 10, e2120563119, 2022. DOI: 10.1073/pnas.2120563119.

[50] X. L. Ji, J. K. Jing, W. Jiang, and B. Z. Jiang, "Tensile modulus of polymer nanocomposites", *Polymer Engineering & Science*, vol. 42, no. 5, pp. 983–993, 2002. DOI: 10.1002/pen.11007.

[51] S.-Y. Fu, X.-Q. Feng, B. Lauke, and Y.-W. Mai, "Effects of particle size, particle/matrix interface adhesion and particle loading on mechanical properties of particulate–polymer composites", *Composites Part B: Engineering*, vol. 39, no. 6, pp. 933–961, 2008. DOI: 10.1016/j.compositesb.2008.01.002.

[52] S. R. White, N. R. Sottos, P. H. Geubelle, J. S. Moore, M. R. Kessler, S. R. Sriram, E. N. Brown, and S. Viswanathan, "Autonomic healing of polymer composites", *Nature*, vol. 409, no. 6822, pp. 794–797, 2001. DOI: 10.1038/35057232.

[53] J. F. Patrick, M. J. Robb, N. R. Sottos, J. S. Moore, and S. R. White, "Polymers with autonomous life-cycle control", *Nature*, vol. 540, no. 7633, pp. 363–370, 2016. DOI: 10.1038/nature21002.

[54] M. M. Caruso, B. J. Blaiszik, H. Jin, S. R. Schelkopf, D. S. Stradley, N. R. Sottos, S. R. White, and J. S. Moore, "Robust, double-walled microcapsules for self-healing polymeric materials", *ACS Applied Materials & Interfaces*, vol. 2, no. 4, pp. 1195–1199, 2010. DOI: 10.1021/am100084k.

[55] M. Hu, Z. Ma, M. Kim, D. Kim, S. Ye, S. Pané, Y. Bao, R. W. Style, and L. Isa, "Self-reporting multiple microscopic stresses through tunable microcapsule arrays", *Advanced Materials*, p. 2 410 945, 2024. DOI: 10.1002/adma.202410945.

[56] C.-H. Stamp, J. Stumpp, and C. Calvino, "Adhesives with debonding-on-demand capability: Leveraging responsive microcapsules for mechanically-induced debonding", en, *Adv. Mater.*, e2414308, 2025. DOI: 10.1002/adma.202414308.

[57] H. Kodama, "Automatic method for fabricating a three-dimensional plastic model with photo-hardening polymer", *Review of Scientific Instruments*, vol. 52, no. 11, pp. 1770–1773, 1981. DOI: 10.1063/1.1136492.

[58] T. D. Ngo, A. Kashani, G. Imbalzano, K. T. Nguyen, and D. Hui, "Additive manufacturing (3d printing): A review of materials, methods, applications and challenges", *Composites Part B: Engineering*, vol. 143, pp. 172–196, 2018. DOI: 10.1016/j.compositesb.2018.02.012.

[59] S. S. Crump, "Apparatus and method for creating three-dimensional objects", pat. 5 121 329, 1992.

[60] S.-H. Ahn, M. Montero, D. Odell, S. Roundy, and P. K. Wright, "Anisotropic material properties of fused deposition modeling abs", *Rapid Prototyping Journal*, vol. 8, no. 4, pp. 248–257, 2002. DOI: 10.1108/13552540210441166.

[61] A. Dey and N. Yodo, "A systematic survey of fdm process parameter optimization and their influence on part characteristics", *Journal of Manufacturing and Materials Processing*, vol. 3, no. 3, p. 64, 2019. DOI: 10.3390/jmmp3030064.

[62] M. M. M. Haque, S. R. Dhrubo, A.-F. Z. Pranto, A. Ahmed, M. M. Arefin, M. Arifuzzaman, and M. S. Islam, "Impact of process parameters and material selection on the mechanical performance of fdm 3d-printed components", *Hybrid Advances*, vol. 10, p. 100 502, 2025. DOI: 10.1016/j.hybadv.2025.100502.

[63] H. I. Medellin-Castillo and J. Zaragoza-Siqueiros, "Design and manufacturing strategies for fused deposition modelling in additive manufacturing: A review", *Chinese Journal of Mechanical Engineering*, vol. 32, no. 1, p. 53, 2019. DOI: 10.1186/s10033-019-0368-0.

[64] DIN EN ISO/ASTM 52910, *Additive manufacturing - design - requirements, guidelines and recommendations*, 2020. DOI: 10.31030/3111254.

[65] DIN EN ISO/ASTM 52920, *Additive manufacturing - qualification principles - requirements for industrial additive manufacturing processes and production sites*, 2023. DOI: 10.31030/3481398.

[66] X. Wang, M. Jiang, Z. Zhou, J. Gou, and D. Hui, "3d printing of polymer matrix composites: A review and prospective", *Composites Part B: Engineering*, vol. 110, pp. 442–458, 2017. DOI: 10.1016/j.compositesb.2016.11.034.

[67] C. Duran, V. Subbian, M. T. Giovanetti, J. R. Simkins, and F. R. Beyette Jr, "Experimental desktop 3d printing using dual extrusion and water-soluble polyvinyl alcohol", *Rapid Prototyping Journal*, vol. 21, no. 5, D. Eujin Pei, Ed., pp. 528–534, 2015. DOI: 10.1108/rpj-09-2014-0117.

[68] Z. Hou, X. Tian, J. Zhang, and D. Li, "3d printed continuous fibre reinforced composite corrugated structure", *Composite Structures*, vol. 184, pp. 1005–1010, 2018. DOI: 10.1016/j.compstruct.2017.10.080.

[69] Z. Hu, Z. Wei, K. Wang, Y. Chen, R. Zhu, G. Huang, and G. Hu, "Engineering zero modes in transformable mechanical metamaterials", *Nature Communications*, vol. 14, no. 1, p. 1266, 2023. DOI: 10.1038/s41467-023-36975-2.

[70] J. Gong, O. Seow, C. Honnet, J. Forman, and S. Mueller, "Metasense: Integrating sensing capabilities into mechanical metamaterial", in *The 34th Annual ACM Symposium on User Interface Software and Technology*, ser. UIST '21, ACM, 2021, pp. 1063–1073. DOI: 10.1145/3472749.3474806.

[71] K. Barri, Q. Zhang, P. Jiao, Z. L. Wang, and A. H. Alavi, "Multifunctional metamaterial sensor and nanogenerator", in *Behavior and Mechanics of Multifunctional Materials XV*, R. L. Harne, Ed., SPIE, 2021, p. 6. DOI: 10.1117/12.2581050.

[72] J. R. C. Dizon, C. C. L. Gache, H. M. S. Cascolan, L. T. Cancino, and R. C. Advincula, "Post-processing of 3d-printed polymers", *Technologies*, vol. 9, no. 3, p. 61, 2021. DOI: 10.3390/technologies9030061.

[73] L. Gillespie, "Deburring precision miniature parts", *Precision Engineering*, vol. 1, no. 4, pp. 189–198, 1979. DOI: 10.1016/0141-6359(79)90099-0.

[74] C. Evans, E. Paul, D. Dornfeld, D. Lucca, G. Byrne, M. Tricard, F. Klocke, O. Dambon, and B. Mullany, "Material removal mechanisms in lapping and polishing", *CIRP Annals*, vol. 52, no. 2, pp. 611–633, 2003. DOI: 10.1016/s0007-8506(07)60207-8.

[75] C. Ye, C. Zhang, J. Zhao, and Y. Dong, "Effects of post-processing on the surface finish, porosity, residual stresses, and fatigue performance of additive manufactured metals: A review", *Journal of Materials Engineering and Performance*, vol. 30, no. 9, pp. 6407–6425, 2021. DOI: 10.1007/s11665-021-06021-7.

[76] J. Butt and R. Bhaskar, "Investigating the effects of annealing on the mechanical properties of fff-printed thermoplastics", *Journal of Manufacturing and Materials Processing*, vol. 4, no. 2, p. 38, 2020. DOI: 10.3390/jmmp4020038.

[77] N. B. Guerra, T. M. Reis, T. Scopel, M. S. de Lima, C. A. Figueroa, and A. F. Michels, "Influence of process parameters and post-molding condition on shrinkage and warpage of injection-molded plastic parts with complex geometry", *The International Journal of Advanced Manufacturing Technology*, vol. 128, no. 1–2, pp. 479–490, 2023. DOI: 10.1007/s00170-023-11782-7.

[78] B. Liu, Y. Wang, Z. Lin, and T. Zhang, "Creating metal parts by fused deposition modeling and sintering", *Materials Letters*, vol. 263, p. 127 252, 2020. DOI: 10.1016/j.matlet.2019.127252.

[79] Y. J. Kim, H. N. Kim, and D. Y. Kim, "A study on effects of curing and machining conditions in post-processing of sla additive manufactured polymer", *Journal of Manufacturing Processes*, vol. 119, pp. 511–519, 2024. DOI: 10.1016/j.jmapro.2024.03.112.

[80] J. Chi, B. Agea Blanco, G. Bruno, J. Günster, and A. Zocca, "Self-organization postprocess for additive manufacturing in producing advanced functional structure and material", *Advanced Engineering Materials*, vol. 24, no. 6, p. 2 101 262, 2021. DOI: 10.1002/adem.202101262.

[81] O. Rifaie-Graham, E. A. Apebende, L. K. Bast, and N. Bruns, "Self-reporting fiber-reinforced composites that mimic the ability of biological materials to sense and report damage", *Advanced Materials*, vol. 30, no. 19, p. 1 705 483, 2018. DOI: 10.1002/adma.201705483.

[82] X. Xia, C. M. Spadaccini, and J. R. Greer, "Responsive materials architected in space and time", *Nature Reviews Materials*, vol. 7, no. 9, pp. 683–701, 2022. DOI: 10.1038/s41578-022-00450-z.

[83] H. Wang, Y. Lyu, S. Bosiakov, H. Zhu, and Y. Ren, "A review on the mechanical metamaterials and their applications in the field of biomedical engineering", *Frontiers in Materials*, vol. 10, p. 1 273 961, 2023. DOI: 10.3389/fmats.2023.1273961.

[84] F. Khan, N. Hossain, J. J. Mim, S. M. Rahman, M. J. Iqbal, M. Billah, and M. A. Chowdhury, "Advances of composite materials in automobile applications – a review", *Journal of Engineering Research*, vol. 13, no. 2, pp. 1001–1023, 2025. DOI: 10.1016/j.jer.2024.02.017.

[85] C. Scazzoli, R. Trigueira, A. Cohades, and V. Michaud, "A novel method to quantify self-healing capabilities of fiber-reinforced polymers", *Frontiers in Materials*, vol. 9, p. 932 287, 2022. DOI: 10.3389/fmats.2022.932287.

[86] J. Dong, G. Ye, Y. Wang, F. Jin, and H. Fan, "Design, manufacture and crushing behaviors of buckling-inspired auxetic meta-lattice structures", *International Journal of Smart and Nano Materials*, vol. 12, no. 4, pp. 491–510, 2021. DOI: 10.1080/19475411.2021.1966855.

[87] O. Skarsetz, V. Slesarenko, and A. Walther, "Programmable auxeticity in hydrogel metamaterials via shape-morphing unit cells", *Advanced Science*, vol. 9, no. 23, p. 2 201 867, 2022. DOI: 10.1002/advs.202201867.

[88] A. Clausen, F. Wang, J. S. Jensen, O. Sigmund, and J. A. Lewis, "Topology optimized architectures with programmable poisson's ratio over large deformations", *Advanced Materials*, vol. 27, no. 37, pp. 5523–5527, 2015. DOI: 10.1002/adma.201502485.

[89] M. F. Berwind, A. Kamas, and C. Eberl, "A hierarchical programmable mechanical metamaterial unit cell showing metastable shape memory", *Advanced Engineering Materials*, vol. 20, no. 11, p. 1 800 771, 2018. DOI: 10.1002/adem.201800771.

[90] M. A. Wagner, F. Schwarz, N. Huber, L. Geistlich, H. Galinski, and R. Spolenak, "Deformation-induced topological transitions in mechanical metamaterials and their application to tunable non-linear stiffening", *Materials & Design*, vol. 221, p. 110 918, 2022. DOI: 10.1016/j.matdes.2022.110918.

[91] H. Yasuda, P. R. Buskohl, A. Gillman, T. D. Murphey, S. Stepney, R. A. Vaia, and J. R. Raney, "Mechanical computing", *Nature*, vol. 598, no. 7879, pp. 39–48, 2021. DOI: 10.1038/s41586-021-03623-y.

[92] C. Coulais, E. Teomy, K. de Reus, Y. Shokef, and M. van Hecke, "Combinatorial design of textured mechanical metamaterials", *Nature*, vol. 535, no. 7613, pp. 529–532, 2016. DOI: 10.1038/nature18960.

[93] N. Gupta and C. Beckwith, "Mechanical properties of metamaterials", in *Architected Metamaterials: Design Principles and Properties*. Springer Nature Switzerland, 2025, pp. 11–39, ISBN: 9783031983306. DOI: 10.1007/978-3-031-98330-6_2.

[94] Y. Pu, S. Zheng, X. Hu, S. Tang, and N. An, "Robotic skins inspired by auxetic metamaterials for programmable bending of soft actuators", *Materials & Design*, vol. 246, p. 113 334, 2024. DOI: 10.1016/j.matdes.2024.113334.

[95] L. Y. W. Loh, U. Gupta, Y. Wang, C. C. Foo, J. Zhu, and W. F. Lu, "3d printed metamaterial capacitive sensing array for universal jamming gripper and human joint wearables", *Advanced Engineering Materials*, vol. 23, no. 5, p. 2 001 082, 2021. DOI: 10.1002/adem.202001082.

[96] R. P. Bohara, S. Linforth, T. Nguyen, A. Ghazlan, and T. Ngo, "Dual-mechanism auxetic-core protective sandwich structure under blast loading", *Composite Structures*, vol. 299, p. 116 088, 2022. DOI: 10.1016/j.compstruct.2022.116088.

[97] D. K. Rajak, D. D. Pagar, R. Kumar, and C. I. Pruncu, "Recent progress of reinforcement materials: A comprehensive overview of composite materials", *Journal of Materials Research and Technology*, vol. 8, no. 6, pp. 6354–6374, 2019. DOI: 10.1016/j.jmrt.2019.09.068.

[98] E. N. Brown, N. R. Sottos, and S. R. White, "Fracture testing of a self-healing polymer composite", *Experimental Mechanics*, vol. 42, no. 4, pp. 372–379, 2002. DOI: 10.1007/bf02412141.

[99] M. Hu, S. Peil, Y. Xing, D. Döhler, L. C. da Silva, W. H. Binder, M. Kappl, and M. B. Bannwarth, "Monitoring crack appearance and healing in coatings with damage self-reporting nanocapsules", *Materials Horizons*, vol. 5, no. 1, pp. 51–58, 2018. DOI: 10.1039/c7mh00676d.

[100] W. Pu, F. Wei, L. Yao, and S. Xie, "A review of humidity-driven actuator: Toward high response speed and practical applications", *Journal of Materials Science*, vol. 57, no. 26, pp. 12 202–12 235, 2022. DOI: 10.1007/s10853-022-07344-z.

[101] M. Chen, M. Gao, L. Bai, H. Zheng, H. J. Qi, and K. Zhou, "Recent advances in 4d printing of liquid crystal elastomers", *Advanced Materials*, vol. 35, no. 23, p. 2 209 566, 2023. DOI: 10.1002/adma.202209566.

[102] A. Amadi, M. Mohyaldinn, S. Ridha, and V. Ola, "Advancing engineering frontiers with niti shape memory alloys: A multifaceted review of properties, fabrication, and application potentials", *Journal of Alloys and Compounds*, vol. 976, p. 173 227, 2024. DOI: 10.1016/j.jallcom.2023.173227.

[103] D. C. Hughes, S. Ellefsen, and K. Baar, "Adaptations to endurance and strength training", *Cold Spring Harbor Perspectives in Medicine*, vol. 8, no. 6, a029769, 2017. DOI: 10.1101/cshperspect.a029769.

[104] N. P. R. Anten, R. Alcalá-Herrera, F. Schieving, and Y. Onoda, "Wind and mechanical stimuli differentially affect leaf traits in plantago major", *New Phytologist*, vol. 188, no. 2, pp. 554–564, 2010. DOI: 10.1111/j.1469-8137.2010.03379.x.

[105] A. Sydney Gladman, E. A. Matsumoto, R. G. Nuzzo, L. Mahadevan, and J. A. Lewis, "Biomimetic 4d printing", *Nature Materials*, vol. 15, no. 4, pp. 413–418, 2016. DOI: 10.1038/nmat4544.

[106] H. Zhang, H. Zeng, A. Priimagi, and O. Ikkala, "Viewpoint: Pavlovian materials—functional biomimetics inspired by classical conditioning", *Advanced Materials*, vol. 32, no. 20, p. 1 906 619, 2020. DOI: 10.1002/adma.201906619.

[107] M. Utzeri, H. Cebeci, and S. Kumar, "Autonomous sensing architected materials", *Advanced Functional Materials*, no. 11, p. 2 411 975, 2024. DOI: 10.1002/adfm.202411975.

[108] P. Auth, S. Conrad, N. Knorr, J. Teichmann, S. Ruppert, T. Speck, and F. Tauber, "Toward more autonomous soft robots: Development and characterization of a 3d-printed pneumatic contact sensor for a six-legged soft robotic walker", *Advanced Intelligent Systems*, e202500430, 2025. DOI: 10.1002/aisy.202500430.

[109] M. A. Kostiainen, A. Priimagi, J. V. I. Timonen, R. H. A. Ras, M. Sammalkorpi, M. Penttilä, O. Ikkala, and M. B. Linder, "Materials inspired by living functions", *Advanced Functional Materials*, vol. 34, no. 37, 2024. DOI: 10.1002/adfm.202402097.

[110] D. Schwarz, J. Liotier, V. Slesarenko, and J. Rühe, "Light induced training of 3d printed mechanical metamaterials", *Advanced Materials Technologies*, e01416, 2025. DOI: 10.1002/admt.202501416.

[111] D. Schwarz and V. Slesarenko, "Correlating fluorescence and residual stiffness in self-reporting microcapsule composites with an intact soft matrix", *Composites Part C: Open Access*, p. 100 586, 2025. DOI: 10.1016/j.jcomc.2025.100586.

[112] D. Schwarz, G. Felsch, F. Tauber, S. Schiller, and V. Slesarenko, "Exploiting self-contact in mechanical metamaterials for new discrete functionalities", *Materials & Design*, vol. 236, p. 112 468, 2023. DOI: 10.1016/j.matdes.2023.112468.

[113] G. Felsch, N. Ghavidelnia, D. Schwarz, and V. Slesarenko, "Controlling auxeticity in curved-beam metamaterials via a deep generative model", *Computer Methods in Applied Mechanics and Engineering*, vol. 410, p. 116 032, 2023. DOI: 10.1016/j.cma.2023.116032.

List of Figures

2.1 Stress state 9
2.2 Stress-strain of brittle and ductile materials 11
2.3 Working principle of the reentrant auxetic 13
2.4 Molding process 17
2.5 Working principle of fused filament fabrication 21

List of Tables

2.1 Overview of selected auxetic metamaterials 14
2.2 Overview of selected metamaterials 16

Nomenclature

ABS	Acrylonitrile Butadiene Styrene
AIE	Aggregation-Induced Emission
AM	Additive Manufacturing
CAD	Computer Aided Design
CFRP	Carbon Fiber Reinforced Plastics
FDM	Fused Deposition Modeling
FFF	Fused Filament Fabrication
PC	Polycarbonate
PDMS	Poly(Dimethyl Siloxane)
PLA	Polylactic Acid
PUF	Poly-(Urea-Formaldehyde)
PVA	Polyvinyl Alcohol
SLA	Stereolithography
STL	Standard Tessellation Language, Stereolithography
TPE	1,1,2,2-Tetraphenylethylene
TPU	Thermoplastic Polyurethane